

1 Response to Editor's comments:
2

3 **Associate Editor Decision: Publish subject to minor revisions (further review by editor)** (02 Feb
4 2020) by [Catherine Mottram](#)

5 Comments to the Author:

6 Editor comments on Roberts et al., 'LA-ICP-MS U-Pb carbonate geochronology: strategies and progress
7 with examples from fracture-fill calcite'

8
9 Overall this paper represents a useful updated review on in-situ carbonate geochronology that will be
10 valuable contribution to the community and particularly those new to the application. It provides a
11 thorough introduction to the method, applications and most importantly the limitations, potential pitfalls
12 and matters of potential concern that any future analyst should be aware of.

13
14 The reviewers were largely supportive of this paper, particularly AKC and the authors have mostly
15 addressed the specific corrections proposed by both reviewers and have presented reasonable responses
16 to reviewers. I am mainly satisfied that these corrections have been made with the following exceptions.

17
18 There are a few points that the authors have not addressed/ might be worth considering before the
19 manuscript is finalised:

20
21 1. Troy Rasbury commented "This manuscript is sort of a funny mix of a review and new datasets... While
22 it is nominally a review of vein dating, it is not a complete review of what is out there." I very much agree
23 with this opinion and I do not think that the authors have made any corrections to address this criticism.
24 The paper is a mix of review and new data and although a lot of what is presented is very useful, it is not
25 really a review of all previous work, instead is a compilation of all the data reported from the BGS lab.
26 Perhaps the authors could make this clear in the abstract/introduction- or include more examples from the
27 published literature (for instance in figures such as figure 14). Troy also commented "my overall take on
28 the manuscript is that it could be more compactly packaged and could do a better job of reviewing all of
29 the U/Pb dating of vein material- perhaps leaving off discussion of speleothems which is well covered by
30 Woodhead and a laundry list of carbonate characterization techniques that aren't tied to examples." Again,
31 I agree with this statement and I do not think that the authors have addressed this- they have made no
32 attempt to make the manuscript any shorter or more compact. I have two suggestions for how you might
33 achieve this:

34
35 We appreciate the comments from those not involved the manuscript, since they can provide an unbiased
36 opinion of the paper. We also understand the general feeling gained by the reviewers and editor – that this
37 paper presents a mixture of review and new data. We however, do not feel that a paper should conform to
38 a simple 'research article' or a 'review paper', these distinctions are given to us by the publishers, and
39 should not limit how we want to present science and scientific methodology. But, we appreciate that the
40 comments may improve the paper, and thus, we have attempted to improve the paper by shortening
41 some aspects, merging some sections, and removing some duplication of text.

42 Although most of our examples draw from vein material, all of our points of discussion are relevant to all
43 carbonate types, and thus we have reworded any text to make it clear that this paper applies to all
44 applications.

45
46 Specifically, we have completely redrawn the figure with the imaging techniques, which we feel provides a
47 more useful tableau, and which is better linked to the text. We have merged the three 'examples' of
48 image-guided dating into a single figure, and dramatically reduced the text, removing any unnecessary
49 background information about the samples. We have removed one of the three image-based dating
50 examples. We have removed the figure with the mu values compiled (but added it to the supp file). We
51 have removed the discussion section and expanded the conclusions, and added all the limitations into a
52 single 'limitation' section. This still comes towards the end of the paper, but we stand by our opinion that
53 is only natural to discuss 'the ways doing things', some 'examples of doing things', and then some
54 'nuances when doing those things'.

55
56 Why not review the published literature as a whole? – (1) if we were to swap figure 4 (the isochron good,
57 bad and ugly) for published literature only, then this section would essentially be unpicking other peoples
58 work (not ideal); (2) It would be difficult to draw from the literature for the section on image-guided
59 dating, as there is very little information within the published literature on how some dates may have been
60 refined, selected, interpreted etc. Instead, we have chosen to include unpublished data, such that we can
61 better demonstrate the methods behind refining data with imagery/compositional data; (3) We have
62 included image-based dating examples from veins, as these are complementary to those published by
63 Drost et al on sedimentary carbonates, and are a better comparison with the image-guided examples also
64 on veins.

65 Hopefully it should be clear where all the data are drawn from, i.e. literature or our own data.

66
67

68 a. Section 2- Discussion of ID vs in-situ techniques- although this is of course a very important topic for
69 discussion in geochronology much of this discussion has already been covered in other publications
70 focused on geochronology methods. I therefore think this text could be shortened. Figure 2 for instance is
71 very useful and I think if the text could be focused on these carbonate-specific examples would help
72 concentrate the discussion.

73 We find that many papers cover the basics of ID versus LA, i.e. the difference in spatial resolution and in
74 precision and accuracy of data, but they do not cover the nuances that make LA so beneficial for
75 carbonates, for example, the ability to hit zones with different U/Pb ratios. We have removed a few
76 sentences that were unnecessary, but overall we have maintained this important section.

77
78

79 b. Section 8- Troy's comment "The modeling of initial disequilibrium is a very important contribution. Why
80 is it so late in the paper?" I agree with this- I think that this section is an important and relatively novel
81 contribution to the community, however, it is buried at the end of this very long paper and I worry that it
82 will be lost due to this. I think that this would make much more impact if this was taken out and made into
83 its own separate manuscript. You could then extend to include details of how to make the corrections with

84 worked examples. This would help the reader understand how to make the corrections as well as why they
85 are important. It is up to the authors what to do with this section- I realise that you won't want to make it
86 into a separate manuscript, but I just wanted you to know that I think it would be much more widely read
87 if you did separate it. Perhaps you could consider adding a worked example as a small addition or refer to
88 an example from the literature?

89 We have kept this section in this paper. Why? We feel that we should not be drawn into the routine of
90 splitting papers up into smaller parts, it can be good for metrics, but generally doesn't make great papers.
91 This particular discussion of diseq is rather immature, certainly not the full story and any answers. It is
92 clearly important to point out, but how we tackle the uncertainty of activity ratios, and how we incorporate
93 these uncertainties into age uncertainties, is not clear. This in fact requires a community-led approach, for
94 example as the zircon and U-Th working groups have worked in the past. Thus, we feel this section is
95 merely paving the way for new investigation and appreciation of a problem. Could it be moved forward
96 within the paper?, yes it could come before other sections, but we do not feel 13500 words is a particularly
97 lengthy paper such that readers will not make it to the limitations section.

98 In addition, Noah McLean, a co-author, is writing up the equations behind integration of U-Pb and U-Th
99 data to incorporate activity ratio measurements – which hopefully will make it into the same special issue.
100 This paper will be more technical, and as such, we feel the broad discussion in the present paper is best
101 staying where it is.

102
103

104 2. Although the methods are clearly presented in the supplementary material, it is not clear whether the
105 primary data for any unpublished examples used by the authors is presented in the Supplementary
106 material? Perhaps the authors could include a data table for any unpublished data?

107 All unpublished data behind the presented isochrons in the image-guided and image-based sections are
108 now included in the supplementary files.

109
110

111 I have also made a few suggestions on the attached annotated manuscript.

112 We have made some of these suggestion in our shortening.

113

114 **LA-ICP-MS U-Pb carbonate geochronology: strategies, ~~and~~ progress,**
115 **~~and~~ and limitations with examples from application to fracture-fill calcite**

116
117
118 Nick M W Roberts¹, Kerstin Drost², Matthew S A Horstwood¹, Daniel J Condon¹, ~~David~~
119 Chew², Henrik Drake³, Antoni E Milodowski⁴, Noah M McLean⁵, Andrew J Smye⁶, Richard J
120 Walker⁷, Richard Haslam⁴, Keith Hodson⁸, Jonathan Imber⁹, Nicolas Beaudoin¹⁰, Jack K
121 Lee⁹
122

123 ¹Geochronology and Tracers Facility, British Geological Survey, Environmental Science
124 Centre, Nottingham, NG12 5GG, UK

125 ²Department of Geology, Trinity College Dublin, Dublin 2, Ireland

126 ³Department of Biology and Environmental Science, Linnaeus University, 39231 Kalmar,
127 Sweden

128 ⁴British Geological Survey, Environmental Science Centre, Nottingham, NG12 5GG, UK

129 ⁵Department of Geology, University of Kansas, Lawrence, KS 66045, USA

130 ⁶Department of Geosciences, Pennsylvania State University, University Park, PA 16802,
131 USA

132 ⁷School of Geography, Geology, and the Environment, University of Leicester, Leicester,
133 LE1 7RH, UK

134 ⁸Department of Earth and Space Sciences, University of Washington, Seattle, WA 98195,
135 USA

136 ⁹Department of Earth Sciences, Durham University, Science Labs, Durham, UK

137 ¹⁰Laboratoire des Fluides Complexes et leurs Réservoirs-IPRA, E2SUPPA, Total, CNRS,
138 Université de Pau et des Pays de l'Adour, UMR5150, Pau, France

139
140
141 Words: ca. 1350014434

142 Figures: 159

143 Tables: 0

144 References: 13540

145 Supplementary files: 2
146

147

148

Abstract

Laser Ablation Inductively Coupled Plasma Mass Spectrometry (LA-ICP-MS) U-Pb geochronology of carbonate minerals, calcite in particular, is rapidly gaining popularity as an absolute dating method. ~~The technique has proven useful for dating fracture-fill calcite, which provides a powerful record of palaeohydrology, and within certain constraints, can be used to bracket the timing of brittle fracture and fault development.~~ The high spatial resolution of LA-ICP-MS U-Pb carbonate geochronology ~~has~~ is ~~beneficial~~ over traditional Isotope Dilution methods, particularly for diagenetic and hydrothermal calcite, because uranium and lead are heterogeneously distributed on the sub-mm scale. At the same time, this can provide limitations to the method, as locating zones of radiogenic lead can be time-consuming and 'hit or miss'. Here, we present strategies for dating carbonates with in situ techniques, through imaging and petrographic techniques to data interpretation; ~~our; we focus on~~ examples are drawn from dating of fracture-filling calcite, but ~~most of our~~ discussion is relevant to all carbonate applications. ~~We demonstrate these strategies through a series of case studies.~~ We review several limitations to the method, including open system behaviour, variable initial lead compositions, and U-daughter disequilibrium. We also discuss two approaches to data collection: traditional spot analyses guided by petrographic and elemental imaging, and image-based dating that utilises LA-ICP-MS elemental and isotopic map data.

1. Introduction

Calcite (CaCO_3), along with other carbonate minerals (e.g. aragonite, dolomite, magnesite), forms in a wide variety of geological environments as both a primary and secondary mineral phase, including diagenetic, biogenic, igneous, metamorphic and hydrothermal environments. Calcite can incorporate uranium upon its formation, making it a potentially suitable chronometer for U-Pb and U-Th geochronology. Calcite geochronology therefore has the potential to provide direct timing constraints to a broad suite of geoscience applications. Calcite has been dated in the past by chemical dissolution and isotope dilution (ID) with measurement by either Thermal Ionisation Mass Spectrometry (TIMS) or Inductively Coupled Plasma Mass Spectrometry (ICP-MS) (e.g. Smith and Farquhar, 1989; DeWolf and Halliday, 1991; Brannon et al., 1996; Rasbury et al., 1997; Richards et al., 1998; Woodhead et al., 2006; Pickering et al., 2010), collectively referred to here simply as

182 Isotope Dilution (ID). More recently, there has been a proliferation in the use of laser
183 ablation (LA-) ICP-MS applied to calcite geochronology (Li et al., 2014; Coogan et al., 2016;
184 Roberts & Walker, 2016, Ring & Gerdes, 2016; Methner et al., 2016; Goodfellow et al.,
185 2017; Burisch et al., 2017, 2018; Drake et al., 2017, [2019, 2020](#); Hansman et al., 2017;
186 Hellwig et al., 2018; Godeau et al., 2017; Beaudoin et al., 2018; Drost et al., 2018;
187 Manganot et al., 2018; [Nicholson et al., 2020](#); Nuriel et al., 2017, 2019; Parrish et al., 2018;
188 Walter et al., 2018; [Yokoyama et al., 2018](#); Smeraglia et al., 2019; Holdsworth et al., 2019;
189 MacDonald et al., 2019; Scardia et al., 2019). Presently, we are not aware of successful
190 secondary ion mass spectrometry (SIMS) U-Pb dating of carbonate mineralisation, but this
191 presents an alternative microbeam method to LA-ICP-MS.

192
193 The first review of the possibilities for carbonate geochronology was published by Jahn &
194 Cuvellier (1984), and this was substantially updated by Rasbury & Cole (2009). The latter
195 provided up-to-date discussion on U-Pb isotope systematics in carbonates, particularly
196 regarding Pb-Pb and U-Pb isochron methods, as well as a review of the applications to
197 date. At that time, both marine- (e.g. limestone, dolomite) and meteoric-water sourced
198 carbonates (e.g. speleothems and tufas) had received the most attention, due to their often-
199 favourable uranium contents, and studies of hydrothermal carbonate were scarce (e.g.
200 Brannon et al., 1996; Grandia et al., 2000). U-Pb dating of speleothems has been further
201 reviewed by Woodhead et al. (2006 and 2012), ~~again,~~ focussing on data generated by ID,
202 [and more recently Woodhead and Petrus \(2020\) discuss the use of LA-ICP-MS for](#)
203 [speleothem dating.](#)

204
205 Now that microbeam (i.e. LA-ICP-MS and SIMS) U-Pb geochronology is proving to be a
206 useful method for a range of geoscience applications, it is pertinent to address what can be
207 achieved with the method, what the current limitations are, and where improvements can be
208 made in the future. We refer to LA-ICP-MS through the rest of this paper, but acknowledge
209 that nearly all of the points we cover are equally relevant to SIMS methods. The key benefit
210 to LA-ICP-MS dating is that its high spatial resolution can be used to relate U-Pb and other
211 geochemical analyses to imaged textures. This is critical for providing context to the
212 obtained dates. Carbonate materials are heterogeneous in composition elementally,
213 isotopically, and texturally. These factors can all lead to scatter in U-Pb data, and will often
214 hinder the ability to generate high precision (i.e. $<1\% 2\sigma$) U-Pb dates. In fact, after
215 propagation of all relevant uncertainties, final [LA-ICP-MS](#) U-Pb dates typically exceed 3%

216 precision (2σ). For this reason, LA-ICP-MS carbonate U-Pb geochronology is particularly
217 suited for applications in tectonics and crustal fluid-flow, but commonly less suited for
218 applications in stratigraphy and palaeoclimate.

219
220 Here we present a review of LA-ICP-MS U-Pb carbonate geochronology, focusing on its
221 benefits, ~~and application~~ and limitations. We pay, ~~with~~ particular attention to hydrothermal
222 and diagenetic ~~vein-filling~~ carbonates; these can constrain the ages of mineral systems,
223 crustal deformation and fluid-flow, and represent a significant growth area for this method.
224 Using several case studies, we highlight the utility of image-guided analysis, where various
225 imaging techniques provide critical context for interpreting U-Pb data. We also provide case
226 studies for an age-mapping technique that is an alternative to traditional static spot ablation,
227 and can be used in combination with sample imagery to generate U-Pb age data. Finally,
228 we highlight issues surrounding initial lead compositions, initial disequilibrium in the U-Pb
229 system and open-system behaviour.

230

231 2. LA vs ID strategies

232 Geochronology by ID provides the most accurate assessment of the U-Pb age of a sample,
233 through use of ~~using~~ calibrated isotopic tracer solutions, but it is time-consuming and
234 requires a clean laboratory facility for sample dissolution and column chemistry. The spatial
235 resolution of ID is typically much lower than that offered by microbeam techniques, although
236 resolution can be increased by using a high precision micro-drill for direct sampling. A major
237 limiting factor is that carbonate materials typically have very low U concentrations (ca. 10
238 ppb to 10 ppm U) compared with traditional U-bearing accessory minerals (e.g., often >100
239 ppm U in zircon). This means that samples with low Pb concentrations yield higher
240 blank/sample ratios, hindering the accuracy and precision of the resulting data, and
241 secondly that the ~~1)~~ comparatively large volumes of material ~~are~~ needed for ID analyses
242 resulting in an 'averaging' effect and reduction of spread in U/Pb space, ~~and 2) samples~~
243 ~~with lower Pb concentrations yield higher blank/sample ratios, hindering the accuracy and~~
244 ~~precision of the resulting data.~~

245

246 LA-ICP-MS is a much quicker technique than ID, and therefore less expensive per analysis.
247 Several samples can be run in a single day, meaning the technique is ideal for screening of
248 large sample sets to find the most suitable material. The effect of blanks sourced from

249 [dissolution and chemical purification](#) is negated, and very low (<100 ppb) Pb contents can
250 be analysed. However, LA-ICPMS is generally less precise analytically compared to ID
251 approaches. Another major limitation is the need to normalise to a matrix-matched
252 reference material. This means that the uncertainty of the reference material becomes a
253 limiting uncertainty, and matrix effects between materials of different composition will
254 generate scatter and/or bias in the U-Pb dates that are difficult to correct for.

255

256 The biggest benefit of LA-ICP-MS comes from the spatial resolution (less than ca. 100 μm)
257 at which data can be obtained, particularly given the length scales of uranium concentration
258 heterogeneity in carbonate. We find that for hydrothermal and diagenetic calcite in
259 particular, uranium is heterogeneously distributed across veins and vein phases, and within
260 individual crystals (see Figure 1). Uranium concentration heterogeneity typically spans 1 to
261 3 orders of magnitude, with the length-scale of this variation being commonly much less
262 than 1 mm. Targeting of high U domains is therefore difficult without a high spatial-
263 resolution sampling method. Intracrystalline uranium distributions within calcite define
264 several patterns (see Figure 1): concentrated along cleavage planes (**Aa**), growth-zone
265 controlled (**cC**, **dD** and **fF**), concentrated towards grain rims (areas of **Bb** and **eE**), and with
266 apparent disorder (areas of **bB** and **eE**). Laser ablation has the spatial resolution capable of
267 targeting such elemental (and isotopic) zonation, making it easier to avoid distinguishable
268 alteration zones and inclusions at the 10-100 μm scale.

269

270

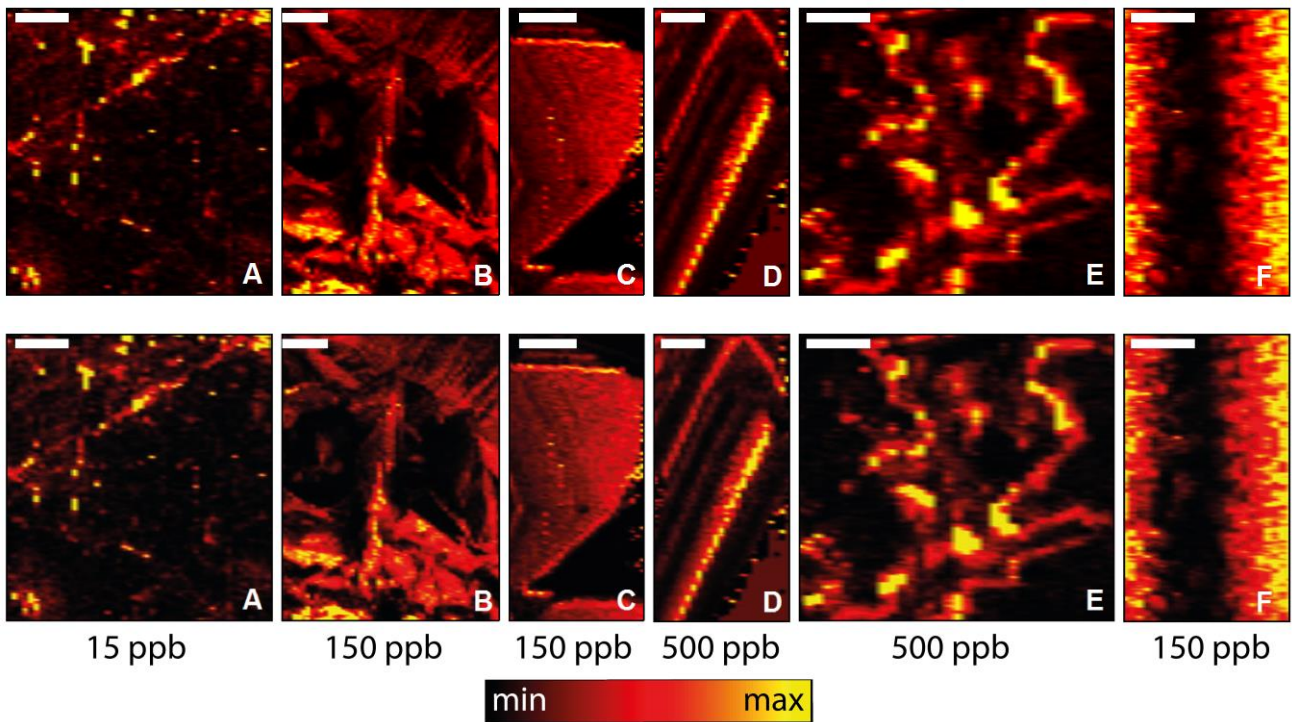


Figure 1. Maps of uranium in vein-filling calcite from a range of geological settings showing varying styles of distribution, see text for explanation.

Maximum concentration (yellow) is shown below each map; (brighter = higher concentration). Maps were generated using LA-ICP-MS trace element analyses and the Iolite data reduction software. Scale bars are 1 mm.

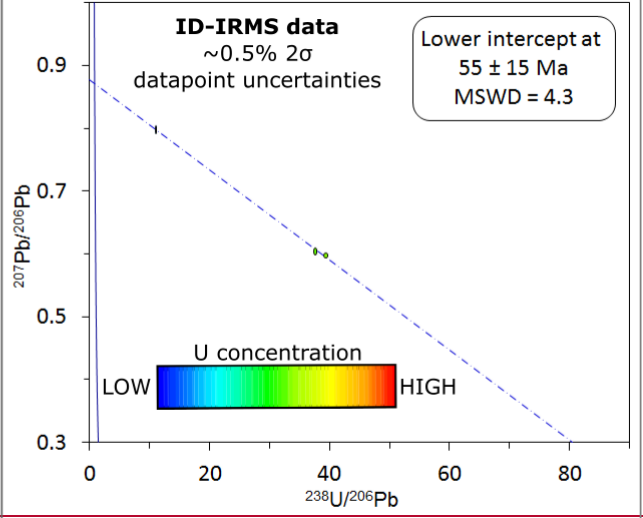
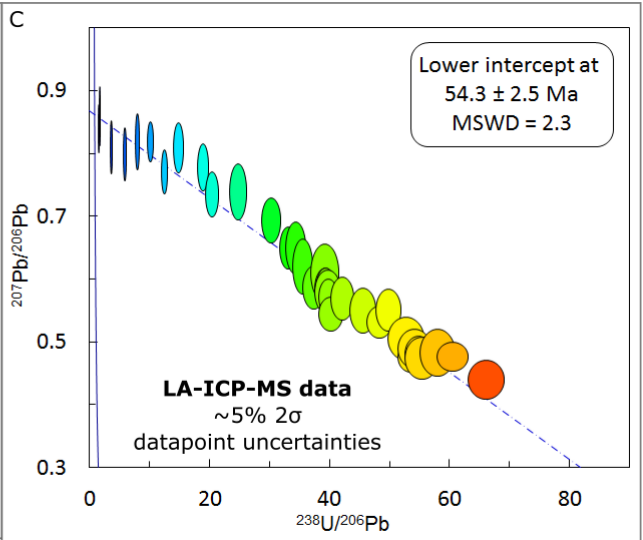
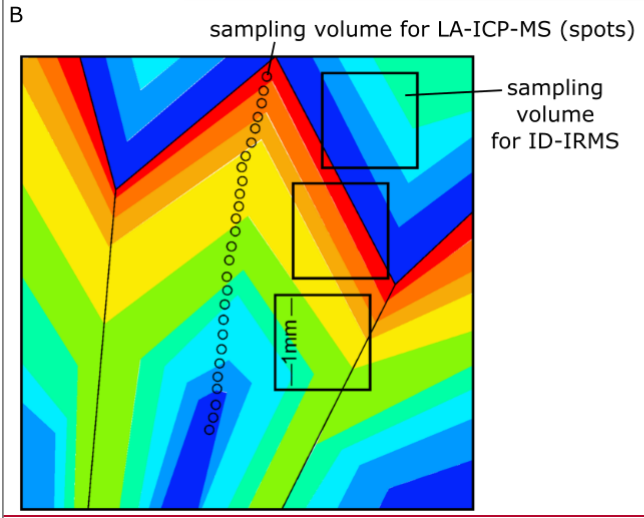
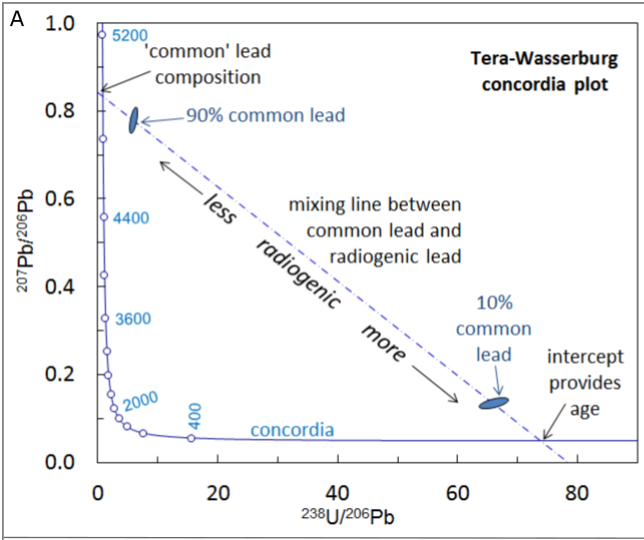
~~For minerals such as zircon, U-Pb ID-TIMS is considered the gold standard of geochronological techniques (Renne et al., 1998). It offers significantly greater accuracy than microbeam techniques by virtue of the use of gravimetrically quantified isotopic spikes, and generally higher detection efficiencies. ID-TIMS does, however, consume greater amounts of material. With ID methods, ages are calculated by absolute determination of the number of atoms of each isotope in the sample material. In contrast, microbeam techniques are relative methods, using ratio normalisation against reference minerals of known composition (generally determined by ID methods).~~

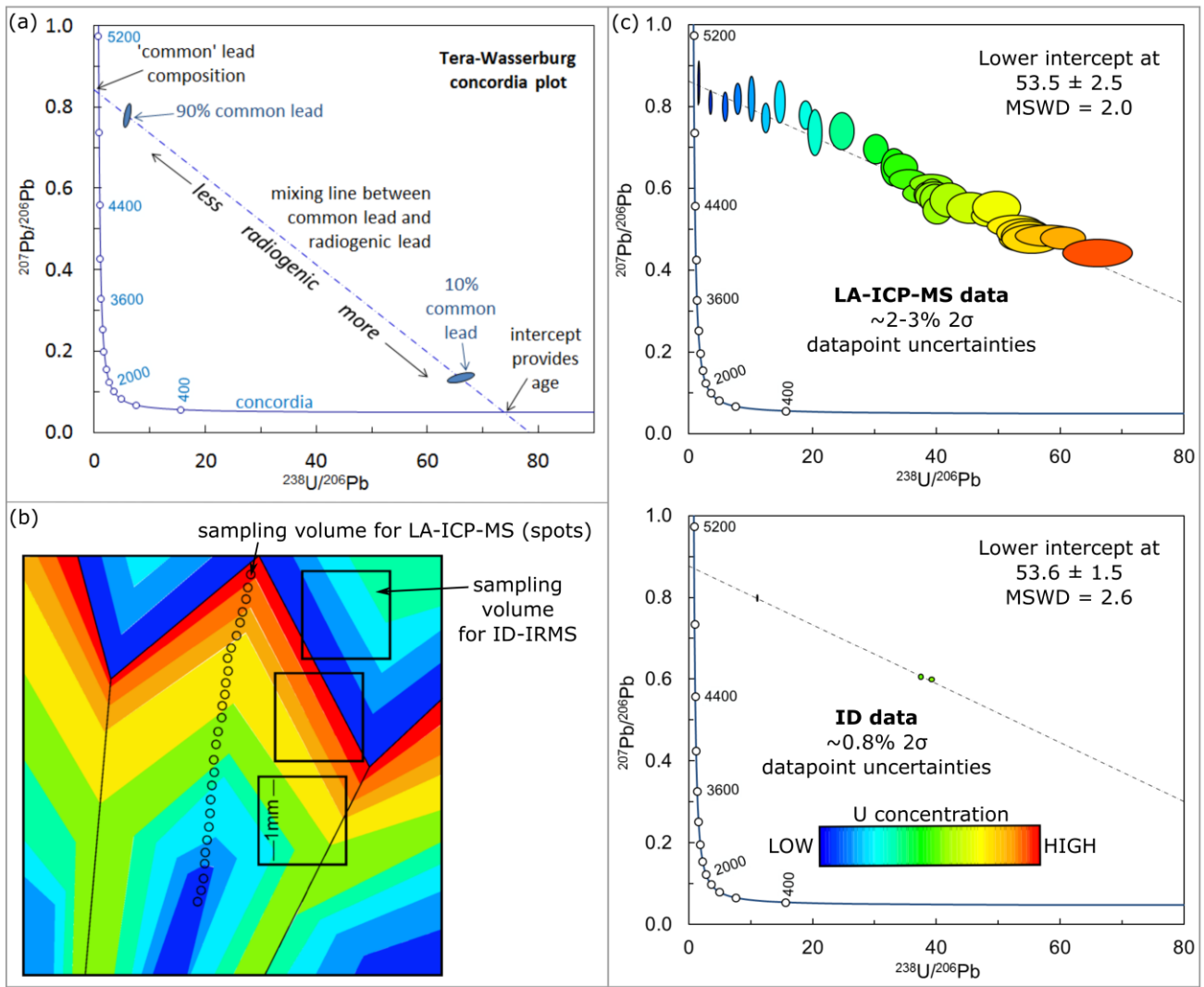
For common-lead bearing minerals such as calcite, the extreme range in parent/daughter ratios encountered (quoted here as ^{238}U divided by initial lead as ^{204}Pb ; a ratio known as μ),

292 means that ID does not always lead to an improvement in precision on the regressed age.
293 This is demonstrated by the schematic model in Figure 2. Sampling for ID provides an
294 average of elemental and isotopic zonation within the analytical volume, perhaps $>1 \text{ mm}^3$,
295 depending on the concentration of U and Pb within the crystal(s). The resulting data should
296 be precise (depending on the sample/blank ratios), but may potentially have a small spread
297 in parent/daughter ratios (i.e. $^{238}\text{U}/^{206}\text{Pb}$) due to the averaging effect during sampling. In
298 contrast, LA sampling has the potential to target and utilise such zonation, better resolving
299 end-member μ compositions, and resulting in analyses with a greater spread in $^{238}\text{U}/^{206}\text{Pb}$
300 ratios. This potentially improves the resolving power of a regression of the measured
301 isotopic ratios allowing definition of, ideally, the high- μ (radiogenic lead) and low- μ (initial
302 lead) end-member compositions of the data array (see Figure 2). Along with the generally
303 high- n datasets generated by the LA-ICP-MS approach, these well-constrained regressions
304 can result in similar ~~or even greater~~ precision for $^{206}\text{Pb}/^{238}\text{U}$ ages ~~determinations~~ than those
305 using ID data alone. ~~However, a caveat to this, is that lower precision data points can mask~~
306 ~~true geological heterogeneity.~~

307

308





310

311

312

313

314

315

316

317

318

319

320

321

322

Figure 2. (Aa) Example Tera-Wasserburg Concordia plot demonstrating the functionality of this plot for common-lead bearing U-Pb data. (bB) Schematic model of a calcite crystal with uranium zonation indicated by the colour-scale. Typical relative sample size for low U (<1 ppm) ID shown by the black squares, and LA-ICP-MS by the circles. (cC) Resultant U-Pb data in Tera-Wasserburg concordia assuming constant Pb concentration across the sample, **and varying U concentration**, for LA-ICP-MS ~~sampling and analyses~~ versus 'bulk' sampling and ID analyses, as represented by the sampling in B. The ~~uncertainties~~ **uncertainties** on the datapoints ~~are~~ **are** 24-36% (2s) for LA-ICP-MS and ~0.85-0.7% for ID.

323 When calculating an age and uncertainty from a regression/isochron, it is assumed that: 1)
324 the dataset describes a single age population whose variability or scatter is derived solely
325 from the analytical process; 2) each analysis represents a closed system, and 3) all
326 analyses share the same initial Pb isotope composition. When these assumptions are
327 satisfied, the MSWD should be about 1 (Mean Squared Weighted Deviation; Wendt and
328 Carl, 1991). LA-ICP-MS data-points generally have a lower precision than those derived by
329 ID. These lower precision data-points can mask scatter that exists within the level of the
330 data-point uncertainties. This caveat must be considered when interpreting regressed data
331 (or weighted means).

332
333 **3.**—In other words, age interpretations rely on isochron assumptions that can only be
334 resolved at the level of the data-point uncertainties. More precise ID data, therefore, have
335 better resolution of scatter and better constrain the likelihood that a sample does not
336 comprise a single population. However, sampling for ID can also contribute to this scatter
337 by analysing larger amounts of material, with a greater chance of including altered zones or
338 zones from different generations. ~~A combination of ID and image-guided LA methods can
339 therefore better elucidate the likely variability in any particular sample.~~ For applications
340 where the best possible precision is needed (e.g. for stratigraphic constraints or
341 ~~characterisation~~ characterisation of potential U-Pb carbonate reference materials), a
342 workflow involving both LA-ICP-MS dating followed by ID on the most favourable material is
343 likely to be the most effective. For applications where the required precision is on the order
344 of several percent, image-guided LA-ICP-MS without ID is suitable.

345
346 **4.**

347 **5.3. Identifying suitable carbonate material for dating**

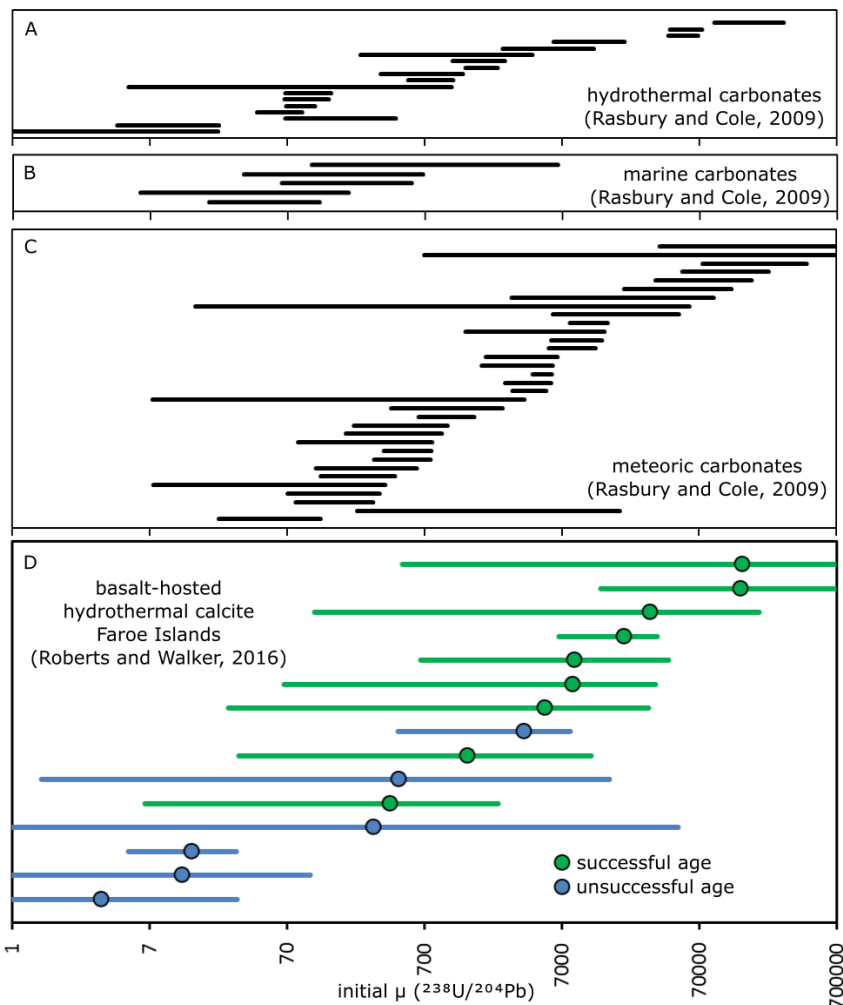
348 **5.1.3.1. μ ($^{238}\text{U}/^{204}\text{Pb}$) in carbonate**

349 An 'ideal' U-Pb chronometer requires incorporation of U (the parent isotopes ^{238}U and ^{235}U
350 which decay to ^{206}Pb and ^{207}Pb respectively), and zero or low concentrations of initial (or
351 'common') Pb during its formation; this is typically expressed as the ratio of parent uranium
352 to initial Pb - $^{238}\text{U}/^{204}\text{Pb}$, or μ . In addition, both the parent and daughter isotopes ideally
353 remain a closed system from formation until present-day. Many chronometers lack these
354 ideal criteria but still provide successful materials for dating: the subset of 'common-lead
355 bearing chronometers' comprise small to large initial lead concentrations that are of uniform

356 composition (e.g. titanite, apatite). The ideal criteria are generally rare in carbonates, but
357 many carbonate materials from a range of different geological environments are successful
358 common-lead bearing chronometers.

359
360 Rasbury and Cole (2009) showed that carbonates of meteoric origin have the highest μ
361 values, and hydrothermal varieties the lowest, with marine varieties in the middle ([see](#)
362 [Supplementary Figure S1](#)) ~~Figure. 3A-C~~). However, the recent literature ~~ee~~ on calcite dating
363 demonstrates that with careful characterisation and sampling, high μ domains can be found
364 in a range of hydrothermal and diagenetic calcite. ~~As an example, we plot the range of μ~~
365 ~~values recorded in very low-U (<200 ppb) and low-Pb (<20 ppb) calcite taken from basalt-~~
366 ~~hosted fractures in the Faroe Islands (Figure. 3D). The range of mean μ values across the~~
367 ~~fifteen samples is very large (ca. 100 to 100,000), and the range within each sample is also~~
368 ~~commonly two to four orders of magnitude. Of the samples providing successful U-Pb~~
369 ~~isochron ages (Roberts & Walker, 2016), μ values extend to as low as ~2000.~~

370



371

372 ~~Figure 3. A-C) Compilation of μ ($^{238}\text{U}/^{204}\text{Pb}$) values taken from Rasbury & Cole (2009).~~
373 ~~Each bar is the range exhibited by an individual sample. These data were acquired using~~
374 ~~sampling by physical separation, i.e. a dental drill. D) Compilation of μ values from basalt-~~
375 ~~hosted vein-filling calcite in the Faroe Islands to highlight the range within crystals and~~
376 ~~across a single region; each datapoint represents the median, and the bar represents the~~
377 ~~range. These data represent laser ablation sampling.~~

378
379

380 The amount of U needed to generate an age is dependent on two factors: (1) the age of the
381 material and (2) the initial μ ratio of the material. The younger a sample is, the less time
382 there is for the growth of radiogenic daughter Pb from parent U. With a higher μ , the ratio of
383 measured radiogenic Pb to common (initial) Pb will be higher, giving greater confidence and
384 (in general) precision and accuracy to the resulting age determination.

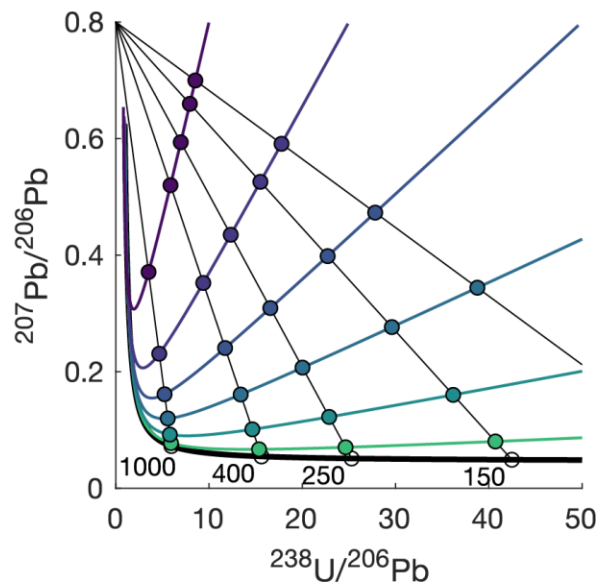
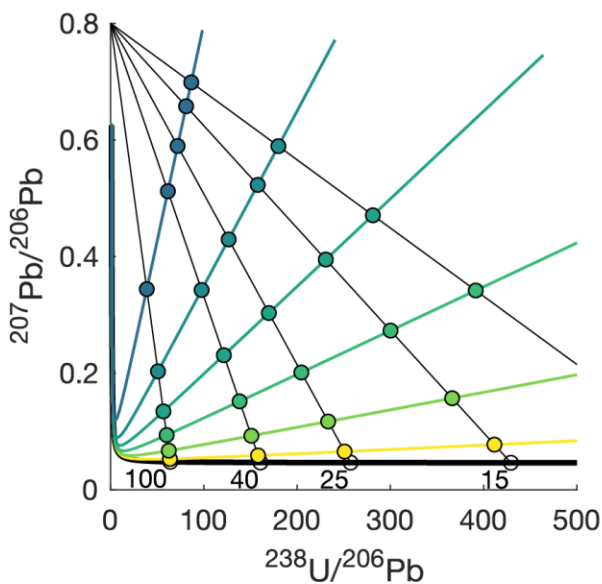
385

386 The effect of these factors is shown in Figure 43. Two Tera-Wasserburg plots are shown,
387 with isochrons for samples of different ages (100 to 10 Ma on the left, 1000 to 100 Ma on
388 the right). The most accurate and precise age determinations, i.e. those that can be
389 interpreted with most confidence, are generated when the sample comprises abundant
390 radiogenic lead, i.e. gets close to the lower part of the concordia curve where the
391 regression intercepts. Each plot shows regressions for individual samples between a
392 common-lead composition (~ 0.8) and a radiogenic end-member (with the age labelled). The
393 colour-coded points along each regression reflect the amount of radiogenic lead that will be
394 created by decay of ^{238}U , based upon the given μ value. For example, utilising the left plot,
395 a sample of 15 Ma, with a μ of 10,000, will have a measured $^{207}\text{Pb}/^{206}\text{Pb}$ of ~ 0.4 , equalling
396 about a 50:50 ratio between radiogenic and initial lead. To get a near concordant
397 measurement of this sample would require a μ value of over 200,000. These plots
398 demonstrate that when simply regarding the abundance of radiogenic lead, how-older
399 samples are more amenable to dating than those young in age, at least when regarding the
400 abundance of radiogenic lead. The preservation of a closed isotopic system over long time
401 periods is what makes dating old samples (i.e. Precambrian materials) potentially difficult.

402
403

$\mu = (^{238}\text{U}/^{204}\text{Pb})_i =$		
200000	20000	5000
50000	10000	2000

$\mu = (^{238}\text{U}/^{204}\text{Pb})_i =$		
20000	2000	500
5000	1000	200



404

405

406

Figure 3-4. Tera-Wasserburg plots showing modelled regressions for samples of different age. Colour-coded spots relate to the measured isotope composition a sample would have at a given μ value (legend above). Ages of each regression in Ma are labelled adjacent to the lower intercept with concordia.

410

411

412 When absent of concordant analyses, both high μ and a significant spread in initial μ values
 413 are required to generate the most robust ages, as these will pin the isochron at the
 414 radiogenic end-member with greater confidence. Some calcite exhibits sufficiently high μ to
 415 generate concordant data (e.g. Richards et al., 1998; Roberts & Walker, 2016; Nuriel et al.,
 416 2017); these ages do not heavily rely on the composition of the common lead end-
 417 member, & but such ~~robust~~ ages are rare with a material that so commonly exhibits high
 418 initial lead abundances. Ages can be derived from isochrons with low amounts of
 419 radiogenic lead, i.e. those with low μ . Such isochrons can be regressed to provide lower
 420 intercept ages, but the confidence in these ages is subject to having well-behaved data
 421 conforming to a single population, requiring precise data-point uncertainties (e.g. Figure
 422 45Gg). Such low μ isochrons can potentially give imprecise and even inaccurate lower
 423 intercept ages if the material is very young, and thus confirmation through multiple samples
 424 and/or alternative age constraints are favoured.

425

426 In Figure 54, we present a selection of 'real-world' data to highlight the potential complexity
427 of carbonate U-Pb data. These data from natural samples broadly range from undesirable
428 to most desirable from aA to h, with the following notable characteristics:

429 (aA) Dominated by common lead with large data-point uncertainties (due to low count-
430 rates) that hamper the distinction between open-system behaviour and radiogenic ingrowth
431 of lead.

432 (bB) All analyses are ca. 100% common lead, with high count-rates providing a precise
433 measurement of the composition of this common lead.

434 (cC) Mixed and scattered data that do not fall on a single linear isochron. This is likely
435 caused by open system behaviour, potentially involving both addition and subtraction of
436 parent ^{238}U .

437 (dD) Majority of data define a linear array with a large spread in U/Pb ratios. Some other
438 analyses fall on a horizontal array, suggesting they experienced open-system behaviour
439 (e.g., local ^{238}U mobility).

440 (eE) Data form an apparent single linear array, but large uncertainties (due to low count-
441 rates) may obscure mixed ages or minor open-system behaviour.

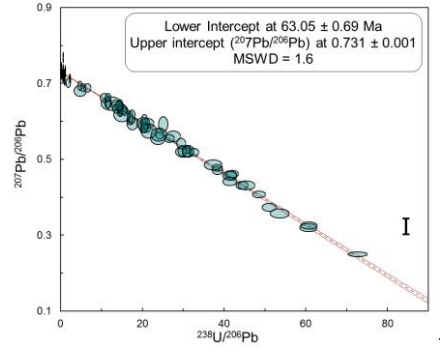
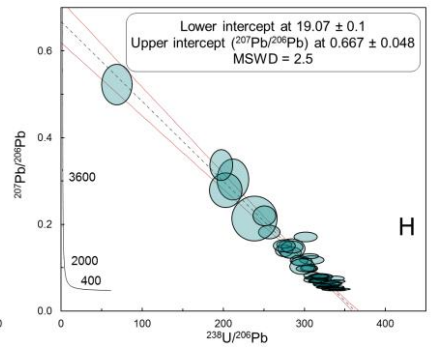
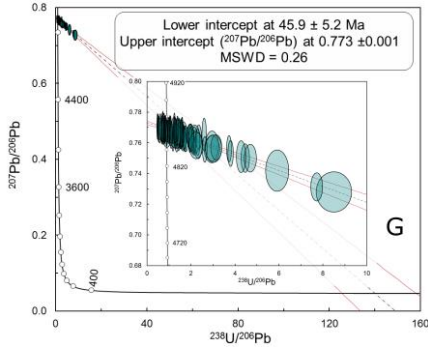
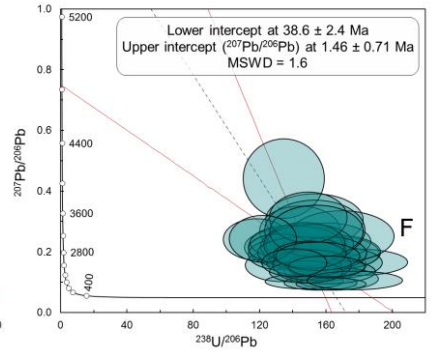
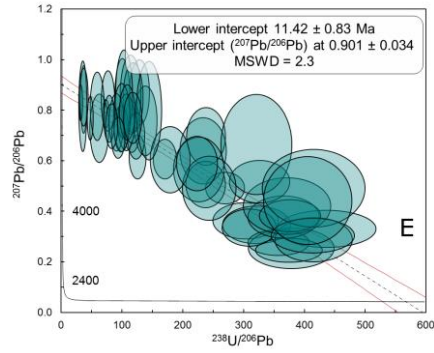
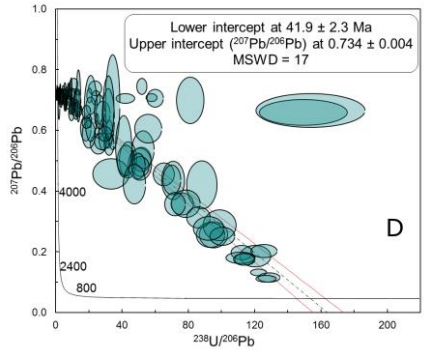
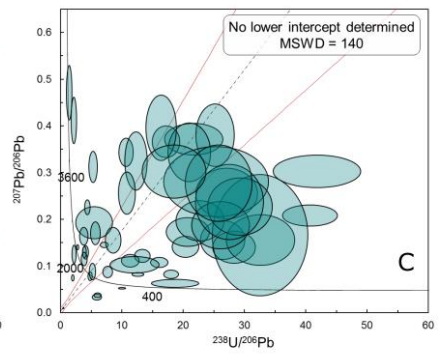
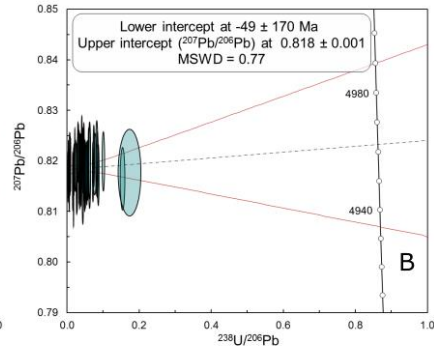
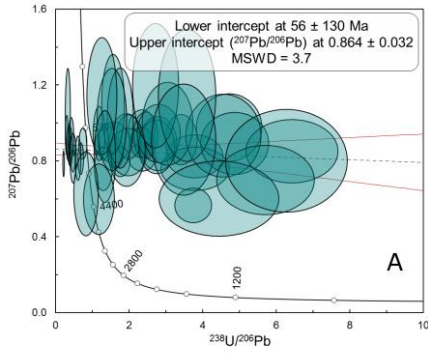
442 (fF) Dominated by relatively radiogenic isotopic compositions, but with large data point
443 uncertainties due to low count-rates. The narrow range in μ leads to a large age uncertainty
444 from extrapolating to the lower concordia intercept. The age uncertainty would be improved
445 with a common lead composition estimated from contemporaneous low- μ samples of the
446 same suite.

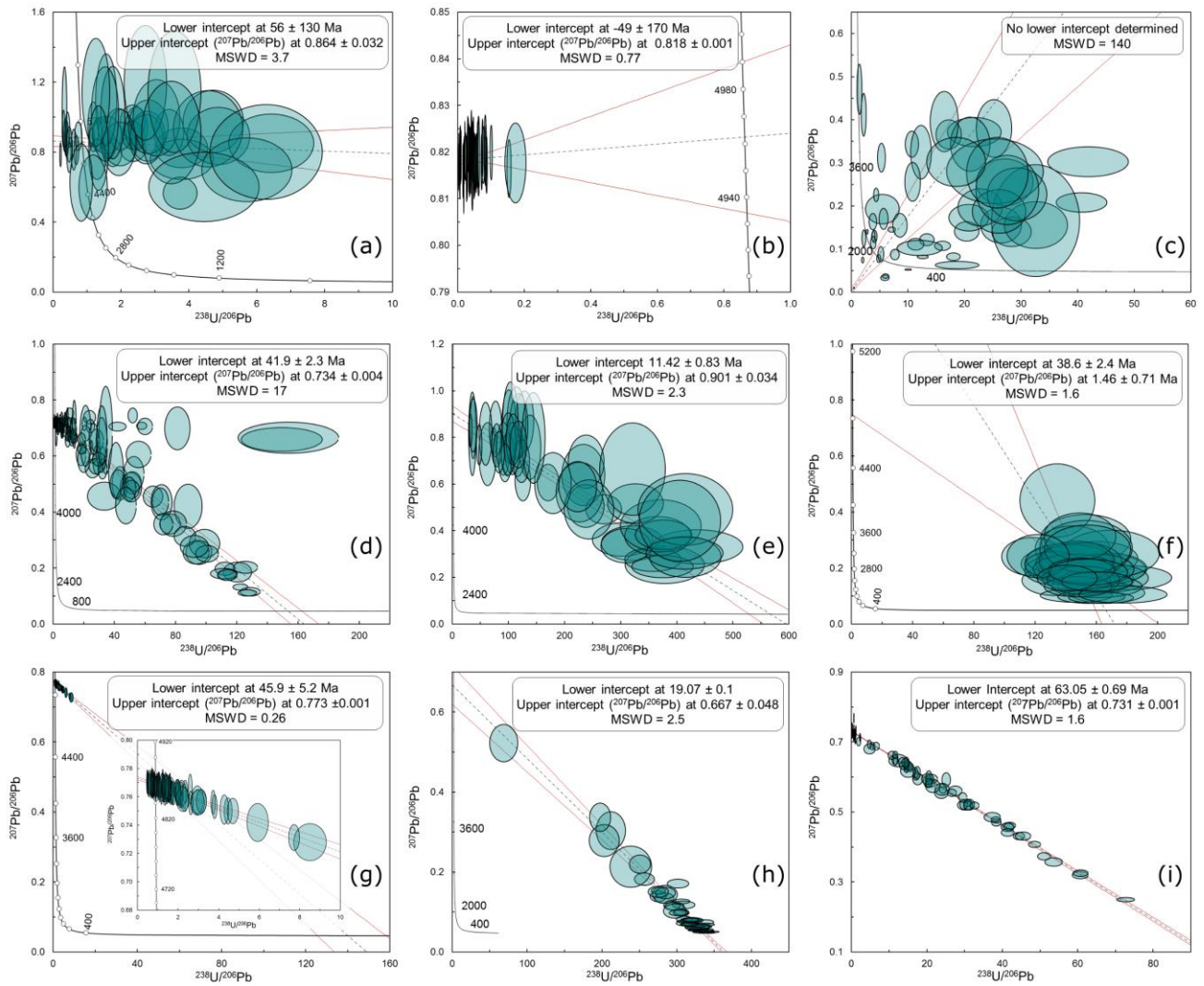
447 (gG) A short isochron, termed a 'small scale isochron' by (see Ring & Gerdes (,2016).
448 There are no radiogenic isotopic compositions to anchor the extrapolation to a lower
449 intercept concordia date, but a tight data array yields a realistic intercept age.

450 (hH) Dominated by radiogenic isotopic compositions, and the spread in the array provides a
451 precise lower intercept date; small data-point uncertainties improve ability to identify
452 potential outliers.

453 (iI) A precise regression due to well-behaved closed system behaviour, high count rates
454 giving small uncertainties, and a large spread in U/Pb ratios providing a precise estimate of
455 both the age and the common lead isotopic composition.

456





458

459

460 *Figure 54. Tera-Wasserburg concordia plots of natural carbonate samples from a variety of*
 461 *settings, with no data rejection. Lower intercept dates are quoted without propagation of*
 462 *systematic uncertainties. See text for explanation.*

463

464

465 **5.2.3.2. U and Pb contents in carbonate**

466 At present, there is a lack of predictive criteria that can be used in the field or in the
 467 laboratory to screen samples prior to analysis for high μ domains. Radionuclide
 468 incorporation in calcite is not well understood despite several decades of interest, primarily
 469 driven by the field of nuclear waste storage and characterisation (e.g. Langmuir, 1978;
 470 Milton & Brown, 1987; Sturchio et al., 1998; Reeder et al., 2000, 2001; Kelly et al., 2003;
 471 Weremeichik et al., 2017; Drake et al., 2018). This is because trace element incorporation
 472 in calcite does not rely on thermodynamically determined partition coefficients, but by a

473 large number of phenomenological variables, including: trace element availability, calcite
474 growth rate, temperature, pH, Eh, pCO₂ and the Ca²⁺:CO₃²⁻ ratio in solution, ionic size, and
475 U complexation. Furthermore, different trace elements can be preferentially incorporated
476 into structurally different growth steps and faces of growing calcite crystals (Paquette and
477 Reeder, 1995; Reeder, 1996).

478
479 Rasbury and Cole (2009) provided a geochronology-focused review of U and Pb in calcite,
480 and we note the following salient features: 1) Pb is both particle reactive and relatively
481 insoluble; 2) Pb is found at very low levels in most fluids (ppt-ppb), providing high Ca/Pb
482 ratios; 3) Pb can substitute for Ca in the crystal lattice, although the Pb cation is larger –
483 ionic radii of Ca²⁺ and Pb²⁺ in six-fold coordination are 114 and 133 pm, respectively; 4) U
484 exists in multiple oxidation states, and its solubility is strongly affected by Eh and pH; and 5)
485 both U(VI) and U(IV) states have been found in calcite, but not with both states together in
486 the same sample with the latter being interpreted as the most likely and most stable form.

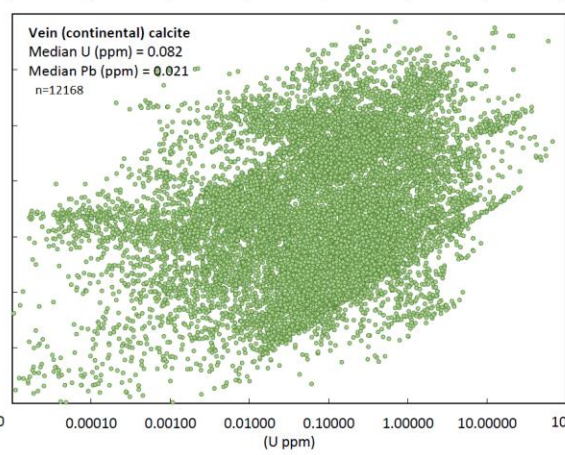
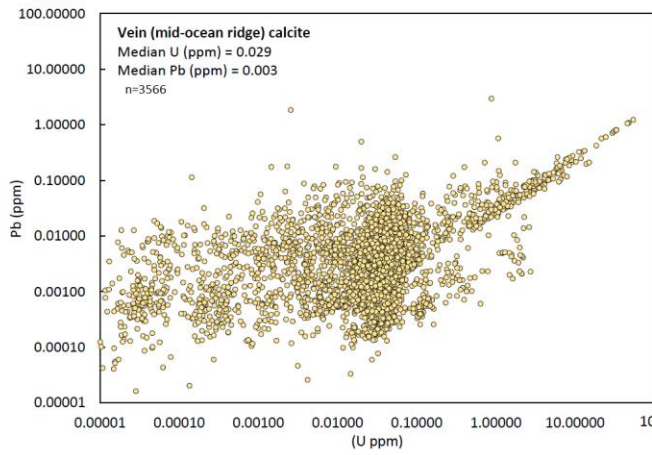
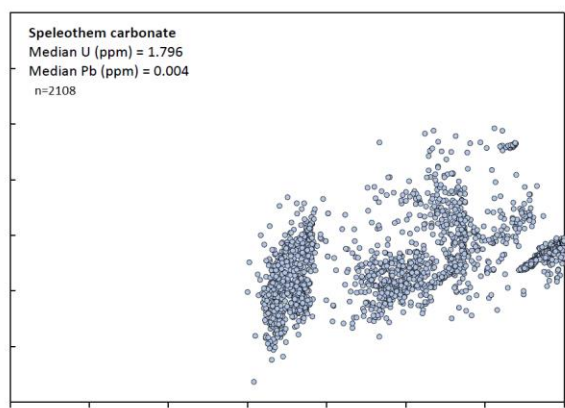
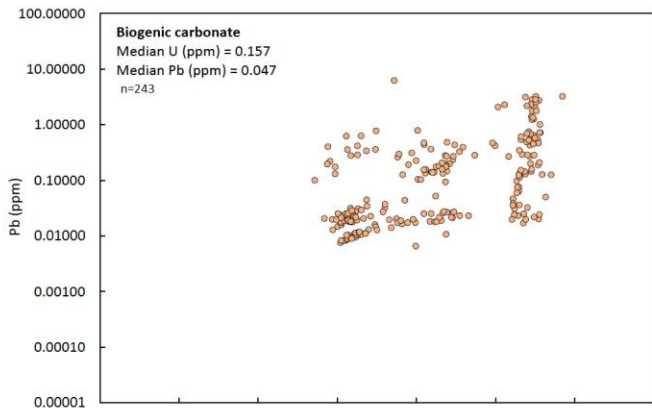
487
488 Points 4 and 5 above are important for understanding why and when uranium is
489 incorporated into calcite, and whether remobilisation is likely. Sturchio et al. (1998), using a
490 combination of X-ray absorption spectroscopy and X-ray microprobe fluorescence,
491 demonstrated that the uranium in a sample of spar calcite was in the form of U(IV), and that
492 U(VI) was less likely based on size and ionic structure (ionic radii of U(IV) and U(VI) in six-
493 fold coordination are 103 and 93 pm, respectively). Given that U(IV) is less mobile than
494 U(VI), this study provided important support for U-daughter geochronology. Kelly et al.
495 (2003) however, found that U(VI) as uranyl (UO₂²⁺) was the dominant species in a natural
496 sample of vein calcite, which they considered to be more representative of typical low-U
497 material than the Sturchio sample. Drake et al. (2018) found much higher concentrations of
498 uranium in calcite precipitated from deep anoxic groundwater than experimental
499 determinations that were performed in oxic conditions, and interpreted this high uranium
500 uptake as due to incorporation of U(IV) and thus that the partition coefficient for U(IV) in
501 these environmental conditions is orders of magnitude larger than for U(VI). It is evident
502 that more data from natural carbonates in different settings are needed to more fully
503 understand the controls on U and Pb incorporation.

504
505 We have compiled uranium and lead concentration data from carbonates analysed in the
506 BGS laboratory over several years (Figure 56). From our data, we see that median U and

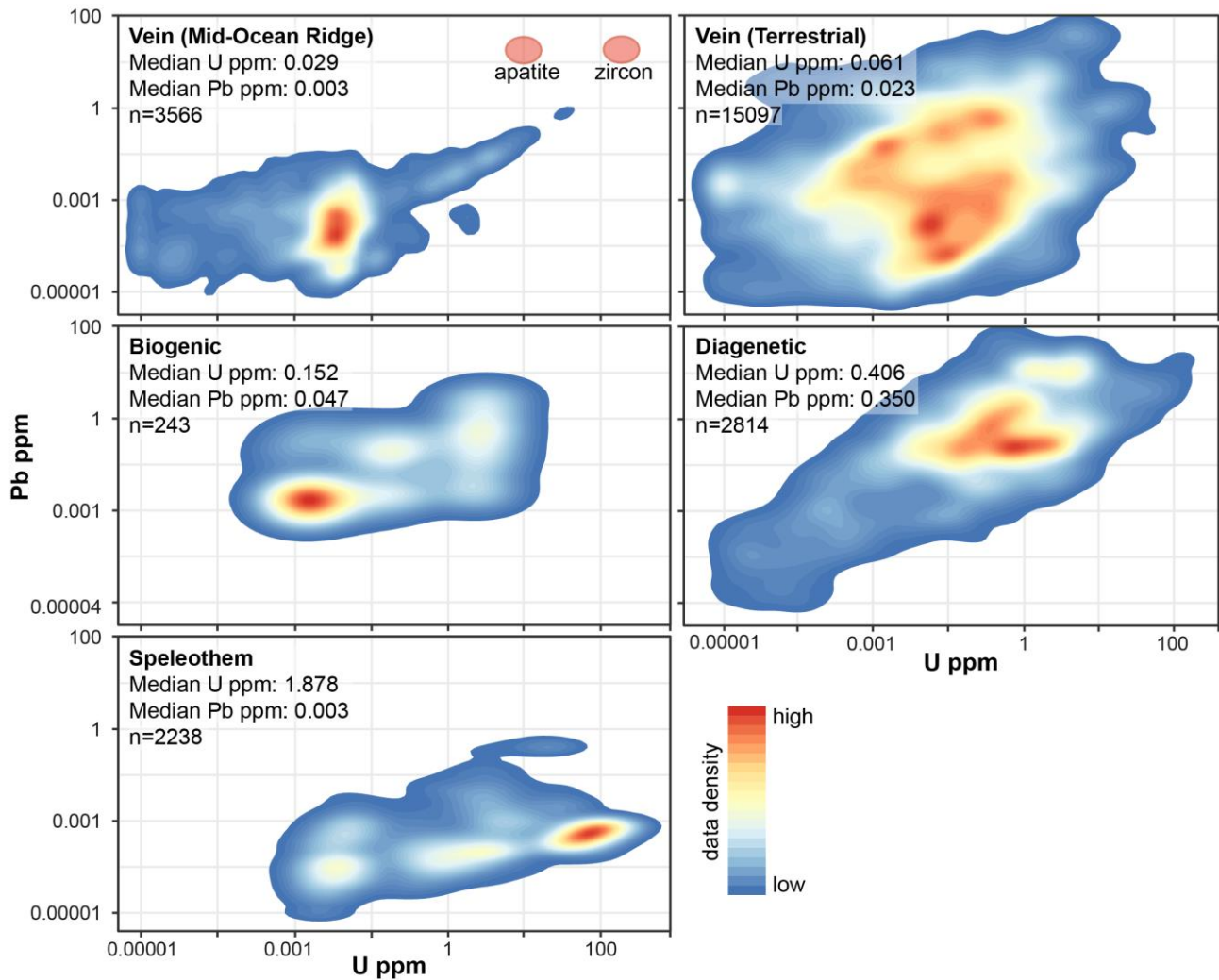
507 ~~/Pb_{total} concentrations are 1.9 and 0.003 ppm, respectively. Diagenetic carbonate has the~~
508 ~~second highest median uranium content (0.4 ppm), but also has high Pb content (0.35~~
509 ~~ppm). Veins in both terrestrial and Mid-Ocean Ridge settings have low U and Pb contents,~~
510 ~~with median values well below 100 ppb for both. Biogenic samples, although a smaller~~
511 ~~dataset, have low contents of U and Pb, generally lower than diagenetic material. ratios for~~
512 ~~speleothems are ~500, whereas median values for Mid-Ocean Ridge (MOR) and~~
513 ~~continental vein calcite are 8.2 and 2.6, respectively. Note that this compilation~~
514 ~~presents these are~~ total Pb contents, and includes radiogenic Pb as well as initial Pb, ~~which~~
515 ~~causes the short linear trends that represent individual samples. The S~~ samples in Figure 56
516 are mostly younger than 200 Ma, or < 4 Ma for the speleothems. The concentration data
517 and U/Pb ratios demonstrate that speleothems in general are much more amenable to U-
518 Pb geochronology, which is why they have been the main focus for this method until the
519 last few years. Dating ~~diagenetic and~~ vein-fill calcite, with more variable and lower contents
520 of U, and higher contents of Pb, has ~~ave~~ a lower chance of success than speleothems
521 (although it should be noted that the speleothems in general have already been visually
522 pre-screened during sampling).

523

524



525



526

527 *Figure 65. Uranium and total lead contents of various carbonate materials, plotted as 2D*
 528 *Kernel Density Estimates, based on a compilation of laser ablation spot data from the*
 529 *British Geological Survey lab over several years. A) Compilation of biogenic carbonates,*
 530 *mostly from corals; B) Speleothem carbonates; C) Veins hosted within mid-ocean ridge*
 531 *oceanic crust; and D) veins hosted within a range of lithologies Median values for high and*
 532 *low common-lead bearing U-Pb geochronometers, apatite and zircon, are shown for*
 533 *comparison. from the upper continental crust, from both outcrop and borehole samples.*

534

535

536 Ideally, a predictive framework could be constructed to aid field sampling and laboratory-
 537 based sub-sampling of carbonate material for geochronological analyses. However, given
 538 the large number of variables controlling U and Pb in carbonate, it is unlikely that such a
 539 tool can be developed without measuring a large number of parameters in the
 540 mineralising/diagenetic system. Relevant information might include the redox history of the

541 system. For example, oxidising fluids may mobilise U as U(VI), which is soluble in hydrous
542 fluids, leading to U loss during fluid-mineral interaction. Conversely, U may undergo much
543 higher precipitation into the mineral phase at redox fronts representing reducing conditions,
544 since reduced U(IV) has lower solubility. Other pertinent information for predicting success
545 includes the nature of the host rock and the source of the fluids. For example, if the
546 mineralising fluids transmit through Pb-rich units, then an undesirable enrichment in the
547 fluid Pb/Ca ~~may potentially would~~ take place, leading to lower initial $^{238}\text{U}/^{204}\text{Pb}$.

548
549 The complex nature of trace element uptake, including Pb and U, in carbonate
550 mineralisation is exemplified by recent studies in hydrothermal settings. Fracture
551 mineralisation in the crystalline basement of southern Sweden has been investigated
552 extensively to evaluate potential geological nuclear waste repository facilities. Several
553 studies have shown that most trace element concentrations vary over an order of
554 magnitude within calcite samples (at the thin section scale), and up to several orders of
555 magnitude across individual fractures (Drake et al., 2012, 2014; Maskenskaya et al., 2014;
556 Milodowski et al., 2018). These authors suggest that: 1) trace element chemistry does not
557 trace the source rock of the metals; 2) the co-variation of most trace elements implies
558 changing metal/Ca ratios in the fracture waters; and 3) in-situ factors affect trace element
559 incorporation, such as microbial activity, metal speciation, crystal habit, water type and co-
560 precipitation of other phases such as barite and pyrite.- Our own experience of vein-filling
561 fractures matches these previous studies, as shown for example by the basalt-hosted
562 calcite in the Faroe Islands (see Figure 97).

564 **6.4. Sample screening, imaging and petrography**

565 As discussed above, it is difficult to predict which carbonate samples are most suitable for
566 U-Pb geochronology. We therefore utilise several methods to screen material, with the aim
567 of limiting the time wasted on unsuitable samples, improving the quality of data that is
568 collected, and enhancing the overall efficacy of LA-ICP-MS U-Pb carbonate geochronology.
569 The purpose of sample imaging is two-fold: it provides important spatial characterisation of
570 U and Pb within the sample and also provides the petrographic and compositional context
571 to assess mineral growth mechanisms and alteration textures that are critical for linking
572 dates to processes.

573

6.1.4.1. Non-destructive techniques

A range of non-destructive imaging techniques ~~is~~are available for sample imaging (see Figure 76), including optical microscopy, cathodoluminescence (CL), back-scattered electron imaging (BSE), charge-contrast imaging (CCI), and etch-track or digital autoradiography techniques. Both reflected light and transmitted light are excellent tools for characterising carbonate minerals; the latter being the mainstay of all petrographic analysis. Features which are usefully distinguished in transmitted light include twinning planes, fluid inclusions and grain boundaries (see Figure 6e). Reflected light is a particularly useful technique for characterising carbonates in polished blocks, when thin sections are not available, and also highlights crystal boundaries, and contrasts between different mineral faces (see Figure 6a and 6b).

~~The latter, in particular storage-phosphor imaging plate autoradiography and direct beta-imaging autoradiography, have been documented previously and are established techniques for meteoric carbonates such as speleothems (e.g. Cole et al., 2003; Woodhead et al., 2012).~~In carbonate minerals, CL intensity is related to trace element contents but not specifically U concentration. CL brightness is generally ascribed to a number of emitters, with Mn^{2+} being the most dominant luminescence activator and Fe^{2+} being the dominant luminescence quencher in calcite and dolomite (e.g. Machel, 1985, 2000; Savard et al., 1995), although rare earth elements (REE) such as Eu^{2+} , Eu^{3+} , Dy^{3+} , Sm^{3+} and Tb^{3+} along with Pb^{2+} may also activate luminescence in some cases (Richter et al., 2003). Despite not being directly related to U, the very high spatial resolution of CL is useful for identifying μ m-scale calcite crystal growth zonation and alteration (Figure 7a and 7b), and for characterising different mineral generations formed from different fluids (e.g. Barnaby & Rimstidt, 1989; Tullborg et al., 2008; Milodowski et al., 2018).

BSE imaging (see Figure 6c and 6d) also does not correlate directly to trace concentrations of uraniumU, but to the mean atomic number of the mineral. It is useful as an imaging tool for characterising zonation, alteration and growth patterns, although we note that the contrast in zonation largely reflects variations in major element composition, and as such it is typically less sensitive than ~~with~~CL. Ukar & Laubach (2016) provide a recent review of high-spatial resolution SEM-based imaging of vein-filling calcite mineralisation.

607 CCI under the SEM directly images differences in dielectric properties, which produce
608 charge or conductivity contrasts in the near-surface of the sample that are detected by the
609 secondary electron emission, and may reflect compositional variations or strain induced by
610 deformation (Watt et al., 2000; Robertson et al., 2005). ~~It is an underutilised method for~~
611 ~~geological materials, a~~ Although the exact origin of charge-contrast is poorly understood, ~~-~~
612 ~~However,~~ it can provide useful information on crystal growth, compositional zoning and
613 microstructural features (see Figure 6a). It is an underutilised method for geological
614 materials, and has been, ~~and CCI has~~ previously ~~been~~ applied to garnet (Cuthbert &
615 Buckman, 2005), feldspar (Flude et al., 2012), limestone (Buckman et al., 2016) and
616 biogenic calcite (Lee et al., 2008). The technique requires very clean and carefully-prepared
617 and polished sample surfaces because it is sensitive to surface contamination and
618 mechanical defects, and imaging needs to be undertaken on uncoated samples under low-
619 vacuum conditions.

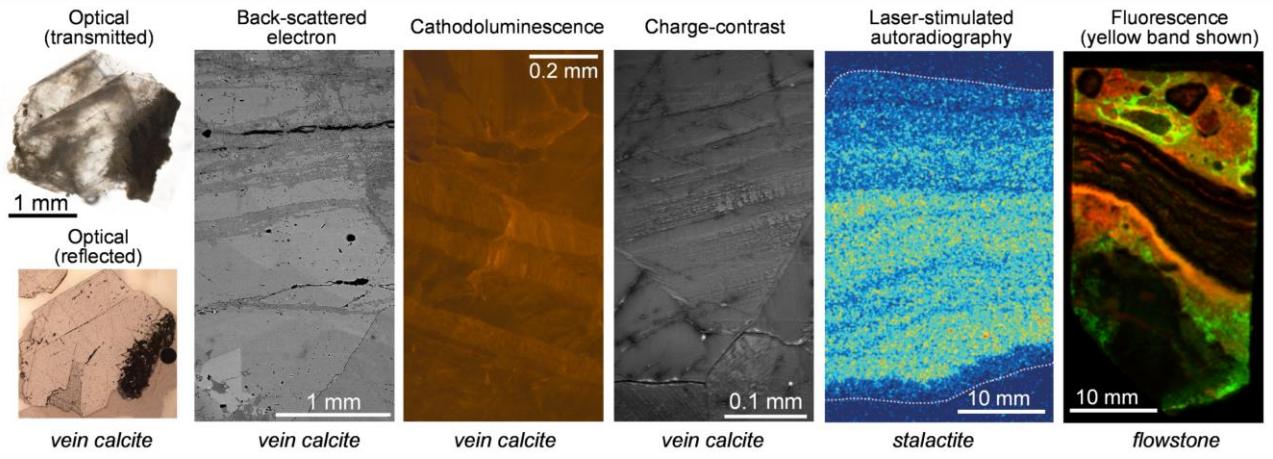
620

621 In addition to the microscopy-based methods listed above, a lower resolution but potentially
622 useful technique is provided by storage-phosphor imaging-plate (IP) autoradiography using
623 a plastic support film coated with a photostimulated phosphor (BaFBr:Eu²⁺) (Hareyama et
624 al., 2000). This technique records an image of the spatial distribution and intensity of total
625 radioactivity (from alpha, beta and gamma emitters) from a flat sample surface. In natural
626 geological materials, IP radiography records radioactivity from U, Th (and their radioactive
627 daughters), ⁸⁷Rb, and ⁴⁰K (Hareyama et al., 2000; Cole et al., 2003). Although U is not
628 specifically discriminated, it has been shown to be a useful screening tool for finding U-
629 bearing domains in carbonate materials (Cole et al., 2005; see Figure 6f). The method has
630 been particularly applied to speleothem studies where its large sample-size capabilities (up
631 to at least 40 cm) are beneficial. Spatial resolution is a few tens of micrometres, depending
632 on the pixel size of the laser scanner. However, the detection limit depends on the
633 exposure time of the IP in direct contact with the sample surface: routinely this is around
634 14-28 days giving a detection limit of a few ppm U, which is typically higher than many
635 carbonate samples. Whilst this may be suitable for speleothems, which typically have
636 higher uranium concentrations, we do not regularly adopt the method for very low U
637 contents in vein-filling or diagenetic carbonates.

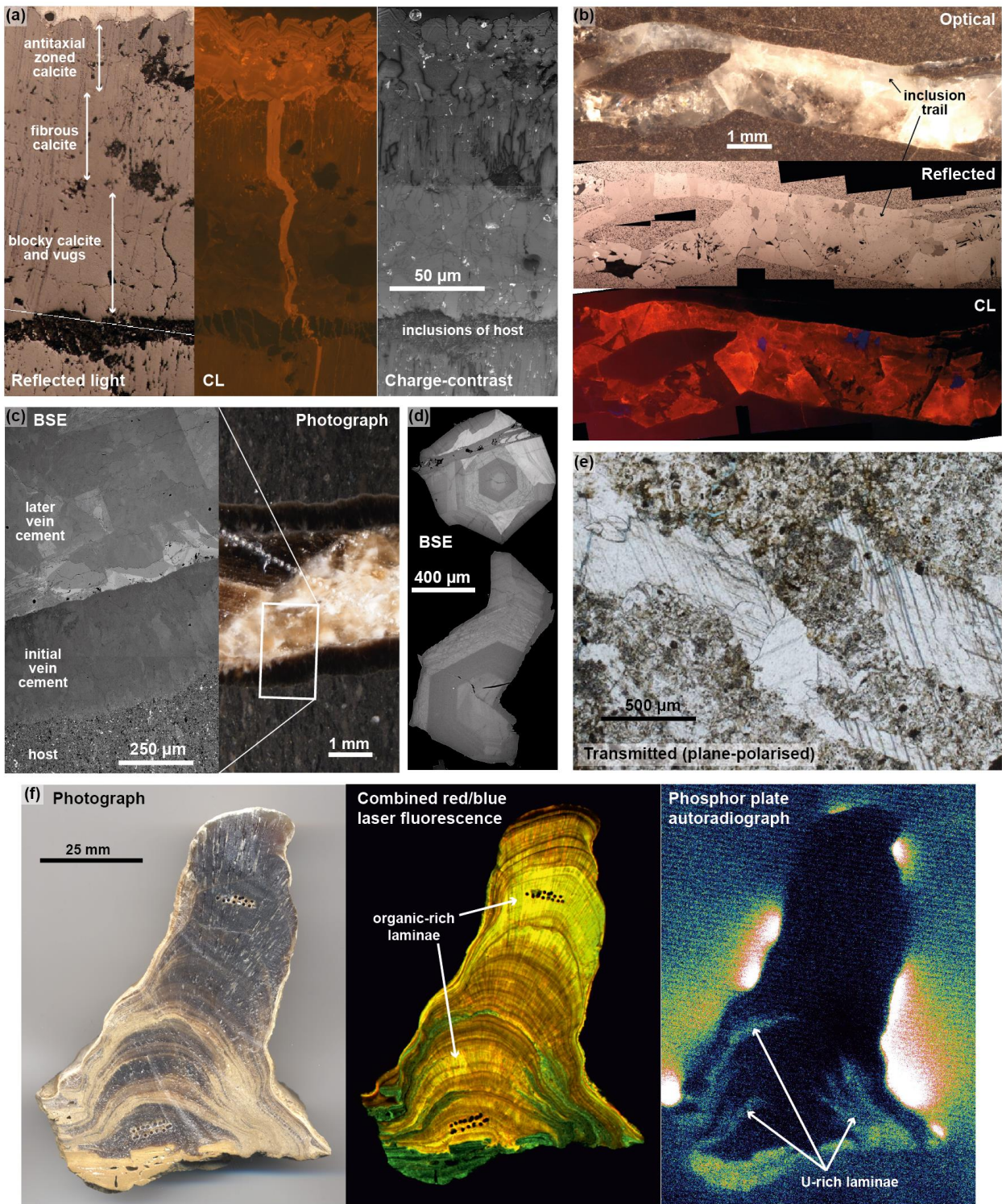
638

639 Fluorescence imaging has long been used in defining and characterising growth fabrics in
640 speleothems, although it does not specifically identify U-rich regions. This usually involves

641 irradiating a sliced sample with UV-light and observing the excited fluorescence emission at
642 a longer (visible light) wavelength, using either a standard UV microscope or digital
643 scanning with a UV laser system (e.g. Shopov et al., 1994; Baker et al., 1995; 2008;
644 Perrette et al., 2005). Fine growth detail with spatial resolutions of between 50 to 100 μm
645 are achievable. Speleothem fluorescence under UV at excitation wavelengths of 300-420
646 nm is dominated by the intrinsic fluorescence of natural high molecular weight and aromatic
647 organic (“humic” and “fulvic”) compounds, with emission between 400-480 nm (Baker et al.,
648 2008). However, we have also successfully imaged speleothems ([see](#) Figure [67f](#)) and other
649 geological materials (Field et al., 2019) by direct laser-stimulated scanning fluorescence
650 imaging (LSSFI) using 635 nm (red) and 450 nm (blue) wavelength excitation with 650 nm
651 and 520 nm low-pass wavelength filters, respectively. Although, such equipment is
652 principally applied to imaging of biological materials labelled with organic fluorescent dyes
653 (fluorochromes) (e.g. fluorescein), it is able to image variations in fluorescence originating
654 from organic laminae and subtle differences between carbonate minerals (calcite,
655 aragonite), revealing microtextural details with a resolution of about 100 [ummicrometres](#).
656



657



658

659

660 *Figure 76. Example imagery from the range of techniques used for sample screening and*

661 *characterisation. (a) mudstone-hosted vein calcite; (b) mudstone-hosted vein calcite; (c)*

662 *carbonate concretion-hosted calcite vein; (d) individual calcite crystals grown in a fracture*

663 *within crystalline bedrock; (e) calcite vein and cement within sediment-fill of an open*

664 *fracture; (f) cave speleothem.*

665

666

667 6.2.4.2. Destructive techniques

668 Several approaches for destructive sample screening using LA-ICP-MS are available.

669 These can include either systematic or non-systematic (random) spot traverses across

670 carbonate samples, and can include full analyses (i.e. a 30 second ablation following a pre-

671 ablation) or a much shorter analysis time (with or without pre-ablation). We commonly adopt

672 systematic traverses across samples utilising shorter ablation times but including a pre-

673 ablation, so as to avoid common Pb from the surface. This is a quick way to determine with

674 reasonable precision and accuracy whether a sample is a single age population that

675 represents a closed isotopic system with a suitable range in μ . For some samples, this

676 provides potentially useable age information that does not require any further refinement

677 (e.g. Figure [45Hh-45Ij](#)). Conversely, this may provide a population of data that exhibits no

678 potential, i.e. dominated by common-lead (e.g. Figure [5Aa-5bB](#)), open-system behaviour

679 (e.g. Figure [45Dd](#)), or mixed analyses (e.g. Figure [45Cc](#)). Screening in this way allows us to

680 analyse several samples or sample-aliquots in a single LA-ICP-MS session, and thus

681 identify the material most likely to provide an accurate and precise age.

682

683 Either as an alternative to spot traverses, or subsequent to spot traverses, we use LA-ICP-

684 MS mapping to determine both the location and nature of U and Pb zonation in the

685 carbonate material. Whereas spot traverses provide rapid screening of multiple

686 samples/aliquots, mapping provides fairly rapid (5 x 5 mm in < 2 hours) screening across

687 complexly zoned samples. Different approaches can be adopted, a suite of major and trace

688 elements can be analysed alone, a suite of elements for age determination (i.e. Pb to U \pm

689 Hg) can be measured, or, depending on ICP-MS instrumentation, these can be combined,

690 i.e. using a quadrupole ICP-MS (Drost et al., 2018) or a split-stream set-up utilising two

691 ICP-MS instruments (e.g. Kylander-Clark et al., 2013). As will be shown by the examples in

692 the subsequent sections, trace element maps are useful for directly comparing U and Pb

693 zonation with other trace and major elements. We have found that in primary vein-filling

694 calcite, U typically correlates with other trace elements, this varies between samples, but

695 can include V, Mn, Y, and the REEs. We can use this information to distinguish primary

696 zones of calcite from those that have been altered (see Section [65](#)). Elements, or elemental

697 ratios such as Ba/Ca, can be used to distinguish alteration zones or secondary material

698 (e.g. a detrital component). For example, in meteoric carbonates, high Th is commonly
699 attributed to detrital matter. The production of trace element maps rapidly produces extra
700 information that can be related to any later age determination, facilitating the relating of the
701 age to a specific growth event, i.e. the petrochronological approach (i.e. Kylander-Clark et
702 al., 2013; Engi et al., 2017).

703

704 An alternative approach is to produce maps that generate U-Pb data directly (see Section
705 [65.25](#)). These have obvious utility in determining suitable domains of calcite; however, for
706 common-lead bearing minerals they can be difficult to interpret by visual inspection. Pb-Pb
707 or Pb-U isotope maps can be created with ease; however, because of the inherent inclusion
708 of common lead, more useful is a map of common lead-corrected $^{206}\text{Pb}/^{238}\text{U}$ ages or ratios.
709 Common lead-corrected age maps require: 1) precise knowledge of the initial lead
710 composition (or upper intercept in Tera-Wasserburg space); and 2) knowledge that the
711 initial Pb composition is homogeneous across the mapped region, something that is not
712 always the case (see Section [57.2-4](#)). However, with the recent advent of more advanced
713 data processing software, such as the Monocle plug-in for Lolite (Petrus et al., 2017),
714 complex age determination from maps is becoming more amenable (see Section [56.52](#)).
715 The caveat with such data processing packages is that non-related domains defining a
716 single age with a good precision can potentially be selected with subjectivity, and without
717 relation to actual geological/mineralogical process. For this reason, we suggest that it is
718 imperative that users relate domains they have selected for U-Pb age determination to
719 specific mineralogical domains that can be identified independently with other means,
720 whether these be entire crystals, domains of crystals, growth bands, or specific veinlets. As
721 suggested by Drost et al. (2018), who demonstrate the method for carbonate sediments, it
722 is also useful to compare conventional spot ablation analyses with the map-generated
723 dates to verify the accuracy of the latter.

724

725 **[7.5.](#) Analytical Protocol**

726 The LA-ICP-MS method for carbonate follows a typical sample-standard bracketing
727 approach using a matrix-matched reference material, i.e. as for other silicate or phosphate
728 minerals (e.g. zircon, monazite, titanite, rutile, apatite, allanite), with only minor
729 modifications. Similarly, uncertainty propagation and data reporting should follow the
730 community-based guidelines for zircon of Horstwood et al. (2016). Details on the LA-ICP-

731 MS method for carbonate adopted by three major laboratories taking a similar approach are
732 provided in Roberts & Walker (2016) and Drake et al. (2017) for the British Geological
733 Survey laboratory (Nottingham, UK); Ring & Gerdes (2016) and Methner et al. (2016) for
734 Goethe-Universität (Frankfurt, Germany), and Nuriel et al., (2017, 2019) for University of
735 California Santa Barbara (Santa Barbara, USA). Ablation spot sizes are typically larger than
736 for silicate/phosphate minerals, generally >40 µm and often >100 µm, and fluences are also
737 often high (>4 J/cm²). As with all U-(Th)-Pb LA-ICP-MS geochronology, we advocate the
738 use of consistent ablation parameters between samples and reference materials.
739

740 There are two key points of the method we feel are worth highlighting that differ from
741 'standard' methods based on silicate minerals such as zircon. Firstly, the heterogeneous
742 nature of the Pb isotope composition of matrix-matched, i.e. calcite/dolomite, minerals (due
743 to variable common Pb incorporation), means that normalisation of the Pb-Pb isotope ratios
744 is currently achieved using a synthetic glass rather than a carbonate, typically NIST612 or
745 NIST614. At present, there is no evidence to suggest that the Pb/Pb mass bias is variable
746 across different matrices. Secondly, calculation of the reproducibility of the primary and
747 secondary matrix-matched reference materials, which is ~~required~~ for uncertainty
748 propagation (Horstwood et al., 2016) and determination of the true method accuracy and
749 precision, is hindered by the fact that the carbonate reference materials currently employed
750 have U/Pb heterogeneity that is equal to or much larger than the analytical uncertainties
751 (Roberts et al., 2017). This means there will typically be a significant excess variance of the
752 reference material U/Pb isotope measurements in any one session (including after
753 correction for common lead), which does not describe the reproducibility of the analytical
754 system but instead reflects the natural variation in the reference material. If propagated
755 onto the sample data-point uncertainties as a within-session excess variance as
756 recommended for zircon in Horstwood et al (2016), these data point uncertainties will be
757 ~~overestimated,~~ masking any smaller-scale, real geological scatter in the sample isochron
758 and ~~resulting~~ in ~~meaningless~~ ages with erroneously high precision. For this reason, it is
759 suggested that calculation of the session-based reproducibility is best estimated using a
760 more homogenous material such as NIST glass or zircon. However, it should be noted that
761 through this practice results can only be compared in a relative sense within session, or
762 between sessions if validation materials are compiled and used. To compare data in an
763 absolute sense, i.e. to assign an age and total uncertainty to a material for comparison
764 between laboratories and/or with other methods, the uncertainty from the primary reference

765 material must be included to reflect the accuracy with which the matrix-matched
766 normalisation is known. In this way, the uncertainty of the primary reference material
767 constitutes a limiting uncertainty on any sample age. Improved reference materials with less
768 scatter around the U/Pb isochron are therefore a pre-requisite for improving this method.
769

770 **8.6. Generating U-Pb data and interpreting ages**

771 Generating ages and relating these to geological processes requires the marriage of
772 spatially-resolved variations in composition (elemental and isotopic) and U-Pb isotopic
773 concentrations. In this section, we present several case studies to highlight how the
774 integration of compositional image-based data with U-Pb data can be used to interpret and
775 refine age data. ~~our approach to dating vein-filling calcite, the potential applications to~~
776 ~~dating faulting and fluid flow, and the type of material commonly encountered.~~ First we
777 present the 'standard' approach, which used independent imagery and analysis to target,
778 refine, and interpret the U-Pb analyses that are based on static spot ablations; ~~.-T~~ this is the
779 same concept approach as using CL imagery to help interpret zircon dates, ~~and that can be~~
780 further refined with information such as companion trace element data. A second
781 approach (age mapping) is to use mapping tools not just to image the sample and its
782 composition, but to extract age data from the map itself (Petrus et al., 2017; Drost et al.,
783 2018).
784

785 **8.1. Image-guided dating**

786 **6.1. Example A – Variscan-related veins in the Northumberland Basin**

787 The aim of most dating studies is to constrain the timing of primary calcite formation rather
788 than subsequent secondary alteration. Trace element mapping using LA-ICP-MS is a
789 particularly useful tool to assist with identification of growth zoning, particularly on the scale
790 of mm- to cm-sized chips. Figures 7a and 7b show examples of vein-fill calcite where
791 uranium zonation can be compared to other major and trace elements. The trace element
792 mapping reveals large variation in trace element contents across the directions of growth,
793 interpretable as changing metal/Ca ratios in the mineralising fluids (e.g. Drake et al., 2014).
794 The trace element zonation in both of these samples can be traced with the optically visible
795 growth zonation, indicating its primary nature. Sample TJN-0-1 (Figure 7a) was presented
796 in Roberts & Walker (2016), and we have re-dated it here locating spots in three separate
797 areas with different uranium concentration. The dates all overlap (Figure 7a), but the

798 precision of the dates is controlled by the amount of radiogenic to common lead, which
799 broadly correlates with the U concentration of the sample and where the traverse was
800 located. For this sample, the trace elements are low, including the Mn content, meaning the
801 entire sample appears dark in cold-stage CL. Therefore, elemental mapping with LA-ICP-
802 MS is one of the few techniques that can be used to characterise the elemental zonation in
803 such samples.

804
805 Sample TJN-6-1 (Figure 7b) is a single large crystal, with a rim of zeolite. Trace element
806 mapping reveals a strong correlation between most elements, again, representing the
807 primary growth zonation. High Mn and V ‘fingers’ intersect the growth zonation, and are
808 visible optically. We interpret these as pathways of secondary alteration. Given that the vein
809 exhibits vuggy textures, it is possible that fluids have precipitated or altered the original
810 calcite much later than the original period of calcite precipitation. Trace element mapping
811 allows us to visualise and fingerprint these alteration zones, and avoid or remove them from
812 analyses used for dating. A benefit to this approach is that the maps can then be used to
813 estimate the trace metal contents of the mineralising fluids, which in turn provides
814 information about rock-water interaction and the redox conditions, for example. These maps
815 also demonstrate that no measurable diffusion of trace elements across the calcite crystals
816 has occurred over a significant time span, as the distribution is interpreted as a primary
817 feature.

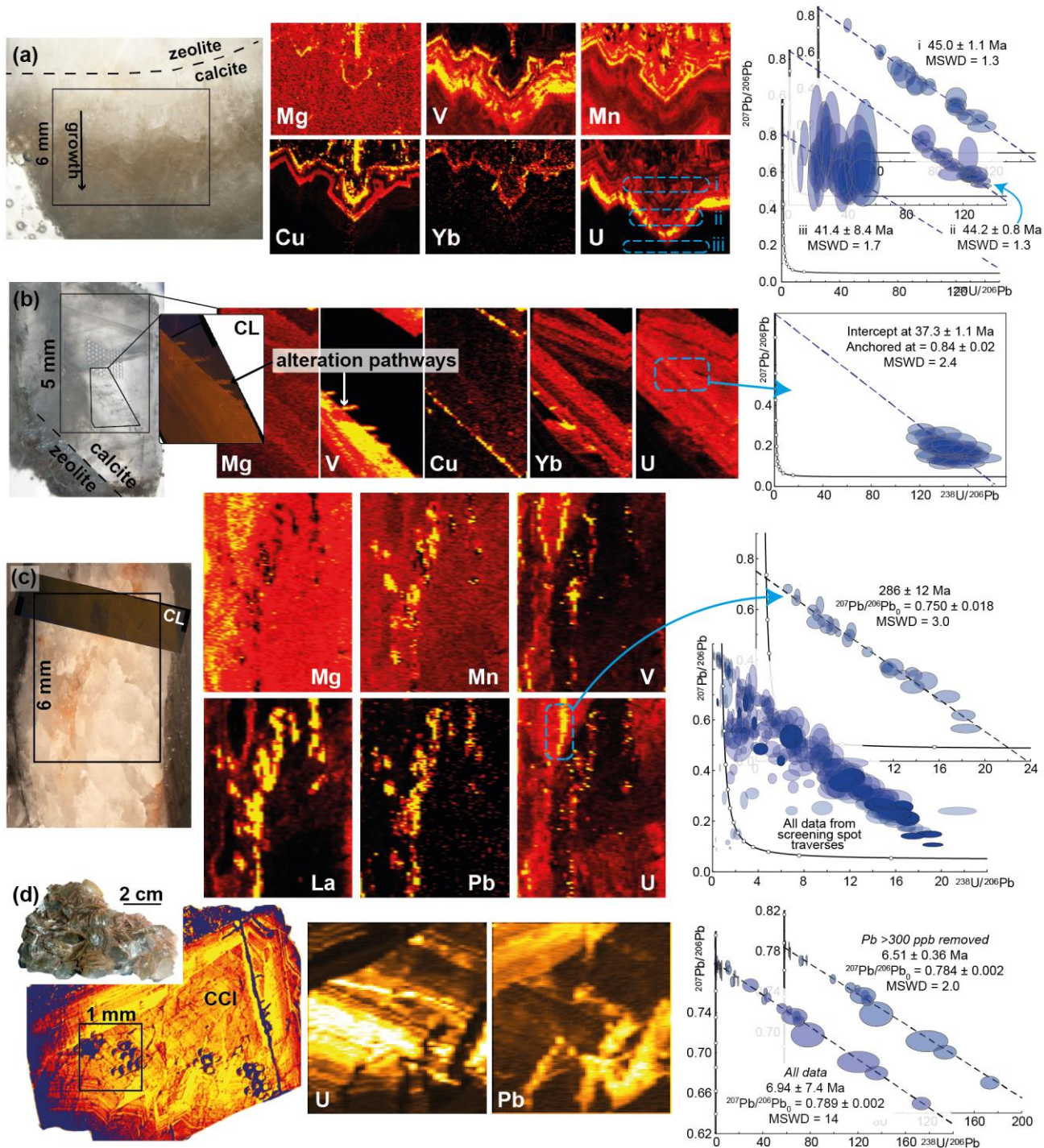
818
819 Alteration zones can sometimes be observed visually, without the need for imaging
820 techniques, as demonstrated by the vein sample in Figure 7c. In this particular sample, the
821 CL emission was rather dark, limiting its use for distinguishing the altered and non-altered
822 parts of the vein. Trace element mapping however, clearly distinguishes a region of
823 alteration running across the vein that is characterised by enrichment and depletion on
824 trace and major elements (e.g. low Mg, high La, Mn and Pb).

825 Figure 8 shows U-Pb calcite data from Howick Bay in the Northumberland Basin, NE
826 England. The mudstone succession in the bay is faulted and weakly folded, which is
827 postulated to be a result of transpressional stress during the Variscan orogeny (De Paola et
828 al., 2005). Syn-kinematic calcite located within fractures has the potential to date this far-
829 field intraplate deformation (c.f. Parrish et al., 2018). Screening data from this sample one
830 sample, comprising randomly located spot traverses across the vein a crystal, are presented
831 in Figure 7c&C. The data yield a regression with have a large array of common to

§32 radiogenic Pb compositions, ~~but~~ with significant scatter (~~MSWD = 577~~) including several
§33 data with low U/Pb and Pb/Pb ratios. The U-Pb data, indicating are compatible with some
§34 alteration and open-system behaviour and/or mixed age domains. Placing spots away from
§35 the altered region, and within a region with high uranium, yields a more robust regression
§36 that we interpret as a primary date of calcite formation.

§37
§38 In the final example (Figure 7d), the only mapped elements were U and Pb, but the sample
§39 was also imaged using CCI. Both the elemental maps and CCI image show laminations that
§40 are interpreted as growth zonation, and a reflection of the primary distribution of trace
§41 elements (U and Pb in this case). Faintly visible on the CCI are thin veinlets that cross-cut
§42 the growth bands. On the elemental maps, these are clearly distinguished as regions of Pb
§43 enrichment and U depletion, suggesting that Pb-rich fluids have percolated through this
§44 fracture-fill calcite. Since the spots that lie on the alteration pathways have high Pb counts,
§45 the age data were culled based on Pb concentration (>300 ppb Pb removed). This
§46 approach reduced the scatter in the regression, providing a more precise age, presumably
§47 through the removal of data that reflect variable common lead compositions.

§48



849

850

851

852

853

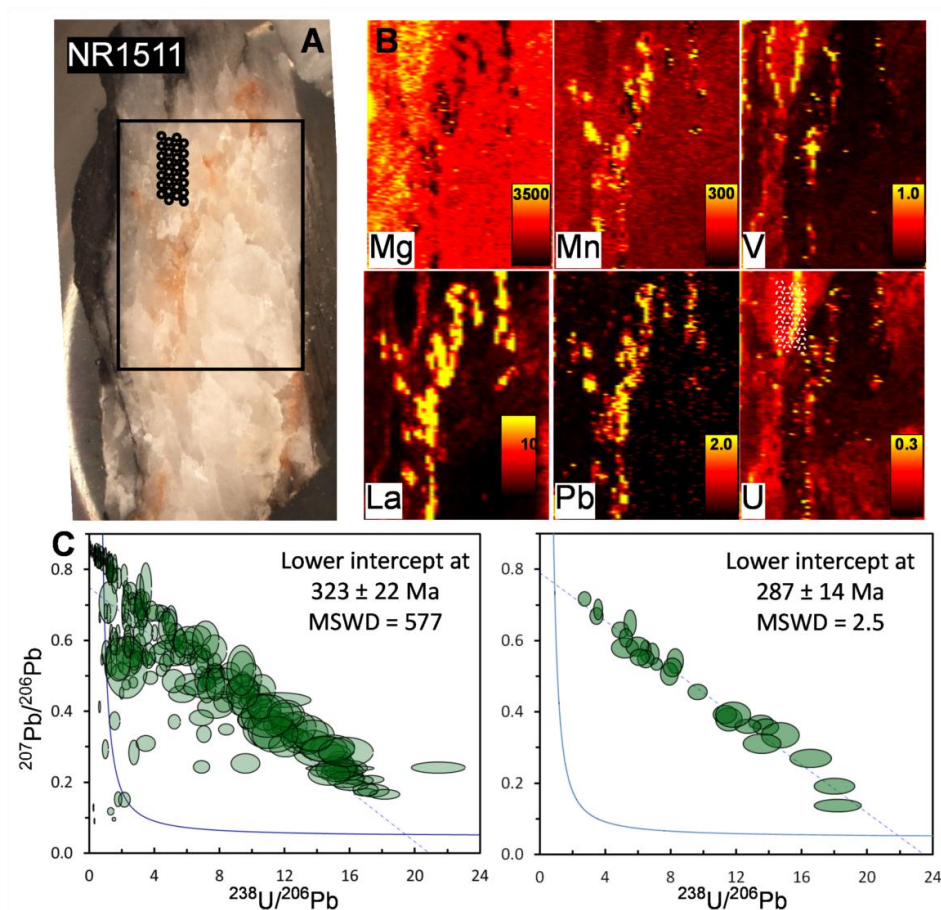
854

855

856

Figure 7. Photographs, LA-ICP-MS elemental maps, CL and CCI imagery and corresponding Tera-Wasserburg plots for four fracture-fill samples. For all maps, brighter = higher concentration. (a) Basalt-hosted fracture-fill calcite grown after zeolite, Faroe Islands. Three spot traverses for U-Pb data are shown, labelled i, ii and iii. (b) Basalt-hosted fracture-fill calcite, with zeolite grown after calcite, Faroe Islands. (c) Mudstone-hosted fracture-fill calcite, UK. U-Pb data are compared between a specific region avoiding the alteration, and from spot traverses across the sample. (d) Sandstone-hosted fracture-fill

§57 *calcite, UK. CCI image is false-coloured. U-Pb data are shown with and without a rejection*
 §58 *criteria based on removal of high Pb counts – corresponding to Pb-rich alteration pathways.*
 §59 *The crystal was subsequently mapped for its trace element distribution, revealing a zone of*
 §60 *low Ca and Mg, and high Mn, REEs and Pb. This zone can be seen optically, and is*
 §61 *interpreted as a zone of alteration. Further U-Pb spot analyses were placed in a domain*
 §62 *away from this feature that exhibits high U, with the data yielding a more precise regression*
 §63 *with an age of 287 ± 14 Ma (MSWD = 2.5). This example highlights the use of trace*
 §64 *element mapping to locate regions of highest U, to assist and refine U-Pb analyses, and*
 §65 *shows the potential for dating calcite veins into the Palaeozoic.*
 §66
 §67



§68
 §69 *Figure 8. A) Photomicrograph of sample NR1511 showing position of mapped area and*
 §70 *ablation spots (in black); B) Trace element maps generated with LA-ICP-MS using line*
 §71 *rasters, the scales are in ppm and white spots show the ablation locations; C) Tera-*
 §72 *Wasserburg concordia of U-Pb data from this sample based on screening spot traverses;*

§73 *D) Tera-Wasserburg concordia of U-Pb spot data placed using constraints from map data,*
§74 *i.e. over the unaltered high U region.*

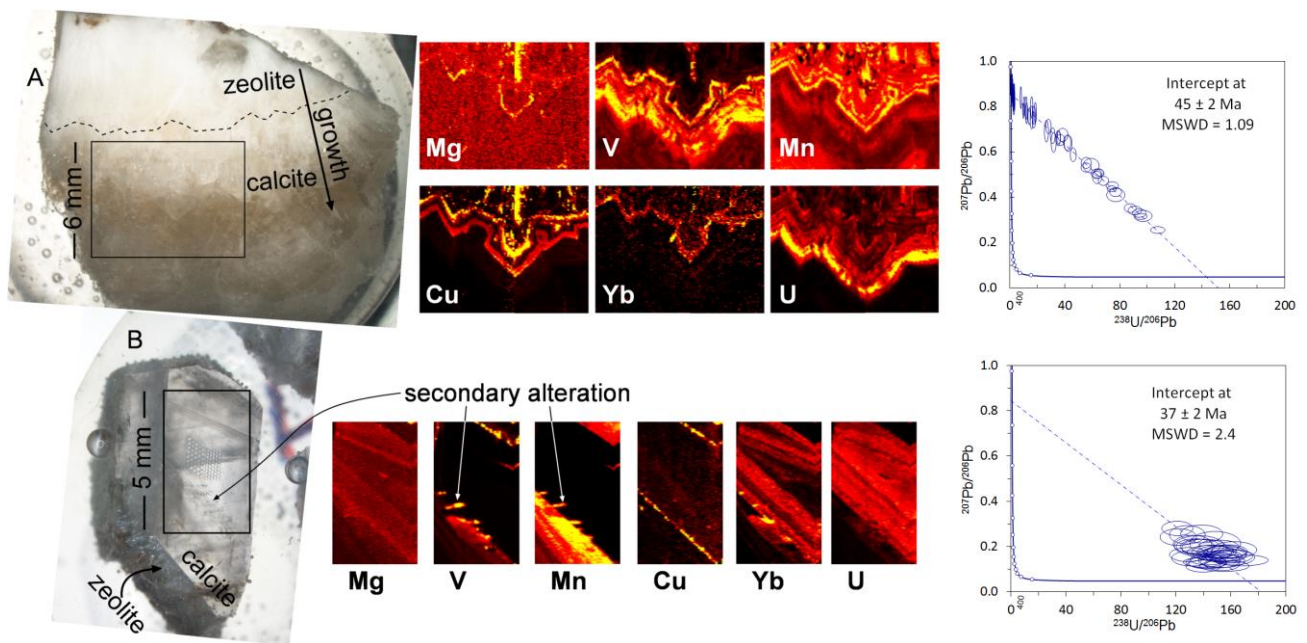
§77 *Example B—Faroe Island vein mineralisation*

§78 The aim of most studies is to date primary calcite formation rather than subsequent
§79 secondary alteration, particularly when dating syn-kinematic calcite for constraining the
§80 timing of fault slip (e.g. Roberts & Walker, 2016; Ring & Gerdes, 2016; Goodfellow et al.,
§81 2017; Hansman et al., 2017; Nuriel et al., 2017, 2019; Parrish et al., 2018; Holdsworth et
§82 al., 2019; Smeraglia et al., 2018). Trace element mapping is a useful tool to assist with
§83 identification of growth zoning, particularly on the scale of mm- to cm-sized chips. Using
§84 standard LA-ICP-MS protocols for trace element determination, with standard sample
§85 bracketing routines, a 5 x 5 mm region can be mapped in less than two hours. As discussed
§86 previously, depending on the analytical set-up, this trace element mapping can be
§87 conducted alongside U-Pb isotope mapping.

§89 Figure 9 shows selected results from dating of syn-kinematic crack-seal-slip calcite
§90 mineralisation from basalt-hosted faults of the Faroe Islands (Roberts & Walker, 2016).
§91 Sample A is from a vein exhibiting a zeolite-calcite-zeolite mineral paragenesis. The calcite
§92 exhibits distinct syntaxial growth zoning towards the centre of the vein. Trace element
§93 mapping reveals large variation in trace element contents in the direction of growth,
§94 interpretable as changing metal/Ca ratios in the mineralising fluid (e.g. Drake et al., 2014).
§95 The trace element zonation clearly follows the optically visible growth zonation, indicating
§96 its primary nature. Uranium increases steadily to the maximum concentrations observed,
§97 then abruptly drops to very low abundances. The U-Pb data define a well-behaved isochron
§98 (low scatter with large spread in U/Pb ratios), determined from spots placed on and near
§99 the high U region, and yields a lower intercept U-Pb age of 45 ± 2 Ma ($MSWD = 1.09$).

901 Sample B is from a large dilational jog (up to 1 m wide) that is filled with zeolite-calcite-
902 zeolite mineralisation, including calcite crystals up to 10 cm long. The mapped grain is
903 composed of calcite with a later rim of zeolite. Trace element mapping reveals a strong
904 correlation between most elements, again, representing the primary growth zonation. High
905 Mn and V ‘fingers’ intersect the growth zonation, and are visible optically. We interpret

906 these as pathways of secondary alteration. Given that the vein exhibits vuggy textures, it is
 907 possible that fluids have precipitated or altered the original calcite much later than the
 908 original fault slip. U-Pb analyses of the primary calcite in this sample reveal fairly radiogenic
 909 Pb compositions, although with large datapoint uncertainties owing to the low U
 910 concentrations, with a lower intercept U-Pb age of 37 ± 2 Ma (MSWD = 2.4; anchored
 911 upper intercept based on other samples on this study at 0.89 ± 0.02). Trace element
 912 mapping allows us to visualise and fingerprint these alteration zones, and avoid or remove
 913 them from analyses used for dating. A benefit to this approach is that the maps can then be
 914 used to estimate the trace metal contents of the mineralising fluids, which in turn provides
 915 information about rock-water interaction and the redox conditions for example. These maps
 916 also demonstrate that no measurable diffusion of trace elements across the calcite crystals
 917 has occurred over a significant time span, as the distribution is interpreted as a primary
 918 feature.



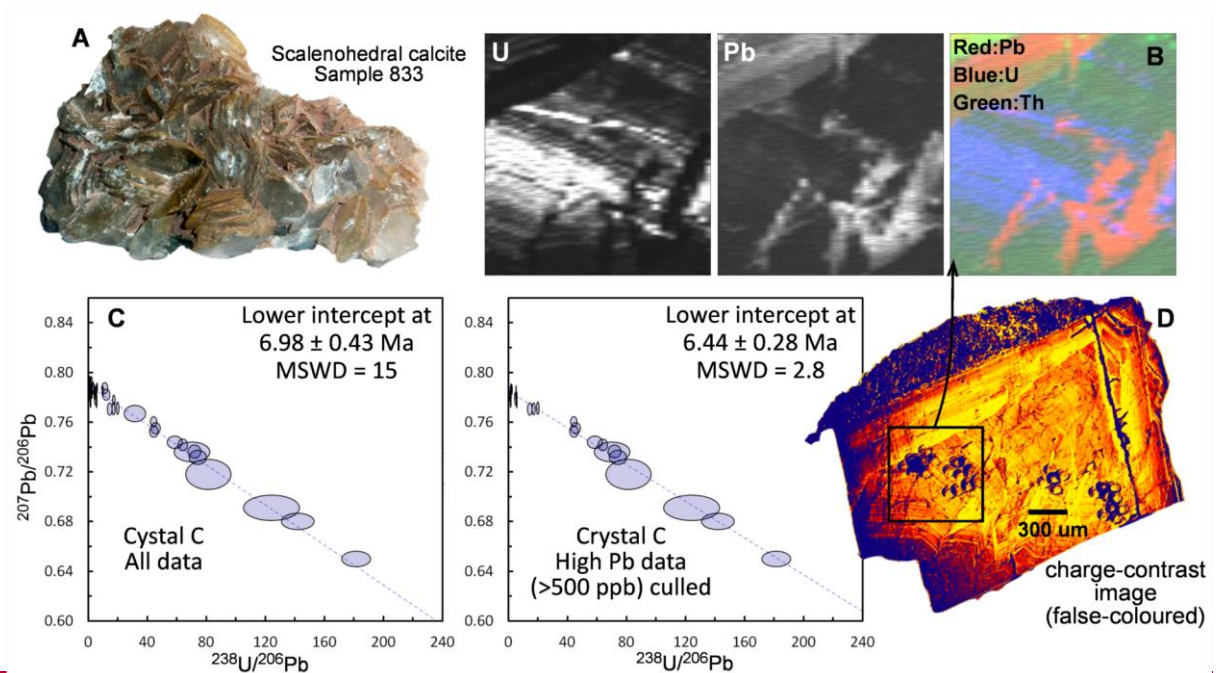
920
 921
 922 *Figure 9. A) Sample microphotographs of epoxy-resin mounted zeolite-calcite vein*
 923 *samples, TJN-0-1 and TJN-6-1, mapped regions shown in black; B) Trace element maps*
 924 *generated with LA-ICP-MS using line rasters; C) Tera-Wasserburg concordia of U-Pb data*
 925 *from each sample (from Roberts and Walker, 2016).*

928 *Example C—Sellafield fracture mineralisation*

929 Figure 10 shows results for fracture mineralisation from Sellafield, NW England. This
930 location was previously investigated (1990–1997) as a potential nuclear waste repository
931 site, and has thus been extensively studied in terms of its structure, stratigraphy,
932 geochemistry and palaeo- to present-day hydrogeology (Michie & Bowden, 1994; Akhurst
933 et al., 1997; Baker et al., 1997; Heathcote and Michie, 2004; Bath et al., 2006; Milodowski
934 et al., 1998, 2018). Deep (up to 2 km) site investigation boreholes revealed a complex
935 sequence of fracture mineralisation within Ordovician greenschist-facies metamorphic
936 basement rocks overlain by Carboniferous Limestone and Permo-Triassic sedimentary
937 strata (Milodowski et al., 1998). Presented here are data from one mineralised zone that
938 show the potential for U-Pb dating of such material.

939
940 Sample 833 is an example of euhedral calcite crystals lining open fractures and
941 representing the latest mineralisation, and which are very closely associated with the
942 present-day fracture-controlled groundwater system (generation ME9 of Milodowski et al.,
943 1998; 2018). The sample has U and Pb concentrations of 0.3–30 ppm and 0.1–3.6 ppm,
944 respectively. U-Pb LA-ICP-MS spot analyses were placed in a single crystal which was
945 optically continuous; the data yielded an age of 6.98 ± 0.43 Ma (MSWD = 15). The dated
946 crystal was subsequently mapped for its U, Th and Pb elemental distribution using LA-ICP-
947 MS. The map shows zoning of U, Th and Pb that is interpreted as growth zoning during
948 primary calcite growth. Pb is distributed similarly, but with high concentrations along narrow
949 veins that are discordant to the primary growth zoning; these are interpreted as alteration
950 pathways where Pb-bearing fluids have invaded the crystals. Crystals were also imaged
951 using charge-contrast imaging (CCI), which highlights structural imperfections in the calcite
952 crystals. The same veinlets that have elevated Pb concentrations are imaged as cracks and
953 disturbances to the growth zoning. Since the spots that lie on the alteration pathways have
954 high Pb counts, the age data were culled based on Pb concentration (>500 ppb Pb
955 removed). This approach reduced the scatter in the regression, presumably removing
956 components with slightly different common lead compositions, giving a more precise age of
957 6.44 ± 0.26 Ma (MSWD = 2.8). These data from Sellafield demonstrate the potential utility
958 of imaging techniques such as CCI and trace element mapping to discriminate primary
959 growth domains from those that are altered at the micro-scale (<100 μ m), and refinement of
960 scattered analyses into those that are interpretable as a single population.

961



962

963 *Figure 10. A) Photograph of sample 833; B) Trace element maps using LA-ICP-MS based*
964 *on line rasters; C) Tera-Wasserburg concordia of U-Pb data before and after refining the*
965 *data; D) False-colour charge-contrast image of the dated crystal, showing the mapped*
966 *region in black.*

967

8.2.6.2. Age mapping of vein-fill carbonates

968

969 *We have demonstrated that elemental mapping data are useful for refining and interpreting*
970 *U-Pb isotopic data. For example, in Example B above, we manually located the spots in a*
971 *high U zone, and in Example C, we manually removed the data with high Pb*
972 *concentrations.* An alternative approach to using elemental maps to 'manually' locate
973 spots or refine spot data, is to generate a combined elemental and U-Pb isotopic 2D
974 dataset (i.e. map); the benefit of this method is that software tools can be used to both
975 discriminate specific isotopic data based upon chosen criteria, and also to show regions
976 within these pooled datasets that have similar compositional characteristics. Lolite (Paton et
977 al., 2011) is one of the most commonly used data reduction tools for both U-Pb isotopic
978 data (Paton et al., 2010), and for generation of elemental 2D maps. Monocle is a software
979 plug-in for Lolite that allows the user to generate maps of isotopic and elemental data
980 (Petrus et al., 2017), and to define and extract regions of pooled compositional data,
981 including those used for age calculations. Drost et al. (2018) demonstrated the efficacy of
982 the software for dating carbonate sediments, whereby features such as bioclasts and

983 detrital components are removed. For a detailed explanation of the protocol, see Drost et al.
984 (2018). In brief, each pixel of the elemental and isotope ratio maps corresponds to one duty
985 cycle of the ICP-MS. First, pixels are removed, using user-defined selection criteria that are
986 believed to be related to alteration, secondary material, or a younger or older carbonate
987 generation. This is usually conducted after an initial inspection of the mapping data
988 combined with prior imaging and petrography; however, the screening can also employ an
989 iterative approach after generation of initial U-Pb isochrons. After this screening/filtering, the
990 remaining data are pooled into a number of pseudo-analyses (each corresponding to the
991 same number of pixels) based on a suitable isotope ratio, such as $^{238}\text{U}/^{208}\text{Pb}$ or $^{235}\text{U}/^{207}\text{Pb}$.
992 The pooling is achieved using an empirical cumulative distribution function (ECDF) to
993 maximise the spread in U/Pb ratios, and an appropriate number of pixels to produce a
994 reasonable population of data, for example twenty to forty data-points. Here, we present
995 examples of this approach applied to vein-filling calcite.

996

997 ~~Example D — BH11~~

998 ~~This example is of a fine-scale vein cross-cutting a sedimentary host rock; the objective is~~
999 ~~to use Monocle-based criteria to discriminate the vein from the host rock and determine a~~
1000 ~~robust age. Only two criteria of filtering were needed to distinguish the vein from the host:~~
1001 ~~Mg of less than 5000 ppm, and Th of less than 0.1 ppm. The remaining data were pooled~~
1002 ~~using $^{238}\text{U}/^{208}\text{Pb}$ ratios into 26 analyses, and yielded a robust lower intercept~~
1003 ~~$^{238}\text{U}/^{206}\text{Pb}$ date of $53.95_{90} \pm 0.36_{33}$ Ma, with an MSWD of 1.0_{21} (Figure. 11). This~~
1004 ~~sample was previously dated using conventional spot analyses located within the vein at~~
1005 ~~53.51 ± 0.39 Ma (MSWD = 2.0; Beaudoin et al., 2018). These dates, quoted without~~
1006 ~~propagation of systematic uncertainties, show good agreement between two different labs~~
1007 ~~using different instrumentation and data reduction methods.~~

1008

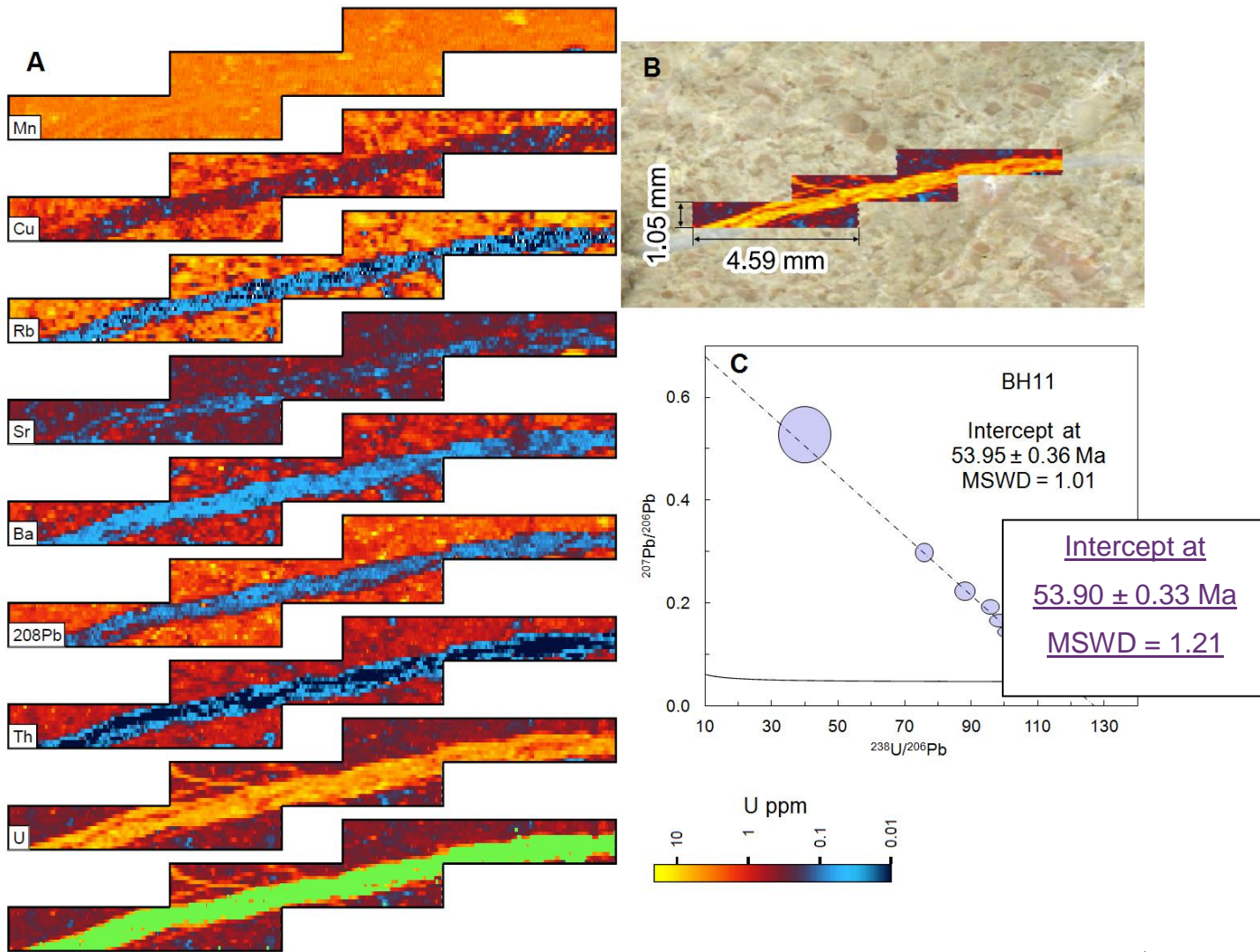


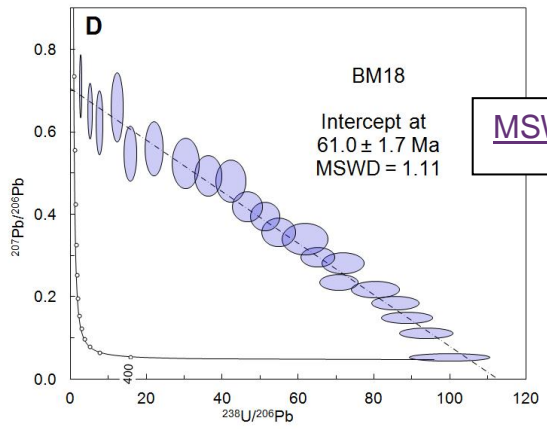
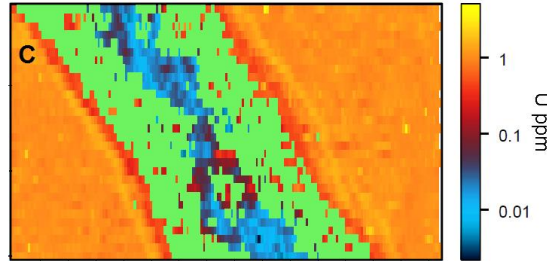
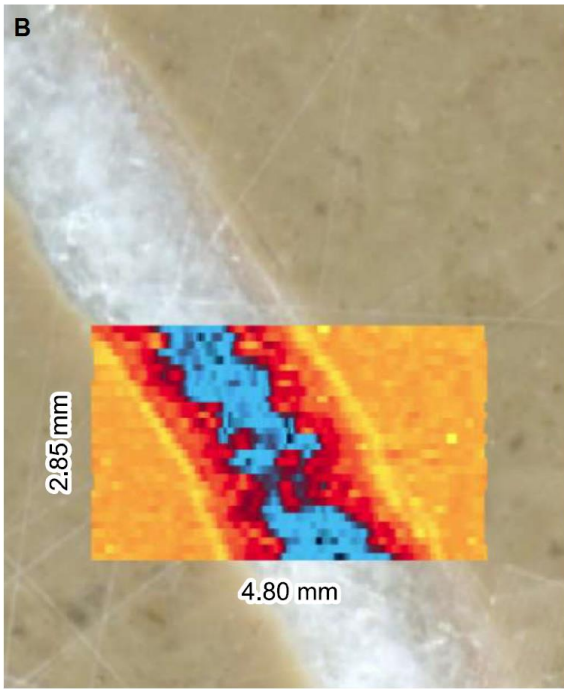
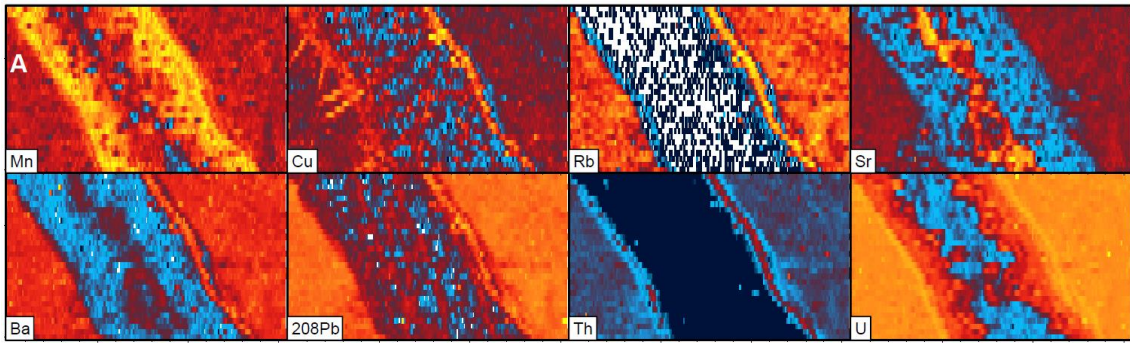
Figure 11. Image-based dating (Monocle plug-in for Iolite) of sample BH11. A) Trace element maps of the analysed region, the final map shows the region of interest selected for the U-Pb date highlighted in green; B) Photomicrograph of the sample surface showing the mapped region as a U map; C) Tera-Wasserburg concordia of U-Pb data after pooling and filtering using the Monocle plug-in (see text for description).

Example E—BM18

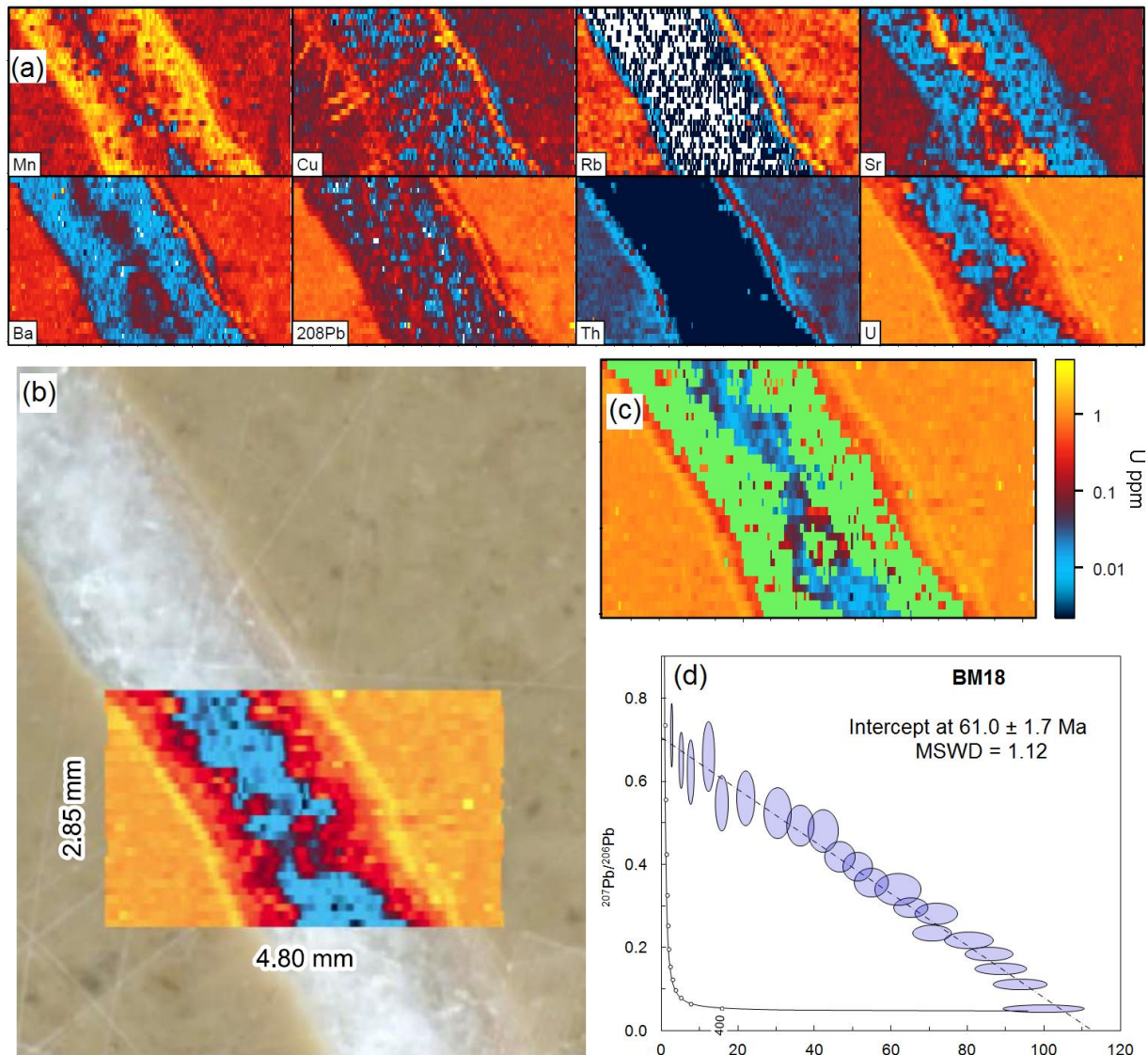
Figure 8 shows an ~~BM18 is another~~ example of a vein cross-cutting a sedimentary host-rock, with. This time, there is clear zonation within of the vein (Figure. 12). Since it is a syntaxial vein (crystals growing from the wall rock to the centre), this zonation probably represents changing fluid chemistry as the calcite crystals were precipitating. However, it could represent multiple generations of calcite precipitation. Criteria were selected for filtering of the data to highlight the outer regions of the vein; Rb < 0.05 ppm, Th < 0.01 ppm,

1024 and Sr < 400 ppm. The U-Pb data were then filtered to remove data with low U and Pb
1025 signals, since no initial rejection of data based on detection limit was conducted using this
1026 data reduction method; criteria for acceptance were $^{238}\text{U} > 500$ cps, and $^{207}\text{Pb}/^{206}\text{Pb} < 1.5$.
1027 The remaining data produce a robust isochron with a lower intercept date of 61.0 ± 1.7 Ma
1028 (MSWD = 1.44; 21 pooled analyses). This date overlaps that previously obtained using
1029 spot analyses that were derived from the entire width of the vein (59.5 ± 1.7 Ma; Beaudoin
1030 et al., 2018).

1031



1032

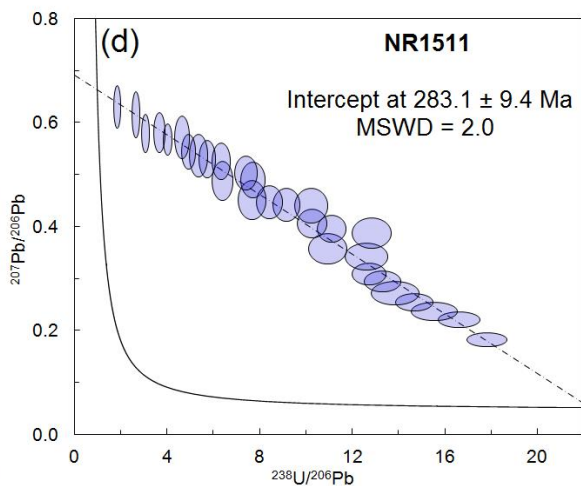
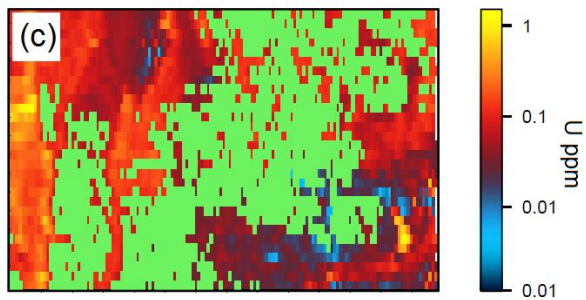
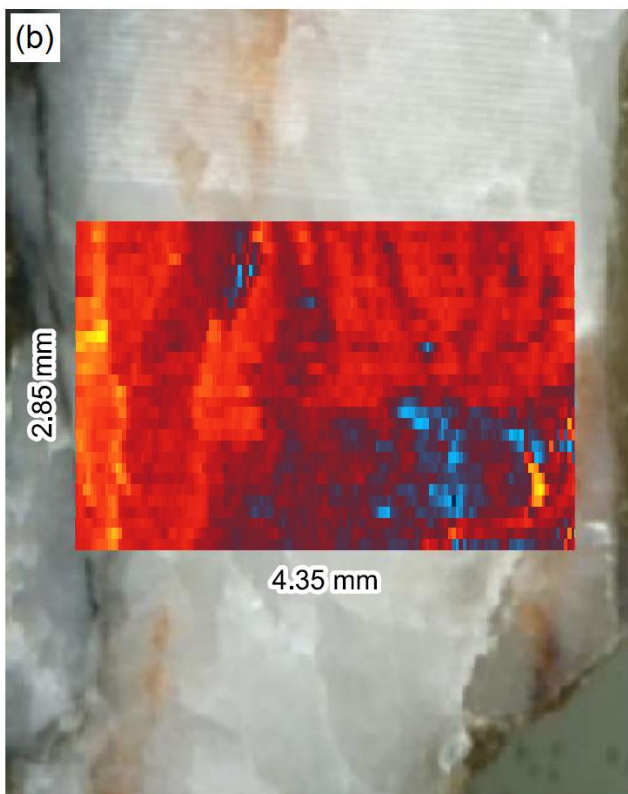
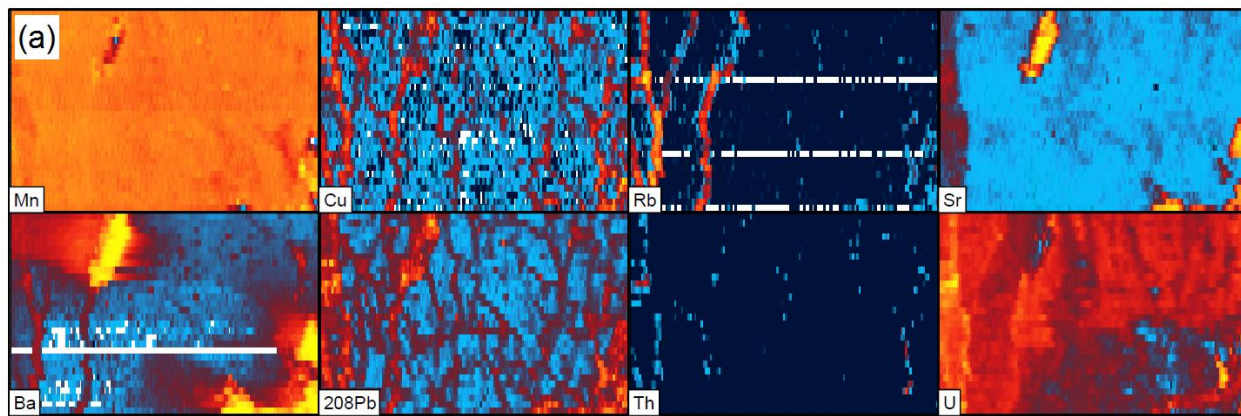


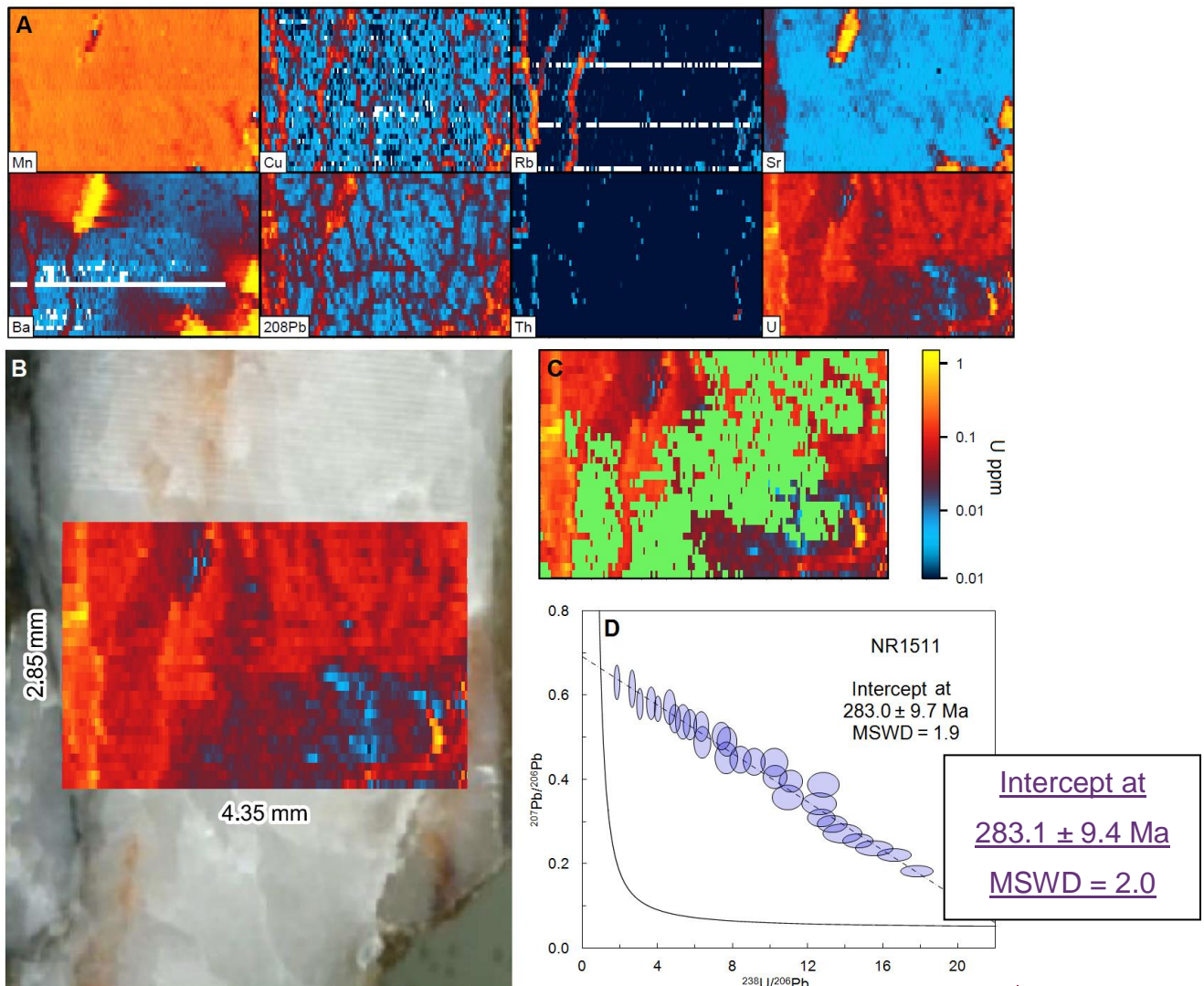
1033
 1034 *Figure 128. Image-based dating (Monocle plug-in for Iolite) of sample BM18. (aA) Trace*
 1035 *element maps of the analysed region; (bB) Photomicrograph of sample surface showing*
 1036 *mapped region as U map; (cC) U map showing the region of interest selected for the U-Pb*
 1037 *date in green; (dD) Tera-Wasserburg concordia of U-Pb data after pooling and filtering*
 1038 *using the Monocle plug-in (see text for description).*

1039
 1040
 1041 **Example F—NR1511**

1042 To demonstrate The third example of image-based dating on another is from a complex
 1043 sample, we re-dated the vein presented in Figure 7c (NR1511). vein already described in
 1044 section 5.1 above (Example A). This vein features visible textures and chemistry associated
 1045 with alteration. (Figure. 13). The mapped region (see Figure 9) is entirely within the vein

1046 (no host rock). High concentrations in several elements (e.g. Cu, ~~Ba~~, Rb, Sr, Ba and Pb)
1047 reflect veinlets that can be seen optically as a yellow altered region. The remaining portion
1048 of the vein varies in U content, which likely represents chemical zonation across the coarse
1049 sparry calcite growth. A fairly robust isochron (MSWD = 4.92.0) was obtained after filtering
1050 of the data for the clearly altered regions, cleaning up the U-Pb data to remove low U and
1051 Pb signals, and pooling the data based on $^{207}\text{Pb}/^{235}\text{U}$. The criteria for acceptance were: Cu
1052 < 0.2 ppm, Ba < 10 ppm, Rb < 0.01 ppm, and ^{238}U < 10000 cps (for removal of alteration),
1053 and ^{238}U > 500 cps, $^{207}\text{Pb}/^{206}\text{Pb}$ > 0.15 < 1.5, and $^{206}\text{Pb}/^{208}\text{Pb}$ > 0.1 < 10 (for 'cleaning up'
1054 the U-Pb data). These data yielded a date of 283.1 ± 9.74 Ma, which overlaps that obtained
1055 from spot analyses and manual location of the spot data based on prior LA-ICP-MS
1056 mapping (2867 ± 142 Ma; see Figure 8D7c), ~~but with an improvement in the precision (4.9~~
1057 ~~to 3.43 %).~~
1058





1060
1061
1062
1063
1064
1065
1066
1067
1068
1069
1070
1071
1072
1073

Figure 139. Image-based dating (Monocle plug-in for Iolite) of sample NR1511. (aA) Trace element maps of the analysed region; (bB) Photomicrograph of sample surface showing mapped region as U map; (cC) U map showing the region of interest selected for the U-Pb date in green; (dD) Tera-Wasserburg concordia of U-Pb data after pooling and filtering using the Monocle plug-in (see text for description).

7. Limitations

9.7.1. Isotopic composition of common lead

Carbonates nearly always take up some amount of lead during their formation, referred to as 'common' or initial lead. Contamination during handling (i.e. during cutting and polishing) or from recent exposure to the environment will have a modern isotopic composition of common lead, i.e. approximating the Stacey & Kramers (1975) model for terrestrial lead composition at present-day, roughly $^{207}\text{Pb}/^{206}\text{Pb} = 0.84$. Distinguishing between such

1074 contamination and the common lead incorporated during formation can be difficult. Well
1075 behaved U-Pb isotopic systematics in a carbonate sample should yield a single mixing line
1076 between the common and radiogenic end-members, and ideally will have enough spread in
1077 U/Pb ratios to yield a precise regression with low uncertainties at both the lower (radiogenic
1078 lead) and upper (common lead) intercepts. However, many samples will exhibit a lack of
1079 spread in U/Pb ratios, or will be dominated by radiogenic compositions (e.g. Figure 4f5F).
1080 Although a best-fit line may be calculated for such data, the slope, and thus age, may be
1081 inaccurate. Thus, it is useful for such samples to have an estimation of the common lead
1082 composition through other means, such as from nearby cogenetic samples formed at the
1083 same age, or from different minerals also believed to have been formed at the same age.

1084
1085 For some mineral chronometers, such as the phosphate mineral monazite, it is common to
1086 use an estimate of the common lead composition based on the Stacey and Kramers (1975)
1087 model (e.g. Palin et al., 2013; Regis et al., 2016). In our experience, this is an acceptable
1088 approach because from a number of different studies, we find that the common lead
1089 composition determined from other minerals (i.e. feldspar, biotite, apatite) overlaps the
1090 Stacey and Kramers (1975) composition (e.g. Stübner et al., 2014; Warren et al., 2014). For
1091 carbonate however, we find this is not always such a suitable approach. Our experience,
1092 particularly from fracture-fill, but also evident in diagenetic and sedimentary carbonates,
1093 from hydrothermal carbonate in particular, is that common lead compositions are often
1094 more radiogenic (lower $^{207}\text{Pb}/^{206}\text{Pb}$ ratios) than those predicted by the terrestrial lead model
1095 (Stacey and Kramers, 1975) for the age of carbonate crystallisation. This situation can
1096 occur if the carbonate has incorporated unsupported radiogenic lead during its formation.
1097 This most readily occurs by incorporation of radiogenic lead that is derived from an ancient
1098 sources, i.e. lead that has been decaying from produced by uranium decay in a closed
1099 system for a long time, but which is decoupled from its parent uranium before being
1100 incorporated into the measured carbonate.

1101
1102 We have compiled sample data with robust U-Pb regressions from the BGS laboratory
1103 (both published and unpublished), and presented these as a Figure 14 shows a
1104 compilation of common lead intercepts ($^{207}\text{Pb}/^{206}\text{Pb}$). The data are split into fracture-fill and
1105 diagenetic samples, and from a number of studies of fracture-filling calcite (compilation of
1106 BGS laboratory data). The data represent different host lithologies, different ages
1107 (dominated by Cretaceous to Miocene), and different geological regions. It is clear that for

1108 many samples in this compilation, anchoring at a value close to the terrestrial lead model
1109 composition for Phanerozoic ages, i.e. $^{207}\text{Pb}/^{206}\text{Pb} \sim 0.84$, will lead to calculated ages older
1110 than the true age due to steepening of the regression. The importance of the common lead
1111 composition in providing constraints on a calculated age will depend on the amount of
1112 measured radiogenic lead in a given sample; samples dominated by common lead and
1113 lacking in radiogenic lead will need a ~~well-defined~~well-defined array to produce a confident
1114 lower intercept. We find that within individual vein samples, the apparent composition of the
1115 common lead end-member can vary, limiting the precision of the regression and derived
1116 age. For speleothems, Woodhead et al. (2012) demonstrate that most samples analysed in
1117 their lab yield common lead compositions overlapping Stacy and Kramers (1975), and thus
1118 their ages are largely insensitive to the common lead compositions. This likely reflects the
1119 fact that they are precipitated from meteoric water that ~~reflects the~~incorporates modern
1120 lead derived from a regional upper crustal lead~~Pb~~ composition. ~~Although, they add the~~
1121 ~~caveat that samples with~~ $^{238}\text{U}/^{206}\text{Pb}$ ~~below 1300 (equivalent to~~ $\mu \approx 20,000$ ~~), have large~~
1122 ~~inaccuracies.~~

1123
1124 The highly radiogenic initial lead values ($^{207}\text{Pb}/^{206}\text{Pb} < \sim 0.75$) recorded in our compilation
1125 are mostly from two settings, young fractures in Proterozoic crystalline crust of Sweden (n=
1126 ~~10 of 104~~), and young fractures in the Bighorn Basin that overlies Archaean basement
1127 (n=~~24-24 of 104~~). In both cases, lead leached from the bulk~~whole-rock~~ Pb, although
1128 ancient, is not radiogenic enough to produce the measured values. Instead, leaching of
1129 unsupported radiogenic lead from uraniferous minerals (i.e. high μ) is required (e.g.
1130 titanite, allanite, monazite, xenotime and zircon) as a causative mechanism. Radiogenic
1131 lead is in fact a well-known widespread feature found in ore deposits across Sweden (e.g.
1132 Johansson & Rickard, 1984; Romer & Wright, 1993).

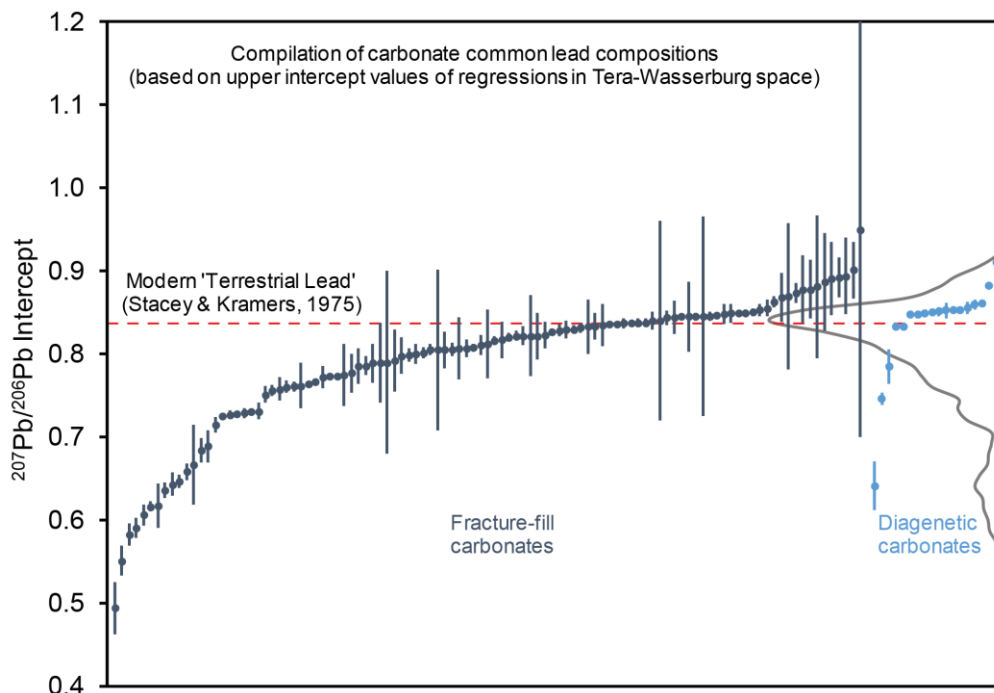
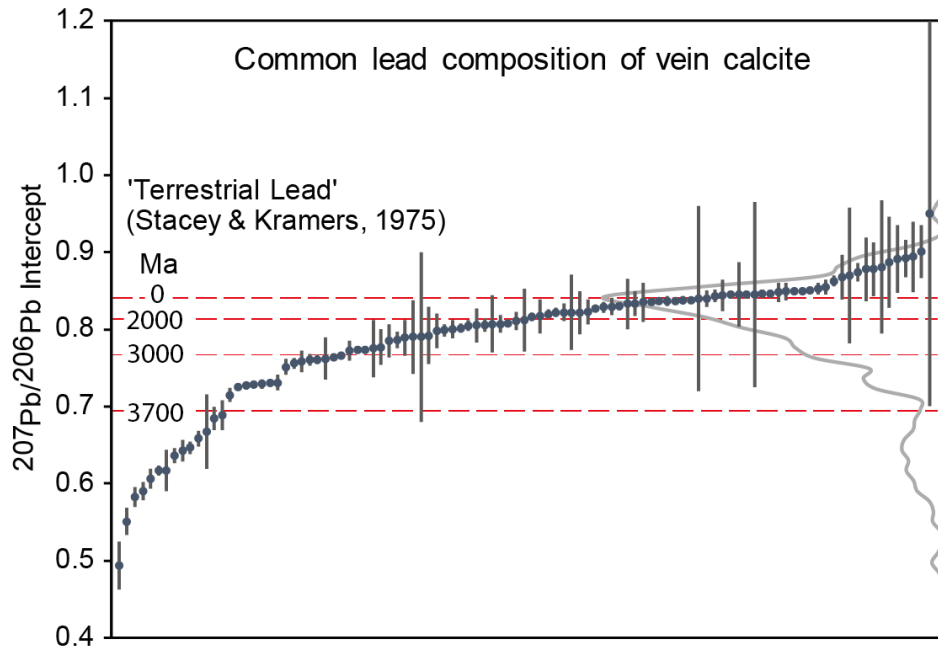


Figure 104. Compilation of upper intercept $^{207}\text{Pb}/^{206}\text{Pb}$ compositions from fracture-fill and diagenetic carbonates in filling calcite, off from samples dated in the British Geological Survey laboratory ($n=12304$). The grey curve is a Kernel Density Estimate showing the distribution of mean compositions. The red bars show the ~~two-stage~~ Stacey and Kramers (1975) compositions of terrestrial lead at present-day, at 0, 2000, 2000 and 3700 Ma. Samples with very large uncertainties in the $^{207}\text{Pb}/^{206}\text{Pb}$ composition are those with very low Pb count-rates.

1145 An additional complexity in interpreting carbonate U-Pb data, is that fine-scale variability in
1146 initial lead compositions may exist. This is because the fluids involved in carbonate
1147 precipitation may vary on very short timescales, with varying fluid-rock interaction leading to
1148 different Pb components being leached into the fluids. The time-scale of varying fluid
1149 involvement may be much shorter than the resolution of the U-Pb data, such that data with
1150 variable initial lead compositions may not be resolvably different in age, and hence, will
1151 merely lead to increased scatter on the U-Pb isochron. Heterogeneous initial lead
1152 compositions can be seen in an example of sandstone-hosted vein material from the Moab
1153 fault, southeast Utah (Figure 11).

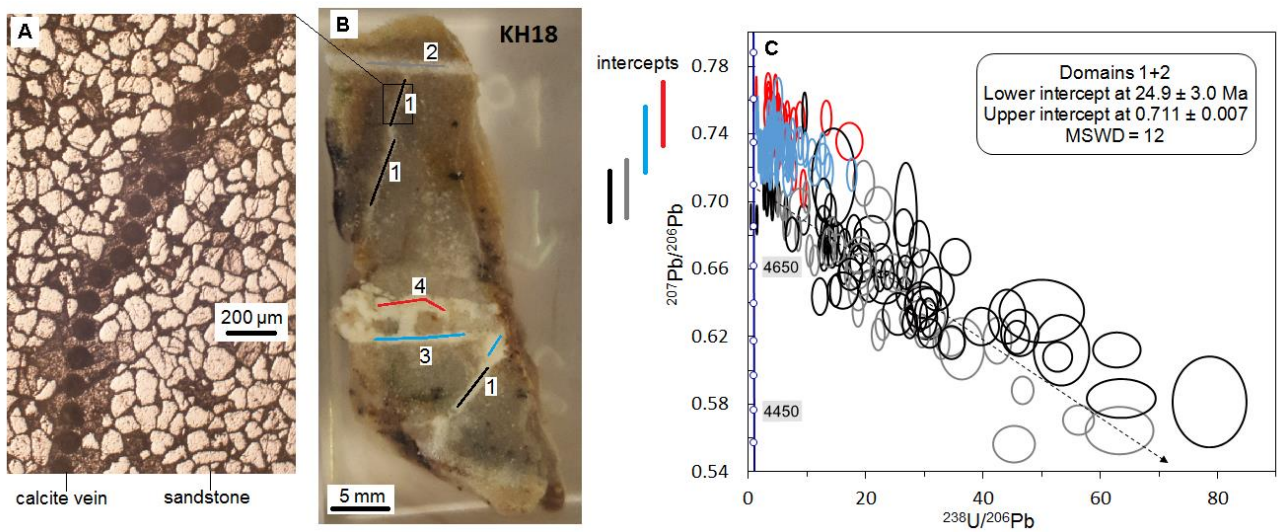
1154 ~~Example G - Moab fault~~

1155 ~~Figure 15 shows results from a sample taken from the Moab fault in southeast Utah, USA.~~
1156 ~~The sample presented here (CHJ15-KH08) is collected from the Courthouse Junction fault~~
1157 ~~segment intersection. This locality has a complex, multi-phase deformation history~~
1158 ~~(Davatzes et al., 2005; Johansen et al., 2005) associated with multiple episodes of~~
1159 ~~mineralization and a range of diagenetic fluids (Chan et al., 2000; Eichhubl et al., 2009;~~
1160 ~~Bergman et al., 2013; Hodson et al., 2016).~~

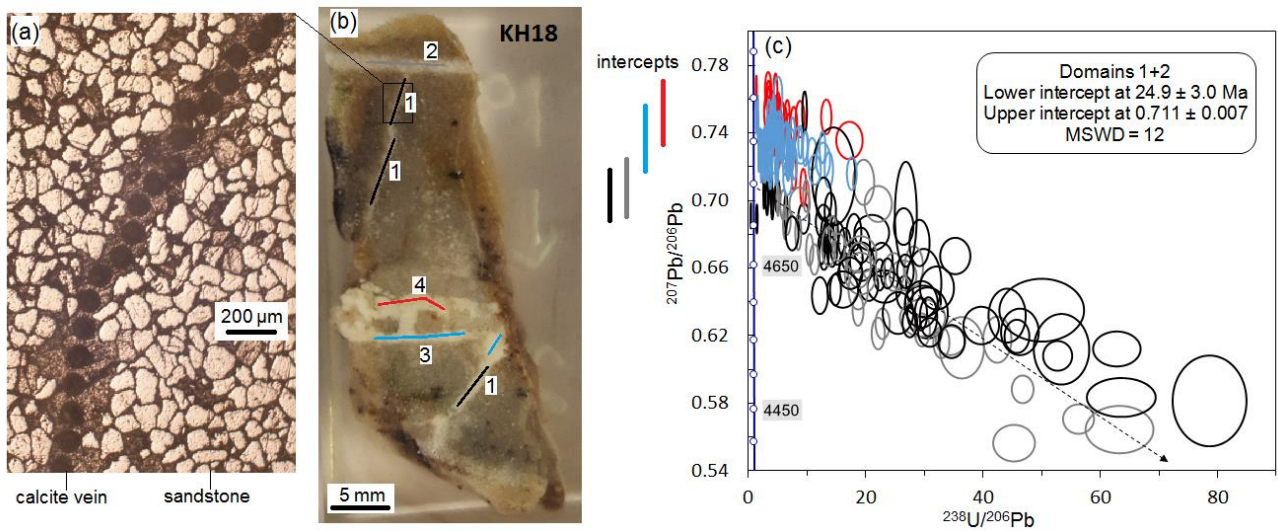
1161
1162
1163 U-Pb data were obtained from different sections of the vein material formed along different
1164 orientations. ~~(See Figure 15).~~ The data exhibit a high level of common/initial lead, with
1165 limited spread in radiogenic lead contents, but still forming a scattered regression to a lower
1166 intercept value. Using different colours to discriminate different sections of vein, it is clear
1167 that they have subtly different initial lead compositions, as indicated by the upper intercept
1168 ($^{207}\text{Pb}/^{206}\text{Pb}$ value) of the data arrays. These lead compositions are more radiogenic
1169 ~~different~~ from that predicted by the Stacey & Kramers (1975) terrestrial composition,
1170 ~~which we find is a common feature of many vein-filling carbonates. This is likely due to the~~
1171 ~~hydrothermal fluids that are precipitating the carbonate comprising unsupported radiogenic~~
1172 ~~lead components derived from leaching of older uraniumiferous minerals or rocks.~~

1173
1174 The existence of variable Pb compositions on small length-scales (<1 mm) means that
1175 careful attention is required to interpret complex data. However, the spatial resolution of LA-
1176 ICP-MS means that these details can potentially be teased out. ~~This case study also shows~~
1177 ~~the potential of the method for measuring veinlets that are only ~150 µm wide (see Figure~~
1178 ~~15), a task that would be difficult for ID analyses.~~

1179



1180



1181

1182 **Figure 15.1.** U-Pb data from a series of calcite veins (sample KH18) along the Moab Fault at
 1183 Courthouse Junction, Utah. **(Aa)** Reflected light image of a region of veining showing the
 1184 100 μm spots; **(bB)** Photomicrograph of the dated sample, with different dated domains of
 1185 veining shown by blue, red, black and grey lines; **(cC)** Tera-Wasserburg plot with U-Pb spot
 1186 data colour-coded to match the different domains. The bars on the left show the variable
 1187 $^{207}\text{Pb}/^{206}\text{Pb}$ upper intercept values for each domain.

1188

1189

1190 In summary, vein-filling, diagenetic and hydrothermal carbonates often do not exhibit Stacy
 1191 & Kramers (1975) model Pb compositions for their assumed age, but typically yield more
 1192 radiogenic compositions. This means that regressions anchored with assumed common
 1193 lead compositions are susceptible to inaccuracy. Mixed common lead compositions in

1194 samples hampers derivation of single age regressions, implying multiple fluid sources.
1195 Mixed ages and atypical lead compositions can also make age mapping problematic.
1196

1197 10.7.2. Dating young material – dealing with disequilibria

1198 As described in Section 3, the younger the age of the sample analysed, the lower the
1199 potential for precise and accurate age determination due to the lack of radiogenic ingrowth
1200 of lead. However, young carbonates are a high priority in many applications, because they
1201 can date events more relevant to the Earth system at present, and because U-Pb can
1202 extend the age range of sample suites or study areas where U-Th age dating is also
1203 feasible. For example, records of environmental change in deep time require the dating of
1204 speleothems that are older than 500 ka (see Woodhead et al., 2012, 2019), and dating of
1205 veins that record seismic cycles extending beyond 500 ka (see Uysal et al., 2011; Williams
1206 et al., 2017) can provide constraints on earthquakes and other hazards associated with
1207 subsurface fractures. These particular applications are likely to require high levels of
1208 precision, i.e. for the Quaternary, of much less than ± 100 ka, and potentially even less than
1209 ± 10 ka or < 1000 years for the Holocene. Achieving such precision requires very high U to
1210 achieve abundant radiogenic lead and higher μ values (see Figure 34).
1211

1212 A major issue for accurate dating of young samples (i.e. < 10 Ma) is the potential effect of
1213 initial daughter isotope disequilibrium within the uranium decay chains. The simplest form of
1214 the U-Pb and Pb-Pb age equations, often used for older samples, assume that all long-lived
1215 daughter isotopes in the U decay chain are initially present in secular equilibrium. Both the
1216 U decay series contain long-lived daughter isotopes, including ^{234}U ($t_{1/2} = 245$ ka), ^{230}Th ($t_{1/2} =$
1217 76 ka), and ^{226}Ra ($t_{1/2} = 1.6$ ka) in the ^{238}U decay chain, and ^{231}Pa ($t_{1/2} = 34$ ka) in the ^{235}U
1218 decay chain. Of these, ^{234}U has the longest half-life and therefore the largest potential
1219 effect on U-Pb dates. The excess initial ^{234}U often observed in natural waters will lead to
1220 generation of unsupported ^{206}Pb . If uncorrected, excess initial ^{234}U produces overestimated
1221 $^{206}\text{Pb}/^{238}\text{U}$ and lower intercept dates. An excess of the other intermediate daughter
1222 products, like ^{230}Th , relative to secular equilibrium will bias the age with a smaller
1223 magnitude but in the same direction, whereas a deficit will result in dates that are too
1224 young.
1225

1226 Carbonates are commonly precipitated from fluids containing $^{234}\text{U}/^{238}\text{U}$ out of secular
1227 equilibrium. Thus, this initial disequilibrium must be considered in any age determination.
1228 Age corrections for initial U daughter deficits are at maximum ~ 1.44 times the half-life of
1229 the daughter isotope for zero initial abundance. But for initial excesses, the age difference
1230 can be many times larger. ~~(see Figure 17)~~. For most older samples dated by U-Pb, the
1231 effect of disequilibrium is deemed to be insignificant compared to larger measurement
1232 uncertainties. For this reason, initial disequilibrium has thus far not been mentioned in any
1233 publication concerning LA-ICP-MS U-Pb dating except for those dealing with young
1234 speleothems (e.g. Hopley et al., 2019). However, here we demonstrate that initial
1235 disequilibrium may be a very significant cause of uncertainty for carbonates precipitated
1236 from groundwater and other crustal fluids, and not just for very young (<1 Ma) samples.
1237

1238 In young samples, particularly those within the range of U-Th geochronology (<600 ka), the
1239 initial $^{234}\text{U}/^{238}\text{U}$ ratio ($^{234}\text{U}/^{238}\text{U}_0$) can be estimated based on the combination of the present-
1240 day measured $^{234}\text{U}/^{238}\text{U}$ ($^{234}\text{U}/^{238}\text{U}_{\text{now}}$), and either the measured $^{230}\text{Th}/^{238}\text{U}$ or the estimated
1241 date of formation. The robustness of this estimate is highly dependent on the precision and
1242 accuracy at which the isotope ratio(s) can be measured (the atom ratio is very small,
1243 making high precision measurement $>1\%$ difficult). In addition, if the offset between
1244 $^{234}\text{U}/^{238}\text{U}_{\text{now}}$ and secular equilibrium is small, then the measurement may overlap secular
1245 equilibrium within uncertainty. For this reason, the highest precision possible is a necessary
1246 target for any disequilibrium correction measurement.
1247

1248 For older samples (i.e. those older than about four times the half-life of ^{234}U), and/or those
1249 with only a small degree of initial disequilibrium, $^{234}\text{U}/^{238}\text{U}_{\text{now}}$ is likely to have reached
1250 secular equilibrium. This means that $^{234}\text{U}/^{238}\text{U}_0$ cannot be estimated from the measured
1251 data alone. One approach to alleviate this problem is to take known initial ratios from
1252 younger samples (<600 ka) formed in approximately the same geologic setting, and apply
1253 these corrections to the older samples from the same setting (e.g. Woodhead et al., 2006,
1254 2019). This approach is only applicable if the geological environment is well known and the
1255 hydrological system believed to be relatively stable.
1256

1257 There are various causes of ^{234}U excess in fluid-mineral systems, which have been studied
1258 at length (e.g. Osmond & Cowart, 1992, 2000; Porcelli & Swarzenski, 2003; Suksi et al.,
1259 2006). In summary, ^{234}U is generated from α decay of ^{238}U , and may preferentially be

1260 increased in the fluid state during mineral-fluid interaction due to oxidation state and
1261 valence differences between the U species (e.g. Suksi et al., 2006). Uranium activity ratios
1262 record information on the redox state of fluids, the source of uranium in the fluids, and
1263 potentially the timing of uranium residence in the fluid; therefore, they have long been a
1264 focus of groundwater studies (e.g. Osmond et al., 1968; Osmond & Cowart, 2000; Porcelli
1265 & Swarzenski, 2003). Of general interest here, is whether carbonates precipitated from
1266 different geological settings are likely to have significant ^{234}U excess such that any
1267 measured $^{238}\text{U}/^{206}\text{Pb}$ dates will be inaccurate.

1268

1269 Cave drip-water that generates speleothem deposits typically has excess ^{234}U relative to
1270 secular equilibrium, although sometimes ^{234}U is depleted. Overall, most cave systems have
1271 initial activity ratios that are not grossly offset from secular equilibrium. This means that an
1272 uncertainty limit can be placed on such carbonates with reasonable confidence.

1273 Disequilibrium corrections will significantly affect age estimates with high precision, but not
1274 the low precision estimates that typically characterise LA-ICP-MS dates. For example,
1275 Woodhead et al. (2019) used an estimate of 1.0 ± 0.3 for $^{234}\text{U}/^{238}\text{U}_0$ in their study of
1276 speleothems from the Nullarbor plain, Australia, and this had negligible impact on the
1277 resultant compilation of U-Pb dates. Hopley et al. (2019) estimated a range of $^{234}\text{U}/^{238}\text{U}_0 =$
1278 1.26 to 2.99 for the 'Cradle of Humankind' in South Africa, with a mean of 1.9, and
1279 discussed a resulting potential age range of 5.8 to 4.8 Ma. A known excursion from 'typical'
1280 activity ratios is the Transvaal Dolomite Aquifer, also in South Africa. Speleothem deposits
1281 in cave systems that interacted with water from this aquifer have anomalously high U
1282 activity ratios ranging from ca. 2 to 12 (Kronfeld et al., 1994). This well-known occurrence
1283 highlights that speleothem deposits could arise from fluids with variable and anomalous
1284 activity ratios, and thus that attention must be given to accurately estimating the $^{234}\text{U}/^{238}\text{U}_0$
1285 when dating such deposits.

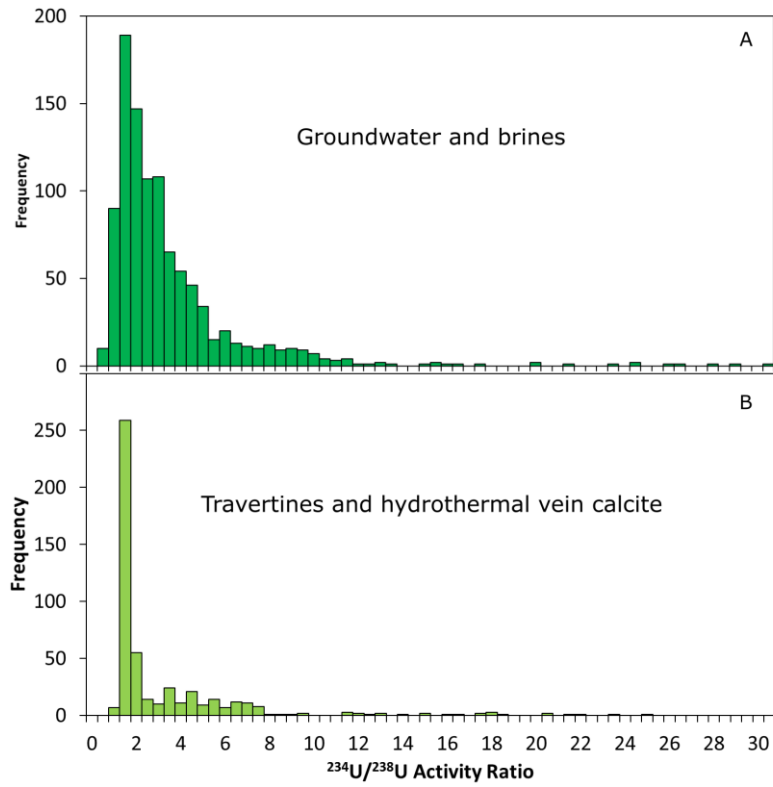
1286

1287 Unfortunately, activity ratio data that is relevant to hydrothermal and other vein-filling
1288 carbonates is sparse and potentially more variable. Carbonates precipitated in the shallow
1289 crust may arise from percolating groundwater, seawater, deep brines, formation waters, or
1290 a mixture of these sources. We can use existing data on these fluid sources to make an
1291 initial estimate of what range may exist in terrestrial carbonates. Groundwater is well known
1292 to have highly variable and significant ^{234}U excess (e.g. Osmond and Cowart, 1976). Figure
1293 [126](#) shows a compilation of $^{234}\text{U}/^{238}\text{U}$ activity ratios taken from a range of literature sources

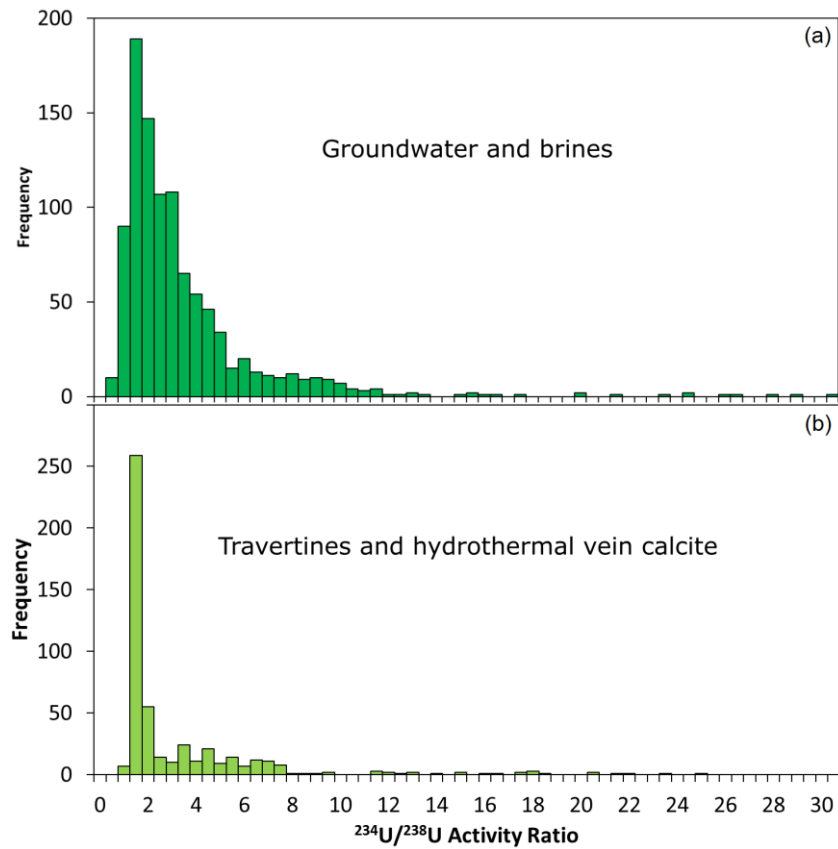
1294 (see supplementary file for sources). The population of data for groundwater (Figure
1295 126Aa), mostly shallow, but including some saline and deeper samples, has a median
1296 activity ratio of 2.25, and is skewed towards higher values, with a significant tail up to ~11.
1297 Data from hydrothermal fluids and deep brines are less abundant in the literature, but can
1298 be estimated from young carbonates precipitated in travertines and hydrothermal veins.
1299 The compilation shown in Figure 126B is dominated byskewed towards samples from
1300 Turkey and surrounding regions.- It has a median of 1.41, and is right-skewed with a tail
1301 ranging up to ~8 and only a few higher values.

1302

1303



1304



1305

1306

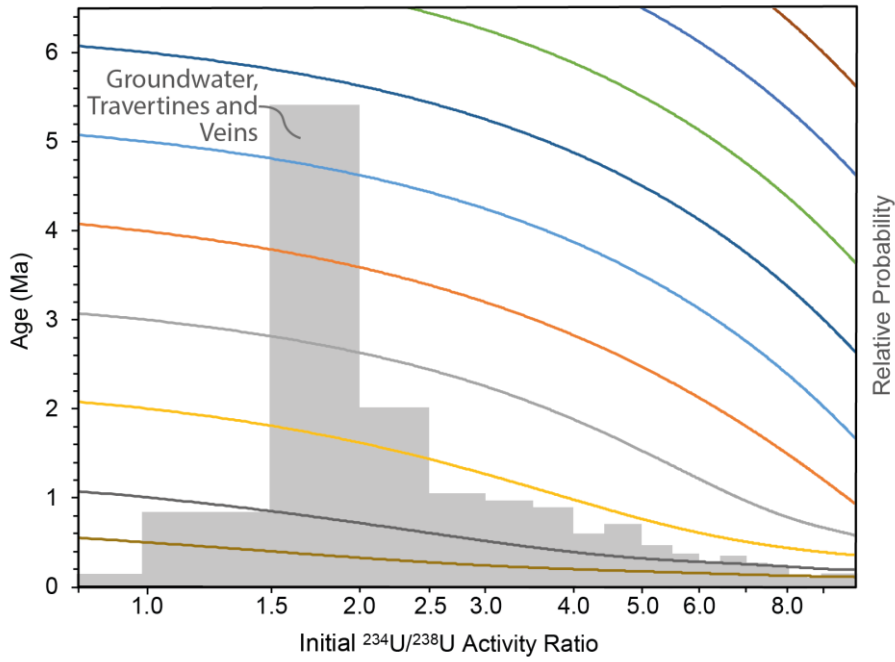
1307

Figure 162. Compilation of uranium $^{234}\text{U}/^{238}\text{U}$ activity ratios from the literature of: (a) groundwater and deep brines - these are present-day $^{234}\text{U}/^{238}\text{U}$ values (note the compilation

1308 is dominated by shallow groundwater rather than brines); and (Bb) travertines and calcite
1309 precipitated in veins, commonly but not exclusively associated with travertines – these are
1310 estimated $^{234}\text{U}/^{238}\text{U}_0$ values.

1311
1312
1313 The compilations in Figure 162 are somewhat alarming, as they suggest that vein-filling
1314 carbonates have a high likelihood of having activity ratios ~~have a high likelihood out of~~
1315 ~~being~~ secular equilibrium (where $^{234}\text{U}/^{238}\text{U} \approx 1$) ~~in vein-filling carbonates~~. The
1316 compilations shown are biased by sampling, so uncertainties on the range of activity ratios
1317 should not be based on these compilations. However, a very conservative view would be
1318 that shallow groundwater $^{234}\text{U}/^{238}\text{U}$ activity ratios average closer to ~2 than they do to ~1;
1319 hydrothermal waters average closer to ~1.5; and permissible values may be extremely out
1320 of secular equilibrium at >10. The data reveal that precise age estimates of young
1321 carbonates derived from crustal fluids are going to be severely hampered by a lack of
1322 knowledge of the U activity ratios.

1323
1324 To demonstrate the effect of initial activity ratios out of secular equilibrium, we have
1325 modelled synthetic data in Figure 173. This figure shows curves representing samples of
1326 ten different ages, which would range from 500 ka to 9 Ma if $^{234}\text{U}/^{238}\text{U}_0$ was in secular
1327 equilibrium (~1) during formation. The true age of the samples get younger as $^{234}\text{U}/^{238}\text{U}_0$
1328 increases. The effect does not decrease in significance as we look at older ages, i.e. the
1329 age offset on a sample with a measured age of 8 Ma is similar to that on a sample of 4 Ma.
1330 The curves are shown on a log scale, because in many systems, the variation in activity
1331 ratio is going to vary a small amount, close to secular equilibrium (~1). For example, in the
1332 Nullarbor plain cave systems, the variation is likely to be within 30% of 1 (Woodhead et al.,
1333 2019). Systems with large variations in initial activity ratios, for example some hydrothermal
1334 systems, would lead to a large uncertainty on the obtained dates. Ignoring the effect of the
1335 likely ^{234}U excess in vein-filling carbonates is likely to lead to significant inaccuracy of dates
1336 by 10s of %, in general by overestimating the age. Considering the impact that
1337 unconstrained initial $^{234}\text{U}/^{238}\text{U}$ ratios have on young dates leads to significant (> 10%)
1338 uncertainties.



1340
 1341
 1342
 1343
 1344
 1345
 1346
 1347
 1348
 1349
 1350
 1351
 1352
 1353
 1354
 1355
 1356
 1357
 1358
 1359
 1360

Figure 173. Curves in different colours showing how an individual $^{206}\text{Pb}/^{238}\text{U}$ age (y-axis) will vary with a change in the initial $^{234}\text{U}/^{238}\text{U}$ activity ratio (x-axis). For example, a sample providing a measured $^{206}\text{Pb}/^{238}\text{U}$ age of 5 Ma will actually have a true age of 3.1 Ma if the initial $^{234}\text{U}/^{238}\text{U}$ is as high as 6. The grey histogram shows the combined compilations of groundwater, travertine and vein data from Figure 162.

1361 So far, the discussion has involved the uncertainties surrounding excess/deficient ^{234}U
1362 during calcite growth. However, there are several other intermediate daughter products in
1363 the uranium decay chains that can pose problems for the accuracy of measured ages; see
1364 Richards et al. (1998) and Woodhead et al. (2006) for previous discussion of these. The
1365 isotope ^{230}Th is a potential consideration in the accuracy of ^{238}U - ^{206}Pb ages. In general,
1366 most speleothem-dating studies assume no initial ^{230}Th in the system, as Th is very
1367 insoluble in water compared to U. Any excess initial ^{230}Th during formation would also result
1368 in artificially old measured ages. ^{231}Pa is another daughter product in the decay chain,
1369 which again, is considered very insoluble, and does not form part of the disequilibrium
1370 corrections at present. ^{226}Ra , another intermediate product, may co-precipitate with U, but
1371 its short half-life of 1.6 ka means it is likely to have little impact on U-Pb ages (Richards et
1372 al., 1998). A final concern is the gas ^{222}Rn , as this may be lost from the system by diffusive
1373 processes. A study into the effect of this showed negligible impact on the ^{238}U - ^{206}Pb ages of
1374 a Quaternary speleothem (Richards et al., 1998).

1375
1376 Although the effects of disequilibrium in these shorter-lived intermediate daughter products
1377 is considered to be minor, and likely within the uncertainty of measured LA-ICP-MS U-Pb
1378 dates, it is worth noting that hydrological systems outside of those concerning speleothems
1379 and meteoric water have not been explored. Most of the issues presented here, particularly
1380 the excess ^{234}U problem, are part of the ^{238}U decay chain, and thus have implications for
1381 $^{238}\text{U}/^{206}\text{Pb}$ and lower intercept ages. The ^{235}U decay chain has different intermediate
1382 daughter products, and thus measured $^{235}\text{U}/^{207}\text{Pb}$ and lower intercept ages will be affected
1383 by a different set of processes. The problem of excess ^{234}U is alleviated if ^{235}U - ^{207}Pb ages
1384 can be used instead of ^{238}U - ^{206}Pb ages. However, there have been few attempts to utilise
1385 ^{235}U - ^{207}Pb dates (e.g. Hopley et al., 2019) because the low abundances of these isotopes in
1386 comparison to ^{238}U and ^{206}Pb are major limitations on the uncertainty of the measurements.
1387 Engel et al. (2019) have provided a solution that will potentially increase the accuracy of
1388 age estimates for speleothems, utilising the ^{235}U decay chain, as well as using ^{208}Pb in
1389 place of ^{204}Pb as the initial lead composition. This approach is based on ID, and it is unclear
1390 how effective it will be for LA-ICP-MS dating, given that ^{204}Pb is difficult to measure at high
1391 precision.

1392
1393 In summary, initial disequilibrium is clearly a major issue for the accuracy of U-Pb dating of
1394 carbonates. The effect is significant for material of any age, but as we get to older

1395 carbonates, the analytical uncertainty contributions will begin to swamp the uncertainties
1396 surrounding disequilibrium. For dating of Neogene-Quaternary carbonates, prior knowledge
1397 of likely activity ratios (e.g. by measuring younger or present-day values of the precipitating
1398 fluid, and inferring no change back in time) is critical for precise and accurate dates. The
1399 variation in hydrothermal systems that mix meteoric water with older brines is likely to be
1400 large in terms of the degree of ^{234}U excess. More information is needed to further
1401 understand what sort of values can be expected in different systems and different settings.
1402 From our preliminary compilation, it is apparent that ^{234}U excess is the norm, rather than the
1403 exception. For now, the absolute values and uncertainties on young dates (late Neogene to
1404 Quaternary) with no estimation of the initial disequilibria should be treated with caution.

1405

1406 [41-7.3.](#) Dating old material – dealing with a potentially open system

1407 Many early carbonate dating studies were attempted on very old material, i.e. Proterozoic
1408 and Archaean (e.g. Moorbath et al., 1987; Jahn, 1998; Taylor and Kalsbeek, 1990;
1409 Whitehouse and Russell, 1997); these mostly utilised Pb-Pb dating. A major issue of the
1410 Pb-Pb method, is that Pb contents of crustal fluids are much higher than that of the primary
1411 carbonates, and therefore, even small amounts of fluid-related alteration can dominate the
1412 measured Pb-Pb composition and lead to an age that is not representative of primary
1413 carbonate precipitation (e.g. Sumner & Bowring, 1996). Although there have been a handful
1414 of studies dating old carbonate material since the 1990s (e.g. Ray et al., 2003; Sarangi et
1415 al., 2004; Babinski et al., 2007; Fairey et al., 2013), Pb-Pb and U-Pb dating of Precambrian
1416 material have become rarely used techniques. This is presumably due to the difficulty in
1417 obtaining meaningful primary ages of old material. The dominant reason for this difficulty
1418 can generally be distilled down to open-system behaviour, i.e. dating material that has
1419 remained a closed isotopic system since its formation is increasingly difficult with
1420 increasingly older material. This is simply because thermal- and/or fluid-induced mobility of
1421 parent and daughter isotopes becomes increasingly likely if the material has been exposed
1422 to multiple deformation-, burial-, uplift-, glaciation-, weathering- or fracture-related events.

1423

1424 Early studies documented various transformative processes and their impact on Pb-Pb/U-
1425 Pb isotope systematics, e.g. fluid infiltration in limestone (Smith et al., 1991), diagenetic
1426 change from aragonite to calcite (Jones et al., 1995), and resetting of Pb isotope signatures
1427 during metamorphism (Russell et al., 1996; Whitehouse and Russell, 1997; Babinski et al.,

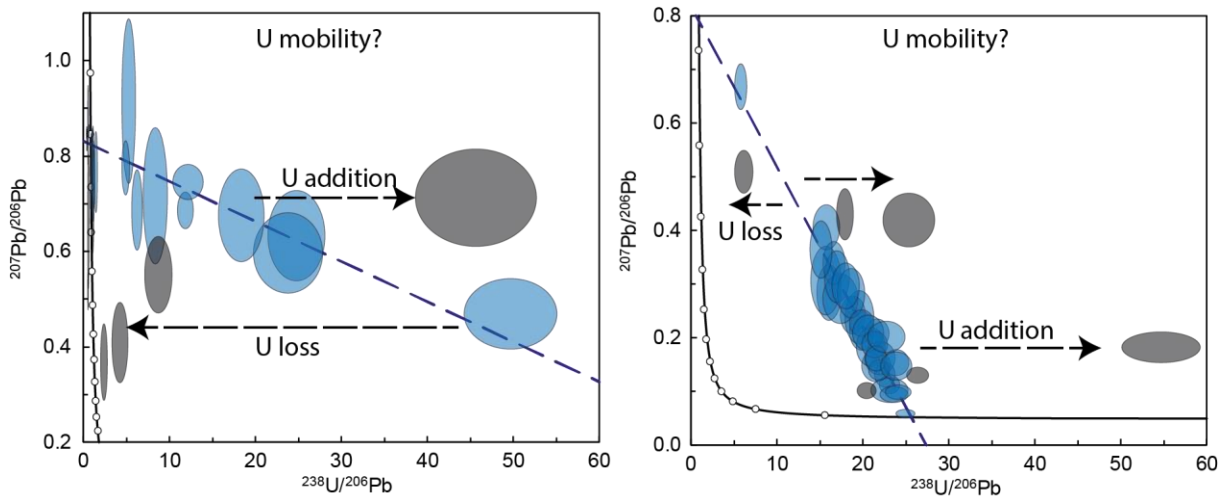
1428 1999). In general, the existence of some form of open-system behaviour within a given
1429 dataset has only been recognised through the isotopic data themselves, not through an
1430 independent dataset. This is simply achieved by assessing the robustness of the Pb-Pb or
1431 U-Pb data array with mathematical means, e.g. using the MSWD value, and explaining
1432 analytical scatter outside of a robust array as due to open system behaviour. With *in situ*
1433 methods, the approaches that we have described in Section 5 may allow for some
1434 independent removal of data that pertains to open-system behaviour, leaving a dataset that
1435 corresponds to a closed system.

1436
1437 A method that has been utilised to screen for altered samples in whole-rock geochemistry,
1438 is to test for effects of modern weathering using $^{234}\text{U}/^{238}\text{U}$ ratios (Albut et al., 2019). Ancient
1439 samples should have measured $^{234}\text{U}/^{238}\text{U}$ activity ratios in ~~in~~ secular equilibrium, and
1440 departure from this in a measured sample would imply a more recent addition or subtraction
1441 of ^{234}U through weathering processes, indicating some modern fluid-rock interaction. This
1442 method of sample screening has not been applied to U-Pb dating, but we suggest is worthy
1443 of investigation.

1444
1445 In Figure [45](#) we documented various U-Pb datasets to demonstrate the range of behaviour
1446 that is seen with natural carbonates. Here we provide some additional comments regarding
1447 open-system behaviour, first in terms of U mobility, followed by that of Pb mobility. Uranium
1448 is mobile in oxidising fluids, so U enrichment and depletion relative to Pb is assumed to be
1449 the most common cause of open-system behaviour that will occur in natural carbonates. In
1450 Tera-Wasserburg space ($^{238}\text{U}/^{206}\text{Pb}$ vs. $^{207}\text{Pb}/^{206}\text{Pb}$), U mobility will be apparent as sub-
1451 horizontal trends in the data, with movement to the right reflecting gain of ^{238}U , and
1452 movement to the left reflecting loss of ^{238}U (see Figure [148](#)). During a period of mobility,
1453 uranium may move into a fluid-phase, such that the remaining carbonate solid remains
1454 variably depleted in ^{238}U , or, uranium may partially move from its original location to another
1455 within the measured sample volume. In the former, this can sometimes be detected from
1456 the isotopic data if a distinct departure from a robust regression is defined by a sub-
1457 horizontal array (see Figures [45d and 18](#)). In the latter case of uranium mobility, some
1458 domains will be depleted, whereas others will be enriched. This may be difficult to ascertain
1459 from the isotopic data alone if the mobility is pervasive through the material, because the
1460 induced scatter in the U-Pb regression (from both positive and negative movement in

1461 $^{238}\text{U}/^{206}\text{Pb}$) cannot be resolved from other causes of scatter, such as mixing between
1462 different age domains.

1463



1464

1465 *Figure 184. Tera-Wasserburg plots for LA-ICP-MS U-Pb data from two slicken-fibre calcite*
1466 *samples that exhibit potential open system behaviour caused by U mobility. Vectors for U*
1467 *loss and gain are schematic. Evidence for such U mobilisation requires additional lines of*
1468 *evidence that are currently lacking.*

1469

1470 Lead can substitute for Ca in the calcite lattice, and is also insoluble in most upper crustal
1471 fluids, for these reasons, U mobility is generally considered in favour of Pb mobility. Fluid-
1472 assisted mobility of U is certainly the most likely cause of open system behaviour because
1473 of the solubility of some U species. However, at high temperatures, solid-state diffusion is
1474 also a factor ~~of~~ for consideration. Based on experimental data, Pb diffusion in calcite is
1475 essentially slow enough to be non-existent below 300°C (when considering the composition
1476 of a grain 1 mm in diameter; Cherniak, 1997); however, at higher temperatures (>400°C),
1477 diffusion of lead is possible if encountered for long periods (> 20 Myrs). Empirical
1478 observations of Pb (or U) diffusion in calcite are lacking. Diffusion is unlikely in the low
1479 temperature calcites that have formed the basis of most modern LA-ICP-MS dating studies;
1480 however, carbonates form in a range of higher temperature environments as well, such as
1481 alteration veins within deeply subducted crust. Understanding how the calcite U-Pb system
1482 works at medium to high-metamorphic grades may therefore become very relevant
1483 information, allowing this chronometer to be used to understand dates and rates in deep
1484 crustal environments.

1485

1486 7.4. Analytical limitations

1487 At present, there is only one reference material in circulation that has been widely used and
1488 documented for the purpose of U-Pb normalisation (WC-1; Roberts et al., 2017). WC-1 has
1489 an uncertainty on its U/Pb ratio of 2.5% 2σ . Using this material for normalisation of U/Pb
1490 ratios, or for validation of the method accuracy, limits the final age uncertainty of any
1491 particular sample to $\sim 2.5\%$. To improve beyond this range requires the characterisation of
1492 natural (or production and characterisation of U and Pb doped synthetic) materials, with a
1493 final U/Pb precision better than 2.5%. There is also a requirement for additional well
1494 characterised materials (i.e. those with robust U-Pb systematics and well documented ID U-
1495 Pb datasets) that can be used as secondary reference materials (i.e. those run as
1496 unknowns), for assessment of accuracy and long-term reproducibility.

1497
1498 Another major limitation is the nature of carbonate matrices, and the lack of quantified data
1499 on the matrix effect between different carbonate minerals and structures. Inter-element
1500 fractionation (i.e. U/Pb in this case) is one of the major limitations on the reproducibility and
1501 accuracy of laser ablation U-Pb dating. For this reason, matching matrices of the reference
1502 material with that of the sample has been standard practise in U-bearing accessory mineral
1503 geochronology. Several groups have tried to limit the effect of this issue by utilising
1504 normalisation and data reduction procedures that reduce the effect (e.g. Burn et al., 2017;
1505 Neymark et al., 2018), but regardless of the matrix used for normalisation, validation of the
1506 method should still utilise a similar matrix to the sample. Carbonates clearly have a large
1507 range of structures, even with calcite, for example, sparry to micritic, with wide-ranging
1508 crystal/grain-sizes and porosity. Nuriel et al. (2019) noted differences between the use of
1509 coarse-grained sparry reference materials to fine-grained polycrystalline reference
1510 materials, with the latter being skewed towards older ages by several percent. To move
1511 towards better precision and accuracy of the LA-ICP-MS U-Pb method, it will be necessary
1512 to have a range of well characterised reference materials that cover variable carbonate
1513 mineralogy (e.g. aragonite, dolomite, calcite), as well as internal morphology and texture.

1514
1515
1516 **12. Discussion**

1517 ~~LA-ICP-MS U-Pb carbonate geochronology has been demonstrated by this and previous~~
1518 ~~studies, to offer a potentially robust technique to date the timing of carbonate mineral~~

1519 formation. Limitations on the technique arise from several challenges. These include the
1520 typically low U content of carbonates in many settings, the propensity for carbonate to
1521 include significant concentrations of Pb upon formation, and the ease with which fluids can
1522 alter or reprecipitate mineral growth. LA-ICP-MS is an *in situ* technique, with high spatial
1523 resolution compared to physical sampling for bulk dissolution studies, which enables many
1524 of the hurdles in carbonate geochronology to be overcome. Rare and localised high U
1525 domains can be located and sampled, a range of U/Pb ratios can be targeted to generate a
1526 spread in isochron regressions, and altered domains, inclusions and secondary
1527 mineralisation can often be avoided.

1528
1529 Accurate and informative U-Pb carbonate geochronology demands careful imaging and
1530 petrographic analysis to establish a link between date and process. Various imaging
1531 techniques can be utilised prior to or after dating to aid with mineral characterisation, and
1532 with refinement and interpretation of the resulting age data. We refer to this as image-
1533 guided analysis. An alternative technique involves directly determining age data from
1534 image-based data itself, which we refer to as image-based analysis. Both techniques have
1535 their different benefits and applicability, and their efficacy depends on the instrumentation
1536 used and the type of material; for example, quadrupole ICP-MS is suited to image-based
1537 analysis, as a large element suite can be measured. Limitations on using quadrupole
1538 instrumentation are the detection limits for U and Pb when counting a large suite of
1539 elements. In contrast, multi-collector instruments can be used for image-based analysis,
1540 and have a very low detection limit, but the mass range is restricted between Hg and U,
1541 meaning that additional elements useful for understanding the U and Pb distribution cannot
1542 be measured simultaneously. Overall, image-based analysis is only nascent in
1543 geochronology, and as such has not been fully explored.

1545 12.1. Limitations

1546 There are several limitations to LA-ICP-MS U-Pb carbonate geochronology. The
1547 heterogeneous nature of carbonate materials pose a problem that is difficult to circumvent.
1548 The relatively high spatial resolution of laser ablation already offers the best solution to this
1549 problem, but detection limits and the very low U and Pb contents mean that spots $>150\ \mu\text{m}$
1550 are commonly employed, hampering the full ability of laser ablation to target fine-scale ($<50\ \mu\text{m}$)
1551 zonation. Improvements in efficiency of ICP-MS instrumentation and of the ablation
1552 process are possible solutions to this issue.

1553

1554 At present, there is only one reference material in circulation that has been widely used and
1555 documented for the purpose of U-Pb normalisation (WC-1; Roberts et al., 2017). WC-1 has
1556 an uncertainty on its U/Pb ratio of 2.5% 2σ . Using this material for normalisation of U/Pb
1557 ratios, or for validation of the method accuracy, limits the final age uncertainty of any
1558 particular sample to ~2.5%. To improve beyond this range requires the characterisation of
1559 natural (or production and characterisation of U and Pb doped synthetic) materials, with a
1560 final U/Pb precision better than 2.5%. There is also a requirement for additional well
1561 characterised materials (i.e. those with robust U-Pb systematics and well documented ID U-
1562 Pb datasets) that can be used as secondary reference materials (i.e. those run as
1563 unknowns), for assessment of accuracy and long-term reproducibility.

1564

1565 Another major limitation is the nature of carbonate matrices, and the lack of quantified data
1566 on the matrix effect between different carbonate minerals and structures. Inter-element
1567 fractionation (i.e. U/Pb in this case) is one of the major limitations on the reproducibility and
1568 accuracy of laser ablation U-Pb dating. For this reason, matching matrices of the reference
1569 material with that of the sample has been standard practise in U-bearing accessory mineral
1570 geochronology. Several groups have tried to limit the effect of this issue by utilising
1571 normalisation and date reduction procedures that reduce the effect (e.g. Burn et al., 2017;
1572 Neymark et al., 2018), but regardless of the matrix used for normalisation, validation of the
1573 method should still utilise a similar matrix to the sample. Carbonates clearly have a large
1574 range of structures, even with calcite, for example, sparry to micritic, with wide-ranging
1575 crystal/grain-sizes and porosity. Nuriel et al. (2019) noted differences between the use of
1576 coarse-grained sparry reference materials to fine-grained polycrystalline reference
1577 materials, with the latter being skewed towards older ages by several percent. To move
1578 towards better precision and accuracy of the LA-ICP-MS U-Pb method, it will be necessary
1579 to have a range of well characterised reference materials that cover variable carbonate
1580 mineralogy (e.g. aragonite, dolomite, calcite), as well as internal morphology and texture.

1581

1582 12.2.8. Applications of carbonate geochronology

1583 To date, LA-ICP-MS U-Pb carbonate geochronology has been utilised for applied to a wide
1584 range of applications. These include the dating of speleothem deposition (Hopley et al.,
1585 2019; Scardia et al., 2019; Nicholson et al., 2020), brittle deformation (Roberts & Walker,

1586 2016; Ring & Gerdes, 2016; Goodfellow et al., 2017; Hansman et al., 2018; Parrish et al.,
1587 2018; Beaudoin et al., 2018; Nuriel et al., 2017, 2019; Smeraglia et al., 2019), hydrocarbon
1588 migration (Holdsworth et al., 2019, [2020](#)), hydrothermal ore mineralisation (Burisch et al.,
1589 2017, 2019), hydrothermal [and deep crustal](#) fluid flow ([Drake et al., 2017, 2019, 2020](#);
1590 Mazurek et al., 2018; Walter et al., 2018; Incerpi et al., 2019; MacDonald et al., 2019),
1591 pedogenesis (Methner et al., 2016; Liivamägi et al., 2019), ocean crust alteration (Coogan
1592 et al., 2016), diagenesis in sedimentary deposits (Li et al., 2014; Pagel et al., 2018;
1593 Mangenot et al., 2018; Godeau et al., 2018; Lawson et al., 2018) and sedimentary
1594 deposition (Drost et al., 2018). Published dates range in age from 0.6 to 548 Ma (see
1595 Figure [195](#)), MSWDs range from 0.2 to 89 (Figure [195a](#)), and quoted uncertainties range
1596 from 0.6 to 143 % (2s; Figure [15b9B](#)). The majority of dated samples so far range from the
1597 Neogene to Jurassic, with ~50% being Oligocene or younger. Across this age range, the
1598 uncertainty is variable and uncorrelated to age or MSWD, demonstrating that the age
1599 uncertainty reflects an interplay of factors, and includes the heterogeneous nature of
1600 carbonate materials. It should be noted however, that many dates with large uncertainties
1601 or mixed results are likely unpublished, biasing this compilation towards successful
1602 samples. For example, it is possible that many unreported and failed attempts at dating
1603 samples that are Palaeozoic and older have been made. [We also note that many samples](#)
1604 [have reported age uncertainties better than the WC-1 RM, indicating that the systematic](#)
1605 [uncertainties have not been fully incorporated for these dates.](#)
1606
1607

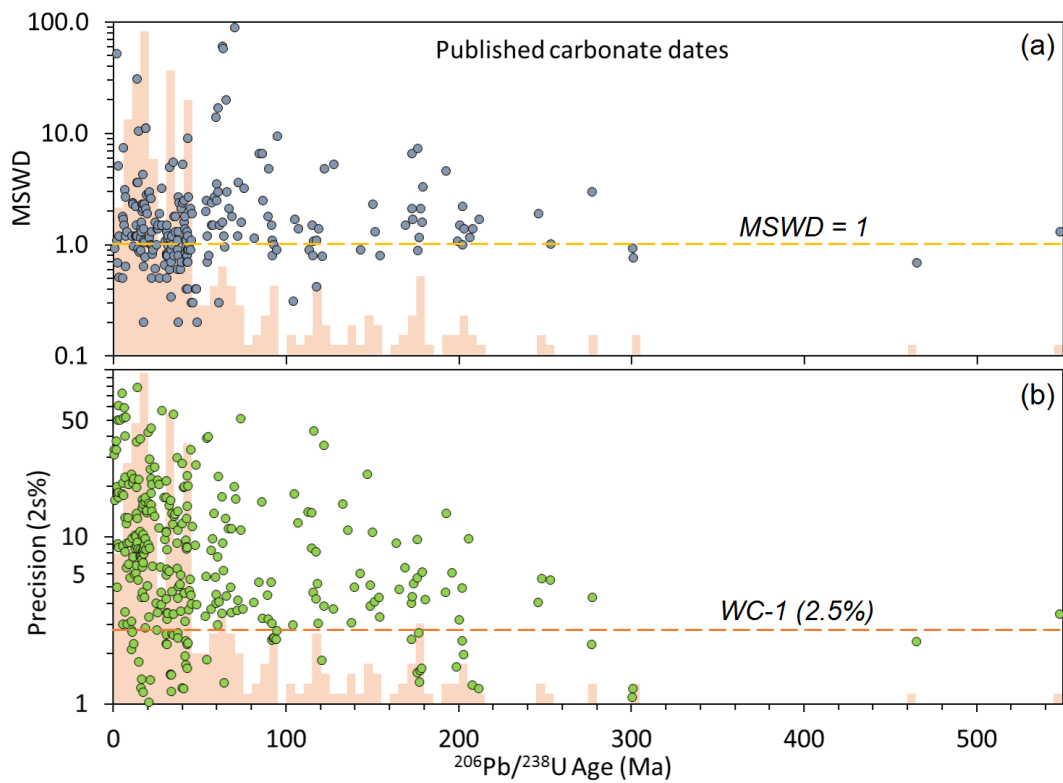
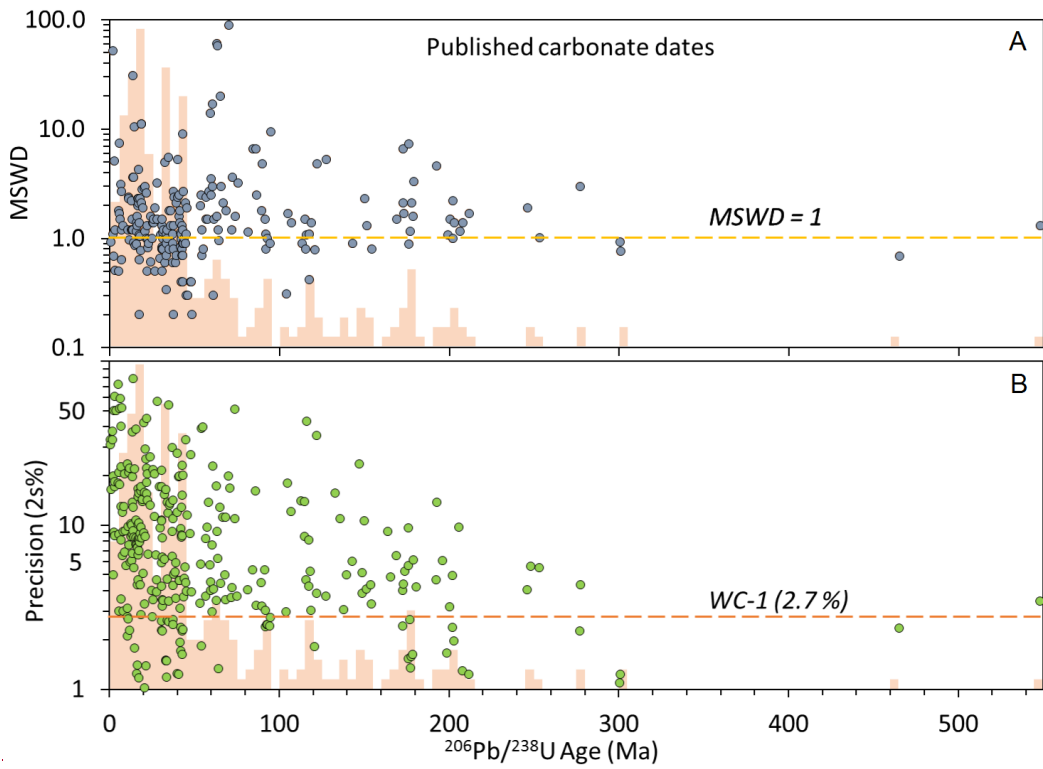


Figure 195. Compilation of published LA-ICP-MS U-Pb dates of carbonate ($n=318$). A) MSWD plotted against $^{206}\text{Pb}/^{238}\text{U}$ age; and B) Precision as 2s % plotted against $^{206}\text{Pb}/^{238}\text{U}$ age. The histograms in the background show the distribution of dates.

1615 A major benefit of carbonate geochronology is that carbonate minerals ~~provide record~~ an
1616 archive of data that can be linked to the age of formation. Fluid inclusions, stable isotopes
1617 (carbon and oxygen), radiogenic isotopes (strontium), and elemental compositions all
1618 reveal insight into the fluid composition that precipitated the mineral. This combination has
1619 long been an approach within the field of palaeohydrology; however, the timing of
1620 mineralisation and hence fluid-flow has generally involved only relative estimates with large
1621 uncertainties, or the dating of phases associated with higher-temperature activity (e.g., Re-
1622 Os dating of Molybdenite). The addition of absolute chronological information is a critical
1623 step to understand the timing of fluid-flow through the crust in a range of settings, for
1624 example, within hydrocarbon-bearing basins, within ore-forming mineral systems, and
1625 within upper crustal bedrock that may be used to host anthropogenic waste/outputs (e.g.
1626 radioactive waste, storage and sequestration of CO₂).

1627

1628 A benefit of utilising LA-ICP-MS as a method of dating, is that the same crystals that have
1629 been dated can be measured for various other chemical proxies and signatures. Several
1630 previous studies have combined fluid inclusions and/or stable carbon and oxygen isotope
1631 analysis with LA-ICP-MS dating (e.g. Mangenot et al., 2018; Pagel et al., 2018; Goodfellow
1632 et al., 2016; Walter et al., 2018), but for most of these, it is not clear if the same volume of
1633 material, or simply the same genetic domain has been sub-sampled for both the dating as
1634 well the additional isotope analyses. Use of petrography and imaging allows for the same
1635 genetic domain to be analysed for several methods; however, there are also several
1636 approaches that allow for an overlapping analytical volume to be analysed. Dated material
1637 can be micro-drilled or -milled following laser ablation, with the powder being analysed for
1638 additional chemical information (e.g. Sr, C, O isotopes). Alternatively, thin sections or
1639 polished blocks can be analysed using a combination of in situ techniques, for example, ion
1640 microprobe measurement of stable isotope and/or elemental compositions, and laser
1641 ablation measurement of Sr isotopes, elemental compositions along with U-Pb dating.

1642 Drake et al. (2017, [2019](#), [2020](#)) demonstrated the utility of combining ion microprobe stable
1643 carbon and oxygen isotope analysis with U-Pb dating to study palaeohydrology and ancient
1644 microbial activity.

1645

1646 In addition to traditional carbon and oxygen isotope measurements ($\delta^{13}\text{C}$ and $\delta^{18}\text{O}$),
1647 clumped isotopes ($\Delta 47$) can provide the temperature of mineral formation (e.g. Eiler, 2007).
1648 Several studies have demonstrated the combination of clumped isotope thermometry with

1649 dating (e.g. Quade et al., 2018; Mangenot et al., 2018; Lawson et al., 2017; MacDonald et
1650 al., 2019). These apply the technique to the dating of paleosols for climatic records,
1651 diagenetic mineralisation for basin histories, and hydrothermal veins to understand crustal
1652 fluid-flow. This combination of techniques is a clear growth area with a range of applications
1653 across earth and environmental science.

1654
1655 Finally, carbonates also comprise a host of major and trace metals that offer further isotopic
1656 information that has yet to be fully explored, for example, stable isotopes of Ca, Zn, Fe, and
1657 Cu. Linking these with U-Pb dates from the same material could provide high resolution
1658 records of natural fractionation processes in subsurface environments.

1660 **9. Conclusions**

1661 LA-ICP-MS U-Pb carbonate geochronology has been demonstrated by this and previous
1662 studies, to offer a potentially robust technique to date the timing of carbonate mineral
1663 formation. Limitations on the technique arise from several challenges. These include the
1664 typically low U content of carbonates in many settings, the propensity for carbonate to
1665 include significant concentrations of Pb upon formation, and the ease with which fluids can
1666 alter or reprecipitate mineral growth. LA-ICP-MS being an *in situ* technique, with high
1667 spatial resolution compared to physical sampling for bulk dissolution studies, enables many
1668 of the hurdles in carbonate geochronology to be overcome.

1669
1670 Accurate and informative U-Pb carbonate geochronology demands careful imaging and
1671 petrographic analysis to establish a link between date and process. Various imaging
1672 techniques can be utilised prior to or after dating to aid with mineral characterisation, and
1673 with refinement and interpretation of the resulting age data. We refer to this as image-
1674 guided analysis. An alternative technique involves directly determining age data from
1675 image-based data itself, which we refer to as image-based analysis. Both techniques have
1676 their different benefits and applicability, and their efficacy depends on the instrumentation
1677 used and the type of material; for example, quadrupole ICP-MS is suited to image-based
1678 analysis, as a large element suite can be measured. Limitations on using quadrupole
1679 instrumentation are the detection limits for U and Pb when counting a large suite of
1680 elements. In contrast, multi-collector instruments can be used for image-based analysis,
1681 and have a very low detection limit, but the mass range is restricted between Hg and U,

1682 meaning that additional elements useful for understanding the U and Pb distribution cannot
1683 be measured simultaneously. Overall, image-based analysis is only nascent in
1684 geochronology, and as such has not been fully explored.

1685
1686 Limitations on the accuracy of ages and their interpretation, comes from several sources.
1687 Variability in initial lead composition needs to be acknowledged when interpreting complex
1688 U-Pb data, and carbonates commonly have initial compositions that are different to that
1689 predicted by model estimates, e.g. Stacey & Kramers (1975). Disequilibrium in the U-Pb
1690 decay chains is typically only explored in very young samples (<1 Ma), but can have a
1691 potentially significant effect on the accuracy of ages throughout the Quaternary to Neogene.
1692 The variability in U isotope ratios in natural waters is a cause for concern in dating young
1693 material, and indicates that more work to understand the natural variability that can be
1694 expected in carbonate precipitates is required.

1695
1696 Limitations on the technique arise from several challenges. These include the typically low
1697 U content of carbonates in many settings, the propensity for carbonate to include significant
1698 concentrations of Pb upon formation, and the ease with which fluids can alter or
1699 reprecipitate mineral growth. LA-ICP-MS is an *in situ* technique, with high spatial resolution
1700 compared to physical sampling for bulk dissolution studies, which enables many of the
1701 hurdles in carbonate geochronology to be overcome. Rare and localised high U domains
1702 can be located and sampled, a range of U/Pb ratios can be targeted to generate a spread in
1703 isochron regressions, and altered domains, inclusions and secondary mineralisation can
1704 often be avoided.

1705
1706 **13.** Accurate and informative U-Pb carbonate geochronology demands careful imaging
1707 and petrographic analysis to establish a link between date and process. Various imaging
1708 techniques can be utilised prior to or after dating to aid with mineral characterisation, and
1709 with refinement and interpretation of the resulting age data. We refer to this as image-
1710 guided analysis. An alternative technique involves directly determining age data from
1711 image-based data itself, which we refer to as image-based analysis. Both techniques have
1712 their different benefits and applicability, and their efficacy depends on the instrumentation
1713 used and the type of material; for example, quadrupole ICP-MS is suited to image-based
1714 analysis, as a large element suite can be measured. Limitations on using quadrupole
1715 instrumentation are the detection limits for U and Pb when counting a large suite of

elements. In contrast, multi-collector instruments can be used for image-based analysis, and have a very low detection limit, but the mass range is restricted between Hg and U, meaning that additional elements useful for understanding the U and Pb distribution cannot be measured simultaneously. Overall, image-based analysis is only nascent in geochronology, and as such has not been fully explored.

~~We have demonstrated the heterogeneous nature of carbonate minerals, in terms of U and Pb distribution and isotopic systematics. Although we have focused on vein-filling calcite, most of the issues highlighted in this paper are relevant to other carbonate dating applications. Various imaging techniques can be used to screen material, and to characterise U-Pb heterogeneity; a combination of these techniques is crucial to understand what exactly has been dated. Linking age information to spatial data, imagery or elemental maps, is crucial to understanding heterogeneous isotopic data. Two main approaches to dating have been presented, the traditional approach of static spot ablations guided by independent image data, and an alternative approach of age mapping using software analysis of 2D isotopic map data. Each of these approaches have benefits and drawbacks, and the choice between them will partly be governed by the instrumentation available.~~ The applications of carbonate U-Pb geochronology are vast, with a key benefit to the laser ablation approach being that specific volumes of material can be analysed for several isotopic and elemental proxies and signatures, whilst also providing absolute chronological information. The LA-ICP-MS method is limited by factors that include the uncertainties on reference material isotope ratios, matrix effects and long-term reproducibility; taking these into consideration, the method is best applied to applications where age uncertainties of greater than 3-4% are of benefit. For applications where high precision (i.e. <1%) is required, such as calibration of palaeoclimate records or of evolutionary change, then follow-up analysis with ID is the only method that can potentially achieve the necessary precision. The future of the method in terms of accuracy and precision requires well characterised (by Isotope Dilution methods) reference materials covering a range of carbonate matrices. The range of studies published over the last five years (2014 to 2019) have revealed a wide array of geoscience applications that are both amenable to, and benefit from, LA-ICP-MS U-Pb carbonate geochronology.

1747 **14.10. Acknowledgements**

1748 The authors acknowledge the Natural Environment Research Council for National
1749 Capability funding of the National Environment [al](#) Isotope Facility. ~~N Roberts, D Condon, M~~
1750 ~~Horstwood, A Milodowski and R Haslam publish with the permission of the Executive~~
1751 ~~Director of the British Geological Survey.~~ D Chew and K Drost acknowledge a Science
1752 Foundation Ireland grant (15/IA/3024) that is partly funded by the Geological Survey of
1753 Ireland and the Environmental Protection Agency, Ireland. HD acknowledges Swedish
1754 Research Council grant (2017-05186) and Formas grant (2017-00766). NR thanks Jeremy
1755 Rushton for continued support and interest in sample petrography, Joe Emmings for help
1756 with R, and Troy Rasbury, Randy Parrish and Chris Smith for discussion and
1757 encouragement during the 'early years' of carbonate dating at the BGS.

1761 **15.11. Appendix**

1762 15.1.11.1. Implications of age data

1763 The focus of this paper is not on the meaning of the age data presented, or its implications
1764 for faulting or fluid-flow; however, we provide brief information for interested readers.

1766 11.1. Figure 7a and 7b - Faroe Island brittle faults

1767 The significance of the Eocene ages has been discussed by Roberts & Walker (2016). This
1768 paper was the first to demonstrate the applicability of LA-ICP-MS U-Pb carbonate
1769 geochronology to dating brittle structures in the upper crust.

1771 15.2.11.2. Figure 7c Example and 9 A and D - Variscan-related veins in the 1772 Northumberland Basin

1773 The age of ca. 287 Ma for the dated calcite crystal can be linked to deformation of the host
1774 rock based on the vein structure. The calcite is taken from a planar fracture forming on the
1775 axial plane of a small fold that has accommodated bedding-plane sliding (Fig. 8). The
1776 fracture is filled with calcite mineralisation of the stretched vein type (Bons et al., 2012), and
1777 that is interpreted to have formed soon after opening of the vein, and synchronous with
1778 deformation. The age of ca. 287 Ma broadly overlaps with the intrusion of the Whin Sill (ca.
1779 297 Ma; Heaman pers. comm. within De Paola et al., 2005), and is therefore compatible

1780 with the model of partitioned transpression of De Paola et al. (2005), who suggest that
1781 deformation was synchronous with the Whin Sill intrusion.

1782
1783 ~~15.3. Example B – Faroe Island brittle faults~~

1784 ~~The significant of the Eocene ages has been discussed by Roberts & Walker (2016). This~~
1785 ~~paper was the first to demonstrate the applicability of LA-ICP-MS U-Pb carbonate~~
1786 ~~geochronology to dating brittle structures in the upper crust.~~

1787
1788 ~~15.4.11.3. Figure 7d~~ Example C - Sellafield fracture mineralisation

1789 Sample 877 was collected from the modern-day saline transition zone between the upper
1790 fresh groundwater system and the deeper saline basinal-basement groundwater system, at
1791 a depth of -635 m OD within the St Bees Sandstone Group (Triassic) in Sellafield borehole
1792 BH10A (equivalent to sample B697 and D750: Appendix Table S2, Milodowski et al., 2018).
1793 Externally, this calcite exhibits a “nailhead” (i.e. c-axis flattened) crystal habit (Figure 10).
1794 However, detailed petrographic analysis reveals it has a complex growth history:
1795 comprising of cores of c-axis-elongated calcite characteristic of the deeper saline
1796 groundwater that are syntaxially-overgrown by later equant and c-axis flattened calcite
1797 characteristic of the overlying fresh groundwater zone (Milodowski et al., 2018). The U-Pb
1798 analyses all come from within the saline groundwater zone type calcite core region (rather
1799 than the later freshwater-type overgrowth that has extremely low U).

1800
1801 Late-stage (generation “ME9”) calcite is a characteristic feature of the present-day fracture-
1802 controlled deep groundwater system in the Sellafield area of the west Cumbrian coastal
1803 plain (Milodowski et al., 2018). The resulting age suggests that ME9 calcite growth in the
1804 sampled fracture was initiated in the late Miocene, and has been preserved (or at least
1805 partially preserved until the present-day). The implication is that the modern groundwater
1806 system was developed following regional Miocene uplift and younger groundwater recharge
1807 relating to glaciations and/or uplift of the region, have not led to complete re-precipitation of
1808 fracture-filling calcite, with calcite precipitation continuing to the present-day. Taken
1809 together with other petrographic, stable isotope, strontium isotope, fluid inclusion,
1810 microchemical analyses and whole-crystal U-Th age dating, the age data support the
1811 interpretation that despite evidence for glacial recharge, the geochemical conditions (e.g.

pH, Eh) have remained stable over this period at potential repository depths (cf. Milodowski et al., 2018).

~~15.5.11.4. Figure 8 Example E and F~~ – Vein sets of the Bighorn Basin, Wyoming

~~Thisese samples is are~~ from ~~a~~ vein sets in the sedimentary cover of the Bighorn Basin, ~~and is. These samples are~~ part of a larger study that analysed the timing of deformation in the foreland of the Sevier and Laramide orogenies, and how this deformation propagated in time and space (Beaudoin et al., 2018). ~~Sample BH11 is related to Laramide deformation, whereas sample BM18 is related to Sevier deformation.~~

~~15.6.11.5. Figure 1 Example 1G~~ - Moab fault

This sample comprises multiple thin (1 to 5 mm wide) veins collected from the footwall damage zone of the Moab Fault in southeast Utah. Regional deformation is primarily driven by salt tectonics (Gutierrez, 2004), and salt dissolution has produced up to one km of offset within the sedimentary rocks along the Moab Fault (Foxford et al., 1996). Fault zone deformation was closely associated with fluid flow and carbonate cementation (Eichhubl et al., 2009; Hodson et al., 2016). Ar-Ar ages from clay fault gauge range from 63 to 43 Ma and are interpreted to record the final episodes of faulting and fracture generation (Pevear et al., 1997; Solum et al., 2005). Our new lower intercept age of 22 Ma is imprecise, but clearly younger than the early-Tertiary ages. This suggests that circulating fluids continued to move along the fault zone long after the cessation of fault related deformation.

~~16.12. References~~

~~1. Akhurst, M.C., Chadwick, R.A., Holliday, D.W., McCormac, M., McMillan, A.A., Millward, D., Young, B., Ambrose, K., Auton, C.A., Barclay, W.J., Barnes, R.P., Beddoe-Stephens, B., James, J.W.C., Johnson, H., Jones, N.S., Glover, B.W., Hawkins, M.P., Kimberll, G.S., MacPherson, K.A.T., Merrit, J.W., Milodowski, A.E., Riley, N.J., Robins, N.S., Stone, P. and Wingfield, R.T.R.: The geology of the west Cumbria district: Memoir of the British Geological Survey, Sheets 28, 37 and 47, British Geological Survey, Keyworth, UK, 1997~~

~~2.1. _____~~ Albut, G., Kamber, B.S., Brüske, A., Beukes, N.J., Smith, A.J. and

Schoenberg, R.: Modern weathering in outcrop samples versus ancient paleoredox information in drill core samples from a Mesoarchaeon marine oxygen oasis in

- 1845 Pongola Supergroup, South Africa. *Geochimica et Cosmochimica Acta*, 265, 330-
1846 353, 2019.
- 1847 ~~3-2.~~ Babinski, M., Van Schmus, W.R. and Chemale Jr, F.: Pb–Pb dating and Pb
1848 isotope geochemistry of Neoproterozoic carbonate rocks from the São Francisco
1849 basin, Brazil: implications for the mobility of Pb isotopes during tectonism and
1850 metamorphism. *Chemical Geology*, 160, 175-199, 1999.
- 1851 ~~4-3.~~ Babinski, M., Vieira, L.C. and Trindade, R.I.: Direct dating of the Sete Lagoas
1852 cap carbonate (Bambuí Group, Brazil) and implications for the Neoproterozoic glacial
1853 events. *Terra Nova*, 19, 401-406, 2007.
- 1854 ~~5. Baker, A.J., Lever, M.C., Thorne, M.C., Tweed, C.J., Wikramaratna, R.S.,
1855 Chambers, A.V., Fitzgerald, P.L., Ghabaee, K., Goodfield, M., Harris, A.W. and
1856 Haworth, A.: NIREX 97: an assessment of the post-closure performance of a deep
1857 waste repository at Sellafield, NIREX, UK, 1997.~~
- 1858 ~~6-4.~~ Baker, A., Smart, P.L., Barnes, W.L., Edwards, R.L. and Farrant, A.: The
1859 Hekla 3 volcanic eruption recorded in a Scottish speleothem?. *The Holocene*, 5, 336-
1860 342, 1995.
- 1861 ~~7-5.~~ Baker, A., Smith, C.L., Jex, C., Fairchild, I.J., Genty, D. and Fuller, L.:
1862 Annually laminated speleothems: a review. *International Journal of Speleology*, 37,
1863 193-206, 2008.
- 1864 ~~8-6.~~ Barnaby, R.J. and Rimstidt, J.D.: Redox conditions of calcite cementation
1865 interpreted from Mn and Fe contents of authigenic calcites. *GSA Bulletin*, 101, 795-
1866 804, 1989.
- 1867 ~~9. Bath, A., Richards, H., Metcalfe, R., McCartney, R., Degnan, P. and Littleboy, A.:
1868 Geochemical indicators of deep groundwater movements at Sellafield, UK. *Journal
1869 of Geochemical Exploration*, 90, 24-44, 2006.~~
- 1870 ~~10-7.~~ Beaudoin, N., Lacombe, O., Roberts, N.M. and Koehn, D.: U-Pb dating of
1871 calcite veins reveals complex stress evolution and thrust sequence in the Bighorn
1872 Basin, Wyoming, USA. *Geology*, 46, 1015-1018, 2018.
- 1873 ~~11. Bergman, S.C., Huntington, K.W. and Crider, J.G.: Tracing paleofluid sources using
1874 clumped isotope thermometry of diagenetic cements along the Moab Fault,
1875 Utah. *American Journal of Science*, 313, 490-515, 2013.~~
- 1876 ~~12-8.~~ Bertok, C., Barale, L., d’Atri, A., Martire, L., Piana, F., Rossetti, P. and
1877 Gerdes, A., 2019. Unusual marbles in a non-metamorphic succession of the SW

1878 Alps (Valdieri, Italy) due to early Oligocene hydrothermal flow. *International Journal*
1879 *of Earth Sciences*, 1-20, 2019.

1880 ~~43.9.~~ Bons, P.D., Elburg, M.A. and Gomez-Rivas, E.: A review of the formation of
1881 tectonic veins and their microstructures. *Journal of Structural Geology*, 43, 33-62,
1882 2012.

1883 ~~44.10.~~ Brannon, J.C., Cole, S.C., Podosek, F.A., Ragan, V.M., Coveney, R.M.,
1884 Wallace, M.W. and Bradley, A.J.: Th-Pb and U-Pb dating of ore-stage calcite and
1885 Paleozoic fluid flow. *Science*, 271, 491-493, 1996.

1886 ~~45.11.~~ Buckman, J.O., Corbett, P.W. and Mitchell, L.: Charge contrast imaging (CCI):
1887 revealing enhanced diagenetic features of a coquina limestone. *Journal of*
1888 *Sedimentary Research*, 86, 734-748, 2016.

1889 ~~46.12.~~ Burisch, M., Gerdes, A., Walter, B.F., Neumann, U., Fettel, M. and Markl, G.:
1890 Methane and the origin of five-element veins: mineralogy, age, fluid inclusion
1891 chemistry and ore forming processes in the Odenwald, SW Germany. *Ore Geology*
1892 *Reviews*, 81, 42-61, 2017.

1893 ~~47.13.~~ Burisch, M., Walter, B.F., Gerdes, A., Lanz, M. and Markl, G.: Late-stage
1894 anhydrite-gypsum-siderite-dolomite-calcite assemblages record the transition from a
1895 deep to a shallow hydrothermal system in the Schwarzwald mining district, SW
1896 Germany. *Geochimica et Cosmochimica Acta*, 223, 259-278, 2018.

1897 ~~48.14.~~ Burn, M., Lanari, P., Pettke, T. and Engi, M.: Non-matrix-matched
1898 standardisation in LA-ICP-MS analysis: general approach, and application to allanite
1899 Th-U-Pb dating. *Journal of analytical atomic spectrometry*, 32, 1359-1377, 2017.

1900 ~~49. Chan, M.A., Parry, W.T. and Bowman, J.R.: Diagenetic hematite and manganese~~
1901 ~~oxides and fault-related fluid flow in Jurassic sandstones, southeastern Utah. *AAPG*~~
1902 ~~*bulletin*, 84, 1281-1310, 2000.~~

1903 ~~20.15.~~ Cherniak, D.J.: An experimental study of strontium and lead diffusion in
1904 calcite, and implications for carbonate diagenesis and metamorphism. *Geochimica et*
1905 *Cosmochimica Acta*, 61, 4173-4179, 1997.

1906 ~~21.16.~~ Cole, J.M., Nienstedt, J., Spataro, G., Rasbury, E.T., Lanzirotti, A., Celestian,
1907 A.J., Nilsson, M. and Hanson, G.N.: Phosphor imaging as a tool for in situ mapping
1908 of ppm levels of uranium and thorium in rocks and minerals. *Chemical Geology*, 193,
1909 127-136, 2003.

- 1910 [22.17.](#) Cole, J.M., Rasbury, E.T., Hanson, G.N., Montañez, I.P. and Pedone, V.A.:
1911 Using U-Pb ages of Miocene tufa for correlation in a terrestrial succession, Barstow
1912 Formation, California. *Geological Society of America Bulletin*, 117, 276-287, 2005.
- 1913 [23.18.](#) Coogan, L.A., Parrish, R.R. and Roberts, N.M.: Early hydrothermal carbon
1914 uptake by the upper oceanic crust: Insight from in situ U-Pb dating. *Geology*, 44,
1915 147-150, 2016.
- 1916 [24.19.](#) Cuthbert, S.J. and Buckman, J.O.: Charge contrast imaging of fine-scale
1917 microstructure and compositional variation in garnet using the environmental
1918 scanning electron microscope. *American Mineralogist*, 90, 701-707, 2005.
- 1919 ~~25. Davatzes, N.C., Eichhubl, P. and Aydin, A.: Structural evolution of fault zones in~~
1920 ~~sandstone by multiple deformation mechanisms: Moab fault, southeast~~
1921 ~~Utah. *Geological Society of America Bulletin*, 117, 135-148, 2005.~~
- 1922 [26.20.](#) De Paola, N., Holdsworth, R.E., McCaffrey, K.J. and Barchi, M.R.: Partitioned
1923 transtension: an alternative to basin inversion models. *Journal of Structural*
1924 *Geology*, 27, 607-625, 2005.
- 1925 [27.21.](#) DeWolf, C.P. and Halliday, A.N.: U-Pb dating of a remagnetized Paleozoic
1926 limestone. *Geophysical Research Letters*, 18, 1445-1448, 1991.
- 1927 [28.22.](#) Drake, H., Heim, C., Hoggmalm, K.J. and Hansen, B.T.: Fracture zone-scale
1928 variation of trace elements and stable isotopes in calcite in a crystalline rock
1929 setting. *Applied Geochemistry*, 40, 11-24, 2014.
- 1930 [29.23.](#) Drake, H., Heim, C., Roberts, N.M.W., Zack, T., Tillberg, M., Broman, C.,
1931 Ivarsson, M., Whitehouse, M.J. and Åström, M.E.: Isotopic evidence for microbial
1932 production and consumption of methane in the upper continental crust throughout
1933 the Phanerozoic eon. *Earth and Planetary Science Letters*, 470, 108-118, 2017.
- 1934 [24.](#) Drake, H., Mathurin, F.A., Zack, T., Schäfer, T., Roberts, N.M.W., Whitehouse, M.,
1935 Karlsson, A., Broman, C. and Åström, M.E.: Incorporation of metals into calcite in a
1936 deep anoxic granite aquifer. *Environmental science & technology*, 52, 493-502,
1937 2018.
- 1938 [30.25.](#) ~~Drake, H., Roberts, N.M.W., Heim, C., Whitehouse, M.J., Siljeström, S.,~~
1939 ~~Kooijman, E., Broman, C., Ivarsson, M. and Åström, M.E., 2019. Timing and origin of~~
1940 ~~natural gas accumulation in the Siljan impact structure, Sweden. *Nature*~~
1941 ~~*communications*, 10, 1-14.~~
- 1942 [31.26.](#) Drake, H., Tullborg, E.L., Hoggmalm, K.J. and Åström, M.E.: Trace metal
1943 distribution and isotope variations in low-temperature calcite and groundwater in

1944 granitoid fractures down to 1 km depth. *Geochimica et Cosmochimica Acta*, 84, 217-
1945 238, 2012.

1946 [32-27.](#) Drost, K., Chew, D., Petrus, J.A., Scholze, F., Woodhead, J.D., Schneider,
1947 J.W. and Harper, D.A.: An Image Mapping Approach to U-Pb LA-ICP-MS Carbonate
1948 Dating, and Applications to Direct Dating of Carbonate
1949 Sedimentation. *Geochemistry, Geophysics, Geosystems*, 19, 4631-4648,
1950 DOI:10.1029/2018GC007850, 2018.

1951 [33-28.](#) Eichhubl, P., Davatz, N.C. and Becker, S.P.: Structural and diagenetic control
1952 of fluid migration and cementation along the Moab fault, Utah. *AAPG bulletin*, 93,
1953 653-681, 2009.

1954 [34-29.](#) Eiler, J.M.: “Clumped-isotope” geochemistry—The study of naturally-
1955 occurring, multiply-substituted isotopologues. *Earth and planetary science
1956 letters*, 262, 309-327, 2007.

1957 [35-30.](#) Engel, J., Woodhead, J., Hellstrom, J., Maas, R., Drysdale, R. and Ford, D.:
1958 Corrections for initial isotopic disequilibrium in the speleothem U-Pb dating
1959 method. *Quaternary Geochronology*, 54, 101009, 2019.

1960 [36-31.](#) Engi, M., Lanari, P. and Kohn, M.J.: Significant ages—An introduction to
1961 petrochronology. *Reviews in Mineralogy and Geochemistry*, 83, 1-12, 2017.

1962 [37-32.](#) Fairey, B., Tsikos, H., Corfu, F. and Polteau, S.: U–Pb systematics in
1963 carbonates of the Postmasburg Group, Transvaal Supergroup, South Africa: primary
1964 versus metasomatic controls. *Precambrian Research*, 231, 194-205, 2013.

1965 [38-33.](#) Field, L.P., Milodowski, A.E., Evans, D., Palumbo-Roe, B., Hall, M.R.,
1966 Marriott, A.L., Barlow, T. and Devez, A.: Determining constraints imposed by salt
1967 fabrics on the morphology of solution-mined energy storage cavities, through
1968 dissolution experiments using brine and seawater in halite. *Quarterly Journal of
1969 Engineering Geology and Hydrogeology*, 52, 240-254, 2019.

1970 [39-34.](#) Flude, S., Lee, M.R., Sherlock, S.C. and Kelley, S.P.: Cryptic microtextures
1971 and geological histories of K-rich alkali feldspars revealed by charge contrast
1972 imaging. *Contributions to Mineralogy and Petrology*, 163, 983-994, 2012.

1973 [40-35.](#) Foxford, K.A., Garden, I.R., Guscott, S.C., Burley, S.D., Lewis, J.J.M., Walsh,
1974 J.J. and Watterson, J.: The field geology of the Moab fault, in: *Geology and
1975 Resources of the Paradox Basin*, Utah Geological Association, 25, 265-283, 1996.

1976 [41-36.](#) Godeau, N., Deschamps, P., Guihou, A., Leonide, P., Tendil, A., Gerdes, A.,
1977 Hamelin, B. and Girard, J.P.: U-Pb dating of calcite cement and diagenetic history in

1978 microporous carbonate reservoirs: Case of the Urgonian Limestone,
1979 France. *Geology*, 46, 247-250, 2018.

1980 ~~42.37.~~ Goodfellow, B.W., Viola, G., Bingen, B., Nuriel, P. and Kylander-Clark, A.R.:
1981 Palaeocene faulting in SE Sweden from U–Pb dating of slickenfibres calcite. *Terra*
1982 *Nova*, 29, 321-328, 2017.

1983 ~~43.38.~~ Grandia, F., Asmerom, Y., Getty, S., Cardellach, E. and Canals, A.: U–Pb
1984 dating of MVT ore-stage calcite: implications for fluid flow in a Mesozoic extensional
1985 basin from Iberian Peninsula. *Journal of Geochemical Exploration*, 69, 377-380,
1986 2000.

1987 ~~44.39.~~ Hansman, R.J., Albert, R., Gerdes, A. and Ring, U.: Absolute ages of multiple
1988 generations of brittle structures by U-Pb dating of calcite. *Geology*, 46, 207-210,
1989 2018.

1990 ~~45.40.~~ Hareyama, M., Tsuchiya, N., Takebe, M. and Chida, T.: Two dimensional
1991 measurement of natural radioactivity of granitic rocks by photostimulated
1992 luminescence technique. *Geochemical Journal*, 34, 1-9, 2000.

1993 ~~46. Heathcote, J.A. and Michie, U.M.: Estimating hydrogeological conditions over the~~
1994 ~~last 120 ka: an example from the Sellafield area, UK. *Journal of the Geological*~~
1995 ~~*Society*, 161, 995-1008, 2004.~~

1996 ~~47.41.~~ Hellwig, A., Voigt, S., Mulch, A., Frisch, K., Bartenstein, A., Pross, J., Gerdes,
1997 A. and Voigt, T.: Late Oligocene to early Miocene humidity change recorded in
1998 terrestrial sequences in the Ili Basin (south-eastern Kazakhstan, Central
1999 Asia). *Sedimentology*, 65, 517-539, 2018.

2000 ~~48.42.~~ Hodson, K.R., Crider, J.G. and Huntington, K.W.: Temperature and
2001 composition of carbonate cements record early structural control on cementation in a
2002 nascent deformation band fault zone: Moab Fault, Utah, USA. *Tectonophysics*, 690,
2003 240-252, 2016.

2004 ~~49.43.~~ Holdsworth, R.E., McCaffrey, K.J.W., Dempsey, E., Roberts, N.M.W.,
2005 Hardman, K., Morton, A., Feely, M., Hunt, J., Conway, A. and Robertson, A.: Natural
2006 fracture propping and earthquake-induced oil migration in fractured basement
2007 reservoirs. *Geology*, in press, [DOI:10.1130/G46280.1](https://doi.org/10.1130/G46280.1), 2019.

2008 ~~50.44.~~ Hopley, P.J., Reade, H., Parrish, R., De Kock, M. and Adams, J.W.:
2009 Speleothem evidence for C3 dominated vegetation during the Late Miocene
2010 (Messinian) of South Africa. *Review of Palaeobotany and Palynology*, 264, 75-89,
2011 2019.

- 2012 [51.45.](#) Horstwood, M.S.A., Košler, J., Gehrels, G., Jackson, S.E., McLean, N.M.,
2013 Paton, C., Pearson, N.J., Sircombe, K., Sylvester, P., Vermeesch, P. and Bowring,
2014 J.F.: Community-derived standards for LA-ICP-MS U-(Th-) Pb geochronology–
2015 Uncertainty propagation, age interpretation and data reporting. *Geostandards and*
2016 *Geoanalytical Research*, 40, 311-332, 2016.
- 2017 [52.46.](#) Incerpi, N., Martire, L., Manatschal, G., Bernasconi, S.M., Gerdes, A.,
2018 Czuppon, G., Palcsu, L., Karner, G.D., Johnson, C.A. and Figueredo, P.H.:
2019 Hydrothermal fluid flow associated to the extensional evolution of the Adriatic rifted
2020 margin: Insights from the pre-to post-rift sedimentary sequence (SE Switzerland, N
2021 ITALY). Basin Research, in press, DOI:10.1111/bre.12370, 2019.
- 2022 [53.47.](#) Jahn, B.M.: Pb–Pb dating of young marbles from Taiwan. *Nature*, 332, 429,
2023 1988.
- 2024 [54.48.](#) Jahn, B.M. and Cuvellier, H.: Pb-Pb and U-Pb geochronology of carbonate
2025 rocks: an assessment. *Chemical Geology*, 115, 125-151, 1994.
- 2026 [55.49.](#) ~~Johansen, T.E.S., Fossen, H. and Kluge, R.: The impact of syn-faulting~~
2027 ~~porosity reduction on damage zone architecture in porous sandstone: an outcrop~~
2028 ~~example from the Moab Fault, Utah. *Journal of Structural Geology*, 27, 1469-1485,~~
2029 ~~2005. Johansson, Å. and Rickard, D., 1984. Isotopic composition of Phanerozoic ore~~
2030 ~~leads from the Swedish segment of the Fennoscandian Shield. *Mineralium*~~
2031 ~~*Deposita*, 19(4), pp.249-255.~~
- 2032 [56.50.](#) Jones, C.E., Halliday, A.N. and Lohmann, K.C.: The impact of diagenesis on
2033 high-precision U-Pb dating of ancient carbonates: An example from the Late
2034 Permian of New Mexico. *Earth and Planetary Science Letters*, 134, 409-423, 1995.
- 2035 [57.51.](#) Kelly, S.D., Newville, M.G., Cheng, L., Kemner, K.M., Sutton, S.R., Fenter, P.,
2036 Sturchio, N.C. and Spötl, C.: Uranyl incorporation in natural calcite. *Environmental*
2037 *Science & Technology*, 37, 1284-1287, 2003.
- 2038 [58.52.](#) Kreissl, S., Gerdes, A., Walter, B.F., Neumann, U., Wenzel, T., Markl, G.:
2039 Reconstruction of a >200 Ma multi-stage “five element” Bi-Co-Ni-Fe-As-S system in
2040 the Penninic Alps, Switzerland. *Ore Geology Reviews* 95, 746-788, 2018.
- 2041 [59.53.](#) Kronfeld, J., Vogel, J.C. and Talma, A.S.: A new explanation for extreme
2042 ²³⁴U/²³⁸U disequilibria in a dolomitic aquifer. *Earth and Planetary Science*
2043 *Letters*, 123, 81-93, 1994.
- 2044 [60.54.](#) Kylander-Clark, A.R., Hacker, B.R. and Cottle, J.M.: Laser-ablation split-
2045 stream ICP petrochronology. *Chemical Geology*, 345, 99-112, 2013.

2046 [61-55.](#) Langmuir, D.: Uranium solution-mineral equilibria at low temperatures with
2047 applications to sedimentary ore deposits. *Geochimica et Cosmochimica Acta*, 42,
2048 547-569, 1978.

2049 [62-56.](#) Lawson, M., Shenton, B.J., Stolper, D.A., Eiler, J.M., Rasbury, E.T., Becker,
2050 T.P., Phillips-Lander, C.M., Buono, A.S., Becker, S.P., Pottorf, R. and Gray, G.G.:
2051 Deciphering the diagenetic history of the El Abra Formation of eastern Mexico using
2052 reordered clumped isotope temperatures and U-Pb dating. *GSA Bulletin*, 130, 617-
2053 629, 2018.

2054 [63-57.](#) Lee, M.R., Hodson, M.E. and Langworthy, G.: Earthworms produce granules
2055 of intricately zoned calcite. *Geology*, 36, 943-946, 2008.

2056 [64-58.](#) Li, Q., Parrish, R.R., Horstwood, M.S.A. and McArthur, J.M.: U-Pb dating of
2057 cements in Mesozoic ammonites. *Chemical Geology*, 376, 76-83, 2014.

2058 [65-59.](#) Liivamägi S, Šrodon J, Bojanowski M, Gerdes A, Stanek JJ, Williams L,
2059 Szczerba M.: Paleosols on the Ediacaran basalts of the East European Craton: a
2060 unique record of paleoweathering with minimum diagenetic overprint. *Precambrian*
2061 *Research*, 316, 66-82, 2018.

2062 [66-60.](#) MacDonald, J.M., Faithfull, J.W., Roberts, N.M.W., Davies, A.J., Holdsworth,
2063 C.M., Newton, M., Williamson, S., Boyce, A. and John, C.M.: Clumped-isotope
2064 palaeothermometry and LA-ICP-MS U-Pb dating of lava-pile hydrothermal calcite
2065 veins. *Contributions to Mineralogy and Petrology*, 174, 63, 2019.

2066 [67-61.](#) Machel, H.G.: Cathodoluminescence in calcite and dolomite and its chemical
2067 interpretation. *Geoscience Canada*, 12, 139-147, 1985.

2068 [68-62.](#) Machel, H.G.: Application of cathodoluminescence to carbonate diagenesis,
2069 in: *Cathodoluminescence in geosciences*, edited by Pagel M., Barbin V., Blanc P.
2070 and Ohnenstetter D., Springer, Berlin, Heidelberg, Germany, 271-301, 2000.

2071 [69-63.](#) Mangenot, X., Gasparrini, M., Gerdes, A., Bonifacie, M. and Rouchon, V.: An
2072 emerging thermochronometer for carbonate-bearing rocks: $\Delta 47/(U-Pb)$. *Geology*, 46,
2073 1067-1070, 2018.

2074 [70-64.](#) Maskenskaya, O.M., Drake, H., Broman, C., Hogmalm, J.K., Czuppon, G. and
2075 Åström, M.E.: Source and character of syntaxial hydrothermal calcite veins in
2076 Paleoproterozoic crystalline rocks revealed by fine-scale
2077 investigations. *Geofluids*, 14, 495-511, 2014.

2078 [71-65.](#) Mazurek, M., Davis, D.W., Madritsch, H., Rufer, D., Villa, I.M., Sutcliffe, C.N.,
2079 De Haller, A. and Traber, D.: Veins in clay-rich aquitards as records of deformation

2080 and fluid-flow events in northern Switzerland. *Applied Geochemistry*, 95, 57-70,
2081 2018.

2082 ~~72-66.~~ Methner, K., Mulch, A., Fiebig, J., Wacker, U., Gerdes, A., Graham, S.A. and
2083 Chamberlain, C.P.: Rapid middle Eocene temperature change in western North
2084 America. *Earth and Planetary Science Letters*, 450, 132-139, 2016.

2085 ~~73-67.~~ Michie, U.M. and Bowden, R.A.: UK NIREX geological investigations at
2086 Sellafield. *Proceedings of the Yorkshire Geological Society*, 50, 5-9, 1994.

2087 ~~74-68.~~ Milodowski, A.E., Bath, A. and Norris, S.: Palaeohydrogeology using
2088 geochemical, isotopic and mineralogical analyses: Salinity and redox evolution in a
2089 deep groundwater system through Quaternary glacial cycles. *Applied*
2090 *geochemistry*, 97, 40-60, 2018.

2091 ~~75. Milodowski, A.E., Gillespie, M.R., Naden, J., Fortey, N.J., Shepherd, T.J., Pearce,~~
2092 ~~J.M. and Metcalfe, R.: The petrology and paragenesis of fracture mineralization in~~
2093 ~~the Sellafield area, west Cumbria. *Proceedings of the Yorkshire Geological*~~
2094 ~~*Society*, 52, 215-241, 1998.~~

2095 ~~76-69.~~ Milton, G.M. and Brown, R.M.: Adsorption of uranium from groundwater by
2096 common fracture secondary minerals. *Canadian Journal of Earth Sciences*, 24,
2097 1321-1328, 1987.

2098 ~~70.~~ Moorbath, S., Taylor, P.N., Orpen, J.L., Treloar, P. and Wilson, J.F.: First direct
2099 radiometric dating of Archaean stromatolitic limestone. *Nature*, 326, 865-867, 1987.

2100 ~~71. Neymark, L.A., Holm-Denoma, C.S. and Moscati, R.J.: In situ LA-ICPMS U–Pb~~
2101 ~~dating of cassiterite without a known-age matrix-matched reference material:~~
2102 ~~Examples from worldwide tin deposits spanning the Proterozoic to the~~
2103 ~~Tertiary. *Chemical Geology*, 483, 410-425, 2018.~~

2104 ~~72. Nicholson, S.L., Pike, A.W., Hosfield, R., Roberts, N.M.W., Sahy, D., Woodhead, J.,~~
2105 ~~Cheng, H., Edwards, R.L., Affolter, S., Leuenberger, M. and Burns, S.J., 2020.~~
2106 ~~Pluvial periods in Southern Arabia over the last 1.1 million-years. *Quaternary*~~
2107 ~~*Science Reviews*, 229, DOI:10.1016/j.quascirev.2019.106112.~~

2108 ~~73. Nuriel, P., Craddock, J., Kylander-Clark, A.R., Uysal, T., Karabacak, V., Dirik, R.K.,~~
2109 ~~Hacker, B.R. and Weinberger, R.: Reactivation history of the North Anatolian fault~~
2110 ~~zone based on calcite age-strain analyses. *Geology*, 47, 465-469, 2019.~~

2111 ~~77-74.~~ Nuriel, P., Weinberger, R., Kylander-Clark, A.R.C., Hacker, B.R. and
2112 ~~Craddock, J.P.: The onset of the Dead Sea transform based on calcite age-strain~~
2113 ~~analyses. *Geology*, 45, 587-590, 2017.~~

2114 ~~78-75.~~ Osmond, J.K. and Cowart, J.B.: Ground water, in: Uranium-series
2115 Disequilibrium: Applications to Earth, Marine, and Environmental Sciences, Second
2116 Edition, edited by: Ivanovich, M. and Harmon, R.S., Clarendon Press, Oxford, UK,
2117 290-330.

2118 ~~79-76.~~ Osmond, J.K. and Cowart, J.B.: The theory and uses of natural uranium
2119 isotopic variations in hydrology. *Atomic Energy Review*, 14, 621-679, 1976.

2120 ~~80-77.~~ Osmond, J.K. and Cowart, J.B.: U-series nuclides as tracers in groundwater
2121 hydrology, in: *Environmental tracers in subsurface hydrology*, edited by Cook P.G.,
2122 and Herczeg A.L., Springer, Boston, MA, USA, 145-173, 2000.

2123 ~~81-78.~~ Osmond, J.K., Rydell, H.S. and Kaufman, M.I.: Uranium disequilibrium in
2124 groundwater: an isotope dilution approach in hydrologic investigations. *Science*, 162,
2125 997-999, 1968.

2126 ~~82. Neymark, L.A., Holm-Denoma, C.S. and Moscati, R.J.: In situ LA-ICPMS U-Pb~~
2127 ~~dating of cassiterite without a known-age matrix-matched reference material:~~
2128 ~~Examples from worldwide tin deposits spanning the Proterozoic to the~~
2129 ~~Tertiary. *Chemical Geology*, 483, 410-425, 2018.~~

2130 ~~83. Nuriel, P., Craddock, J., Kylander-Clark, A.R., Uysal, T., Karabacak, V., Dirik, R.K.,~~
2131 ~~Hacker, B.R. and Weinberger, R.: Reactivation history of the North Anatolian fault~~
2132 ~~zone based on calcite age-strain analyses. *Geology*, 47, 465-469, 2019.~~

2133 ~~84. Nuriel, P., Weinberger, R., Kylander-Clark, A.R.C., Hacker, B.R. and Craddock, J.P.:~~
2134 ~~The onset of the Dead Sea transform based on calcite age-strain~~
2135 ~~analyses. *Geology*, 45, 587-590, 2017.~~

2136 ~~85-79.~~ Palin, R.M., Searle, M.P., Waters, D.J., Parrish, R.R., Roberts, N.M.W.,
2137 Horstwood, M.S.A., Yeh, M.W., Chung, S.L. and Anh, T.T.: A geochronological and
2138 petrological study of anatectic paragneiss and associated granite dykes from the Day
2139 Nui C on Voi metamorphic core complex, North Vietnam: constraints on the timing of
2140 metamorphism within the Red River shear zone. *Journal of Metamorphic*
2141 *Geology*, 31, 359-387, 2013.

2142 ~~86-80.~~ Pagel, M., Bonifacie, M., Schneider, D.A., Gautheron, C., Brigaud, B.,
2143 Calmels, D., Cros, A., Saint-Bezar, B., Landrein, P., Sutcliffe, C. and Davis, D.:
2144 Improving paleohydrological and diagenetic reconstructions in calcite veins and
2145 breccia of a sedimentary basin by combining $\Delta 47$ temperature, $\delta^{18}\text{O}_{\text{water}}$ and U-Pb
2146 age. *Chemical Geology*, 481, 1-17, 2018.

2147 [87-81.](#) Paquette, J. and Reeder, R.J.: Relationship between surface structure, growth
2148 mechanism, and trace element incorporation in calcite. *Geochimica et*
2149 *Cosmochimica Acta*, 59, 735-749, 1995.

2150 [88-82.](#) Parrish, R.R., Parrish, C.M. and Lasalle, S.: Vein calcite dating reveals
2151 Pyrenean orogen as cause of Paleogene deformation in southern England. *Journal*
2152 *of the Geological Society*, 175, 425-442, 2018.

2153 [89-83.](#) Paton, C., Hellstrom, J., Paul, B., Woodhead, J. and Hergt, J.: Lolite: Freeware
2154 for the visualisation and processing of mass spectrometric data. *Journal of Analytical*
2155 *Atomic Spectrometry*, 26, 2508-2518, 2011.

2156 [90-84.](#) Paton, C., Woodhead, J.D., Hellstrom, J.C., Hergt, J.M., Greig, A. and Maas,
2157 R.: Improved laser ablation U-Pb zircon geochronology through robust downhole
2158 fractionation correction. *Geochemistry, Geophysics, Geosystems*, 11, Q0AA06,
2159 DOI:10.1029/2009GC002618, 2010.

2160 [91-85.](#) Perrette, Y., Delannoy, J.J., Desmet, M., Lignier, V. and Destombes, J.L.:
2161 Speleothem organic matter content imaging. The use of a Fluorescence Index to
2162 characterise the maximum emission wavelength. *Chemical Geology*, 214, 193-208,
2163 2005.

2164 [92-86.](#) Petrus, J.A., Chew, D.M., Leybourne, M.I. and Kamber, B.S.: A new approach
2165 to laser-ablation inductively-coupled-plasma mass-spectrometry (LA-ICP-MS) using
2166 the flexible map interrogation tool 'Monocle'. *Chemical Geology*, 463, 76-93, 2017.

2167 [93-87.](#) Pevear, D.R., Vrolijk, P.J., Longstaffe, F.J., Hendry, J., Carey, P., Parnell, J.,
2168 Ruffell, A. and Worden, R.: Timing of Moab fault displacement and fluid movement
2169 integrated with burial history using radiogenic and stable isotopes. *Geofluids II*, 97,
2170 42-45, 1997.

2171 [94-88.](#) Pickering, R., Kramers, J.D., Partridge, T., Kodolanyi, J. and Pettke, T.: U-Pb
2172 dating of calcite–aragonite layers in speleothems from hominin sites in South Africa
2173 by MC-ICP-MS. *Quaternary Geochronology*, 5, 544-558, 2010.

2174 [95-89.](#) Porcelli, D. and Swarzenski, P.W.: The behavior of U-and Th-series nuclides
2175 in groundwater. *Reviews in Mineralogy and Geochemistry*, 52, 317-361, 2003.

2176 [96-90.](#) Quade, J., Rasbury, E.T., Huntington, K.W., Hudson, A.M., Vonhof, H.,
2177 Anchukaitis, K., Betancourt, J., Latorre, C. and Pepper, M.: Isotopic characterization
2178 of late Neogene travertine deposits at Barrancas Blancas in the eastern Atacama
2179 Desert, Chile. *Chemical Geology*, 466, 41-56, 2017.

2180 [97-91.](#) Rasbury, E.T. and Cole, J.M.: Directly dating geologic events: U-Pb dating of
2181 carbonates. *Reviews of Geophysics*, 47, 2009.

2182 [98-92.](#) Rasbury, E.T., Hanson, G.N., Meyers, W.J. and Saller, A.H.: Dating of the
2183 time of sedimentation using U-Pb ages for paleosol calcite. *Geochimica et*
2184 *Cosmochimica Acta*, 61, 1525-1529, 1997.

2185 [99-93.](#) Ray, J.S., Veizer, J. and Davis, W.J.: C, O, Sr and Pb isotope systematics of
2186 carbonate sequences of the Vindhyan Supergroup, India: age, diagenesis,
2187 correlations and implications for global events. *Precambrian Research*, 121, 103-
2188 140, 2003.

2189 [100-94.](#) Reeder, R.J.: Interaction of divalent cobalt, zinc, cadmium, and barium with
2190 the calcite surface during layer growth. *Geochimica et Cosmochimica Acta*, 60,
2191 1543-1552, 1996.

2192 [101-95.](#) Reeder, R.J., Nugent, M., Lamble, G.M., Tait, C.D. and Morris, D.E.: Uranyl
2193 incorporation into calcite and aragonite: XAFS and luminescence
2194 studies. *Environmental Science & Technology*, 34, 638-644, 2000.

2195 [102-96.](#) Reeder, R.J., Nugent, M., Tait, C.D., Morris, D.E., Heald, S.M., Beck, K.M.,
2196 Hess, W.P. and Lanzirotti, A.: Coprecipitation of uranium (VI) with calcite: XAFS,
2197 micro-XAS, and luminescence characterization. *Geochimica et Cosmochimica*
2198 *Acta*, 65, 3491-3503, 2001.

2199 [103-97.](#) Regis, D., Warren, C.J., Mottram, C.M. and Roberts, N.M.W.: Using monazite
2200 and zircon petrochronology to constrain the P–T–t evolution of the middle crust in
2201 the Bhutan Himalaya. *Journal of Metamorphic Geology*, 34, 617-639, 2016.

2202 ~~[104.](#) Renne, P.R., Karner, D.B. and Ludwig, K.R.: Absolute ages aren't~~
2203 ~~exactly. *Science*, 282, 1840-1841, 1998.~~

2204 [105-98.](#) Richards, D.A., Bottrell, S.H., Cliff, R.A., Ströhle, K. and Rowe, P.J.: U-Pb
2205 dating of a speleothem of Quaternary age. *Geochimica et Cosmochimica Acta*, 62,
2206 3683-3688, 1998.

2207 [106-99.](#) Richter, D.K., Götze, T., Götze, J. and Neuser, R.D.: Progress in application of
2208 cathodoluminescence (CL) in sedimentary petrology. *Mineralogy and Petrology*, 79,
2209 127-166, 2003.

2210 [107-100.](#) Ring, U. and Gerdes, A.: Kinematics of the Alpenrhein-Bodensee graben
2211 system in the Central Alps: Oligocene/Miocene transtension due to formation of the
2212 Western Alps arc. *Tectonics*, 35, 1367-1391, 2016.

2213 ~~408.~~[101.](#) Roberts, N.M.W., Rasbury, E.T., Parrish, R.R., Smith, C.J., Horstwood,
2214 M.S.A. and Condon, D.J.: A calcite reference material for LA-ICP-MS U-Pb
2215 geochronology. *Geochemistry, Geophysics, Geosystems*, 18, 2807-2814, 2017.

2216 ~~409.~~[102.](#) Roberts, N.M.W. and Walker, R.J.: U-Pb geochronology of calcite-mineralized
2217 faults: Absolute timing of rift-related fault events on the northeast Atlantic
2218 margin. *Geology*, 44, 531-534, 2016.

2219 ~~410.~~[103.](#) Robertson, K., Gauvin, R. and Finch, J.: Application of charge contrast
2220 imaging in mineral characterization. *Minerals Engineering*, 18, 343-352, 2005.

2221 [104.](#) Romer, R.L. and Wright, J.E., 1993. [Lead mobilization during tectonic reactivation](#)
2222 [of the western Baltic Shield. *Geochimica et Cosmochimica Acta*, 57, 2555-2570.](#)

2223 ~~411.~~[105.](#) Russell, J., Chadwick, B., Rao, B.K. and Vasudev, V.N.: Whole-rock PbPb
2224 isotopic ages of Late Archaean limestones, Karnataka, India. *Precambrian*
2225 *Research*, 78, 261-272, 1996.

2226 ~~412.~~[106.](#) Sarangi, S., Gopalan, K. and Kumar, S.: Pb–Pb age of earliest megascopic,
2227 eukaryotic alga bearing Rohtas Formation, Vindhyan Supergroup, India:
2228 implications for Precambrian atmospheric oxygen evolution. *Precambrian*
2229 *Research*, 132, 107-121, 2004.

2230 ~~413.~~[107.](#) Savard, M.M., Veizer, J. and Hinton, R.: Cathodoluminescence at low Fe and
2231 Mn concentrations; a SIMS study of zones in natural calcites. *Journal of*
2232 *Sedimentary Research*, 65, 208-213, 1995.

2233 ~~414.~~[108.](#) Scardia, G., Parenti, F., Miggins, D.P., Gerdes, A., Araujo, A.G. and Neves,
2234 W.A.: Chronologic constraints on hominin dispersal outside Africa since 2.48 Ma
2235 from the Zarqa Valley, Jordan. *Quaternary Science Reviews*, 219, 1-19, 2019.

2236 ~~415.~~[109.](#) Shopov, Y.Y., Ford, D.C. and Schwarcz, H.P.: Luminescent microbanding in
2237 speleothems: high-resolution chronology and paleoclimate. *Geology*, 22, 407-410,
2238 1994.

2239 ~~416.~~[110.](#) Smeraglia, L., Aldega, L., Billi, A., Carminati, E., Di Fiore, F., Gerdes, A.,
2240 Albert, R., Rossetti, F. and Vignaroli, G.: Development of an intra-wedge tectonic
2241 mélange by out-of-sequence thrusting, buttressing, and intraformational rheological
2242 contrast, Mt. Massico ridge, Apennines, Italy. *Tectonics*, 38, 1223-1249, 2019.

2243 ~~417.~~[111.](#) Smith, P.E. and Farquhar, R.M.: Direct dating of Phanerozoic sediments by
2244 the ²³⁸U–²⁰⁶Pb method. *Nature*, 341, 518, 1989.

- 2245 ~~418~~.[112](#). Smith, P.E., Farquhar, R.M. and Hancock, R.G.: Direct radiometric age
2246 determination of carbonate diagenesis using U-Pb in secondary calcite. *Earth and*
2247 *Planetary science letters*, 105, 474-491, 1991.
- 2248 ~~419~~.[113](#). Solum, J.G., van der Pluijm, B.A. and Peacor, D.R.: Neocrystallization, fabrics
2249 and age of clay minerals from an exposure of the Moab Fault, Utah. *Journal of*
2250 *Structural Geology*, 27, 1563-1576, 2005.
- 2251 ~~420~~.[114](#). Stacey, J.T. and Kramers, J.: Approximation of terrestrial lead isotope
2252 evolution by a two-stage model. *Earth and planetary science letters*, 26, 207-221,
2253 1975.
- 2254 ~~421~~.[115](#). Stübner, K., Grujic, D., Parrish, R.R., Roberts, N.M., Kronz, A., Wooden, J.
2255 and Ahmad, T.: Monazite geochronology unravels the timing of crustal thickening in
2256 NW Himalaya. *Lithos*, 210, 111-128, 2014.
- 2257 ~~422~~.[116](#). Sturchio, N.C., Antonio, M.R., Soderholm, L., Sutton, S.R. and Brannon, J.C.:
2258 Tetravalent uranium in calcite. *Science*, 281, 971-973, 1998.
- 2259 ~~423~~.[117](#). Suksi, J., Rasilainen, K. and Pitkänen, P.: Variations in ²³⁴U/²³⁸U activity
2260 ratios in groundwater—A key to flow system characterisation?. *Physics and*
2261 *Chemistry of the Earth, Parts A/B/C*, 31, 556-571, 2006.
- 2262 ~~424~~.[118](#). Sumner, D.Y. and Bowring, S.A.: U-Pb geochronologic constraints on
2263 deposition of the Campbellrand Subgroup, Transvaal Supergroup, South
2264 Africa. *Precambrian Research*, 79, 25-35, 1996.
- 2265 ~~425~~.[119](#). Taylor, P.N. and Kalsbeek, F.: Dating the metamorphism of Precambrian
2266 marbles: Examples from Proterozoic mobile belts in Greenland. *Chemical Geology:*
2267 *Isotope Geoscience Section*, 86, 21-28, 1990.
- 2268 ~~426~~.[120](#). Trudgill, B.D.: Evolution of salt structures in the northern Paradox Basin:
2269 Controls on evaporite deposition, salt wall growth and supra-salt stratigraphic
2270 architecture. *Basin Research*, 23, 208-238, 2011.
- 2271 ~~427~~.[121](#). Tullborg, E.L., Drake, H. and Sandström, B.: Palaeohydrogeology: a
2272 methodology based on fracture mineral studies. *Applied Geochemistry*, 23, 1881-
2273 1897, 2008.
- 2274 ~~428~~.[122](#). Ukar, E. and Laubach, S.E.: Syn-and postkinematic cement textures in
2275 fractured carbonate rocks: Insights from advanced cathodoluminescence
2276 imaging. *Tectonophysics*, 690, 190-205, 2016.
- 2277 ~~429~~.[123](#). Uysal, I.T., Feng, Y.X., Zhao, J.X., Bolhar, R., Işik, V., Baublys, K.A., Yago, A.
2278 and Golding, S.D.: Seismic cycles recorded in late Quaternary calcite veins:

2279 geochronological, geochemical and microstructural evidence. *Earth and Planetary*
2280 *Science Letters*, 303, 84-96, 2011.

2281 ~~430-124.~~ Walter, B.F., Gerdes, A., Kleinhanns, I.C., Dunkl, I., von Eynatten, H., Kreissl,
2282 S. and Markl, G.: The connection between hydrothermal fluids, mineralization,
2283 tectonics and magmatism in a continental rift setting: Fluorite Sm-Nd and hematite
2284 and carbonates U-Pb geochronology from the Rhinegraben in SW
2285 Germany. *Geochimica et Cosmochimica Acta*, 240, 11-42, 2018.

2286 ~~431-125.~~ Warren, C.J., Singh, A.K., Roberts, N.M.W., Regis, D., Halton, A.M. and
2287 Singh, R.B.: Timing and conditions of peak metamorphism and cooling across the
2288 Zimithang Thrust, Arunachal Pradesh, India. *Lithos*, 200, 94-110, 2014.

2289 ~~432-126.~~ Watt, G.R., Griffin, B.J. and Kinny, P.D.: Charge contrast imaging of
2290 geological materials in the environmental scanning electron microscope. *American*
2291 *Mineralogist*, 85, 1784-1794, 2000.

2292 ~~433-127.~~ Weremeichik, J.M., Gabitov, R.I., Thien, B.M. and Sadekov, A.: The effect of
2293 growth rate on uranium partitioning between individual calcite crystals and
2294 fluid. *Chemical Geology*, 450, 145-153, 2017.

2295 ~~434-128.~~ Wendt, I. and Carl, C.: The statistical distribution of the mean squared
2296 weighted deviation. *Chemical Geology: Isotope Geoscience Section*, 86, 275-285,
2297 1991.

2298 ~~435-129.~~ Whitehouse, M.J. and Russell, J.: Isotope systematics of Precambrian
2299 marbles from the Lewisian complex of northwest Scotland: implications for Pb-Pb
2300 dating of metamorphosed carbonates. *Chemical Geology*, 136, 295-307, 1997.

2301 ~~436-130.~~ Williams, R.T., Goodwin, L.B., Sharp, W.D. and Mozley, P.S.: Reading a
2302 400,000-year record of earthquake frequency for an intraplate fault. *Proceedings of*
2303 *the National Academy of Sciences*, 114, 4893-4898, 2017.

2304 ~~437-131.~~ Woodhead, J., Hellstrom, J., Maas, R., Drysdale, R., Zanchetta, G., Devine,
2305 P. and Taylor, E.: U-Pb geochronology of speleothems by MC-ICPMS. *Quaternary*
2306 *Geochronology*, 1, 208-221, 2006.

2307 ~~132.~~ Woodhead, J., Hellstrom, J., Pickering, R., Drysdale, R., Paul, B. and Bajo, P.: U
2308 and Pb variability in older speleothems and strategies for their
2309 chronology. *Quaternary Geochronology*, 14, 105-113, 2012.

2310 ~~438-133.~~ Woodhead, J. and Petrus, J., 2019. Exploring the advantages and limitations
2311 of in situ U-Pb carbonate geochronology using speleothems. *Geochronology*, 1,
2312 69-84.

2313 [439-134.](#) Woodhead, J.D., Sniderman, J.K., Hellstrom, J., Drysdale, R.N., Maas, R.,
2314 White, N., White, S. and Devine, P.: The antiquity of Nullarbor speleothems and
2315 implications for karst palaeoclimate archives. *Scientific reports*, 9, 603, 2019.

2316 [440-135.](#) Yokoyama, T., Kimura, J.I., Mitsuguchi, T., Danhara, T., Hirata, T., Sakata, S.,
2317 Iwano, H., Maruyama, S., Chang, Q., Miyazaki, T. and Murakami, H.: U-Pb dating
2318 of calcite using LA-ICP-MS: Instrumental setup for non-matrix-matched age dating
2319 and determination of analytical areas using elemental imaging. *Geochemical*
2320 *Journal*, 52, 531-540, 2018.